

Espen Andreas Torgersen

Stability assessment of the Ryfylke subsea tunnel passing through weak rock mass

Master's thesis in Engineering Geology and Rock Mechanics

Supervisor: Krishna Kanta Panthi

Co-supervisor: Ahmed Al-Samarray

June 2022



Ryfylke tunnel during construction. Photo: Ahmed Al-Samarray (NPRA)

Espen Andreas Torgersen

Stability assessment of the Ryfylke subsea tunnel passing through weak rock mass

Master's thesis in Engineering Geology and Rock Mechanics
Supervisor: Krishna Kanta Panthi
Co-supervisor: Ahmed Al-Samarray
June 2022

Norwegian University of Science and Technology
Faculty of Engineering
Department of Geoscience and Petroleum



Your ref.: MS/N44T65/IGP/EATKKP

Date: 10.02.2022

**TGB4945 ENGINEERING GEOLOGY - MSc thesis
for
Eng. geo. student Espen Andreas Torgersen**

Stability assessment of Ryfylke subsea tunnel passing through weak rock mass

Background

During project work the candidate has reviewed different investigation methods, extent of investigations to be used in underground excavation and briefly reviewed theoretical aspects of TSP. Prediction of rock mass quality in the tunnel before excavation is an important but challenging task. Different investigation methods covering field mapping, geophysical investigations, drilling and excavation of exploratory tunnels, probe hole drilling and use of measuring while drilling (MWD) technique are being used by Norwegian tunneling industries. However, the Norwegian subsea tunnels passing through weak rock mass are seldom analyzed using analytical approaches. Therefore, this thesis should focus on the stability assessment of Ryfylke subsea tunnel that passes through segments of weak rock mass. The stability assessment should focus on the use of empirical, analytical, and numerical approaches.

MSc thesis task

The MSc thesis will therefore cover following main tasks.

- Brief review on planning and design of road tunnels including review on the importance of engineering geological and mechanical properties of the rock mass.
- Theoretical review on in-situ rock stress, stability assessment methods and design and estimation of rock support.
- Introduce about the case project. Discuss on the extent of planning phase investigations carried out. Discuss about the applied support decision.
- Carry out stability assessment of selected segments of the tunnel passing through weak rock mass using semi-analytical and analytical approaches.
- Carry out stability assessment using numerical modelling.
- Compare, discuss, and summarize the findings

Relevant computer software packages

Candidate shall use *roc-science package* and other relevant computer software.

Background information for the study

- Relevant information such as reports, maps, information, and data collected by the candidate from the project and provided by the Statens Vegvesen.
- Scientific papers, reports and books related to investigations, mechanical properties of the rocks and rock mass.
- Literatures in rock engineering, in-situ stress, stability assessment methods and rock support principles.

Cooperating partner

Statens Vegvesen is the cooperating partner for this project work. Mr. Ahmed Al-Samarray from Statens Vegvesen will be the co-supervisor and contact person for needed project data.

The project work has started on 10th January 2022 and to be completed by 10th June 2022.

The Norwegian University of Science and Technology (NTNU)
Department of Geoscience and Petroleum

February 10, 2022



Dr. Krishna K. Panthi
Professor of geological engineering, main supervisor

Note: This MSc task must be inserted in the MSc thesis after cover page

Abstract

When constructing underground excavations, optimized rock support and design is vital for the long-term stability and safety. The extent of support utilized is mainly dependent on the rock mass quality as well as the supporting tradition of the region in question. In areas with very weak rock mass, more extensive support must be installed to stabilize the tunnel compared to areas of massive, intact rock. For Norwegian road tunnels, the NPRA table of support classes based on the Q-system provides the main guidance for support implementation. For areas where the assigned Q-value is below 0.2, the common method is to install initial support consistent of spiling bolting, radial systematic rock bolts and shotcrete, in addition to the installation of arched ribs of reinforced shotcrete (RRS).

Weak rock mass may undergo plastic deformation if the ratio of the rock mass strength and deformation modulus to the in-situ and induced stress is low. If this issue is not addressed, the tunnel may be subjected to failure and collapse. A tunnel strain level of over $\sim 1\%$ is commonly described as the conditions for when squeezing problems can occur, and heavier rock support need to be installed. In such conditions, in addition to the Q-value being under 0.2, arched RRS support is usually implemented in practice. In some literature, however, it has been claimed that the utilization of arched RRS support in Norwegian road tunnels sometimes may be too excessive.

The main objectives of this thesis were to carry out analyses for the degree of tunnel deformation and the requirement for rock support in weak rock mass which exhibits plastic behavior. Two weakness zones of the Ryfylke subsea tunnel have been studied. Selected analytical, semi-analytical, numerical and empirical methods have been carried out. Obtained results have been compared to the described observations of tunnel stability and the actual performed rock support. In addition to this comparison, it could be studied which of the utilized methods were more realistic.

The results showed that the first weakness zone was expected to be subjected to $\sim 0,5-1,5\%$ tunnel strain, depending on the utilized method. Thus, it was ambiguous as to whether the zone would encounter squeezing problems. Correspondingly, the implementation of arched RRS was deemed too excessive.

For the second weakness zone, the predicted tunnel strains ranged from $\sim 1,25-3,5\%$. Based on these values, it was clear that the zone would encounter moderate-severe squeezing problems, and heavier load bearing support should be installed. However, the Convergence-Confinement Method (CCM) results' indication on rock support clearly shows that initial support consistent of systematic bolting c/c 1m and an 8cm layer of shotcrete is sufficient. This result greatly deviates from the real conditions and is deemed unrealistic. The Panthi-Shresta results were somewhat ambiguous as to whether the arched RRS was needed or not.

Concludingly, it is evaluated that the extent of tunnel deformation hardly represents the total, composite tunnel stability, and other factors may have justified the implementation of arched RRS. However, implementation of the methods presented in this thesis will give good initial estimations of squeezing problems, given that the input parameters are accurate. The Panthi-Shresta method seems like the one which provides the most information and is most realistic when compared to the performed tunnel support and tunnel stability.

Sammendrag

Ved konstruksjon av bergrom er optimalisert bergsikring avgjørende for langtidsstabilitet og sikkerhet. Omfanget av bergsikring er hovedsakelig avhengig av bergmassekvalitet og sikringstradisjonene i det aktuelle området. I områder med veldig svak bergmasse trengs det mer omfattende sikring, sammenlignet med massivt, intakt berg. I Norske vegtunneler er det Q-systemet kombinert med Statens Vegvesens tabell for sikringsklasser som utgjør den viktigste veilederen for bergsikring. For områder der den kartlagte Q-verdien er under 0.2, er det vanlig med bergsikring som inkluderer forbolting, radiell bolting og sprøytebetong, i tillegg til installasjon av armerte sprøytebetongbuer (RRS). RRS er i litteraturen beskrevet som en lastbærende sikringskonstruksjon.

Svak bergmasse kan gjennomgå plastisk deformasjon dersom forholdet mellom bergmassestyrken og stivheten til in-situ og indusert spenning er lav. Hvis dette problemet ikke blir løst, kan tunnelen kollapse. En deformasjon på over $\sim 1\%$ er typisk beskrevet som størrelsesordenen som kan medføre plastiske deformasjonsproblemer (squeezing). Da må ofte tynge bergsikring installeres. Under slike forhold, i tillegg til en Q-verdi under 0.2, er det i praksis vanlig å installere lastbærende sikring. I litteraturen og teorien hevdes det likevel at bruken av lastbærende sikring i Norske vegtunneler noen ganger kan være overflødig.

Formålet med denne oppgaven var å utføre analyser for tunneldeformasjon og nødvendig bergsikring i svak bergmasse som oppfører seg plastisk. To svakhetssoner i Ryfylketunnelen har blitt studert. Utvalgte analytiske, semi-analytiske, numeriske og empiriske metoder har blitt utført og studert. Resultatene har blitt sammenliknet med de beskrevne stabilitetsforholdene og den faktisk utførte sikringen. Utover denne sammenligningen kunne det også vurderes hvilke metoder som var de mest realistiske.

Resultatene viser at den første svakhetssonen var forventet å undergå $\sim 0,5-1,5\%$ tunneldeformasjon, avhengig av hvilken metode en som benyttes. Derfor var det uklart om svakhetssonen ville undergå deformasjonsproblemer. Tilsvarende ble det vurdert at installert RRS var noe overflødig.

I den andre svakhetssonen var den forventede tunneldeformasjonen $\sim 1,25-3,5\%$. Basert på disse resultatene er det tydelig at svakhetssonen støtte på moderate til alvorlige deformasjonsproblemer. Tynge bergsikring ble vurdert til å være nødvendig. Likevel viste Convergence-Confinement Metoden (CCM) sine resultater at førstegangssikring bestående av bolter c/c 1m og 8cm sprøytebetong ville være tilstrekkelig. Denne indikasjonen avviker stort fra de virkelige forholdene, og ble vurdert til å være urealistisk. Resultatene fra Panthi-Shresta metoden var noe tvetydelig angående nødvendigheten av RRS.

Oppsummeringsvis er det vurdert at grad av tunneldeformasjon ikke gjenspeiler den totale tunnelstabiliteten. Dermed kan også andre faktorer rettferdiggjøre implementering av RRS. Likevel vil metodene presentert i denne oppgaven gi gode førstegangsestimater på tunneldeformasjonsproblemer, gitt at inngangsparameterene er nøyaktige. Panthi-Shresta metoden virker til å være metoden som gir mest nyttig informasjon, i tillegg til å være mest realistisk når en sammenligner med utført sikring og observert tunnelstabilitet.

Preface

This thesis concludes my Master of Science degree in the field of engineering geology and rock mechanics. Several aspects of tunnelling, including pre-construction investigation, stability, support design and construction methodology quickly caught my interest during my years at the Institute of Geoscience and Petroleum. I am grateful for the opportunity to learn something new here every day, and thankful that I could write both the Specialization project and Masters thesis within subjects of great interest. This thesis makes up 30 credits, and marks the end of the my time as a student in Trondheim and NTNU.

The ever-present need for underground solutions always motivated me to stay updated on the latest trends and advances in tunnelling and rock mechanics. A science that is rarely exact has for me been captivating. By this, I know that there are endless opportunities to discover new innovations and solutions within the field. This makes up a part of the basis for the thesis subject, and I hope to be able to contribute with clever solutions in real-life projects for years to come! This is just the beginning.

I want to thank my supervisor, professor Krishna Kanta Panthi for always being available and motivating me along the way. Your knowledge, experience and cheerful mood has inspired me during these times, and I am very grateful for that. Your sharing of real tunnel project experience is always helpful.

A big thank you is also addressed to Mr. Ahmed Al-Samarray for your cooperation during the specialization project and this masters thesis. I especially appreciate your shared experience from the Ryfylke and Rogfast tunnels during our conversations. You have always been available and provided relevant background material so that this project could be carried out. For this, the Norwegian Public Roads Administration is also thanked.

Finally, I would like to thank my family and friends, fellow students, and all those who have supported me during completion of my Masters degree. You make the days shine bright, and I am thankful for all of you. During this time, I have collected memories with you that will never fade.

Trondheim, 10th June 2022

Espen Andreas Torgersen

Table of Contents

Abstract	iii
Sammendrag	v
Preface	vii
1 Introduction	1
1.1 Background and motivation	1
1.2 Objectives	2
1.3 Limitations	2
1.4 Outline	2
2 Rock masses and their properties	3
2.1 Rock mass	3
2.2 Continuous and discontinuous rock masses	4
2.3 Plasticity and plastic deformation	5
2.4 Strength anisotropy	6
2.5 Weakness zones	7
2.6 The generalized Hoek-Brown failure criteria and GSI	8
2.6.1 GSI	9
2.6.2 GSI- strengths and limitations	11
3 In-situ and induced rock stress	13
3.1 Stresses induced after opening of excavations	15
3.2 Stability problems due to rock stresses	16
3.3 Shear strength of discontinuities	18
3.4 Critical strain	19

3.5	Singh et al. prediction of tunnel squeezing	21
4	Estimation of rock support	23
4.1	Q-system	23
4.2	NPRA support classes	24
4.2.1	The need for load-bearing support and Ribs of Reinforced Shotcrete (RRS)	26
4.3	Conversion between Q, RMR and GSI	27
5	Engineering geological investigation for road tunnel projects	31
5.1	Standards and requirements for pre-construction investigation in Norway	31
5.2	Investigation methods used	34
6	Subsea tunnels and special requirements	35
6.1	Minimum rock cover	35
6.2	Some challenging conditions and cases in subsea tunnels	37
7	Numerical analysis	39
7.1	Finite element method- FEM	39
7.2	RS2	40
8	Introduction to the Ryfylke tunnel project and two weakness zones	41
8.1	Regional Geology	42
8.2	Geotechnical category	43
8.3	Weakness zones at the Ryfylke tunnel	44
8.4	Weakness zone 1	44
8.5	Weakness zone 2	46
8.6	Support methodology and observations during construction	46
8.7	Other remarks from the weakness zones	48

9	Assessment of input parameters	49
9.1	Intact rock strength	49
9.2	Intact rock modulus	50
9.3	Weathering effect on intact rock properties	51
9.4	GSI	53
9.4.1	Observational estimation	53
9.4.2	Empirical GSI estimation	56
9.4.3	Correlation and remarks on GSI-values in the Ryfylke phyllite	58
9.5	In-situ stresses	58
9.6	Rock mass strength	59
9.6.1	Hoek et al. (2002) rock mass strength	59
9.6.2	Hoek and Marinos (2000) rock mass strength	60
9.6.3	Panthi (2006) rock mass strength	60
9.6.4	Barton (2002) rock mass strength	62
9.6.5	Rock mass strength results and comparison	62
9.7	Rock mass deformation modulus	66
9.7.1	Hoek and Diederichs (2006) rock mass deformation modulus	66
9.7.2	Panthi (2006) deformation modulus and shear modulus	67
9.7.3	Barton (2002) deformation modulus	67
9.7.4	Rock mass deformation modulus results and comparison	68
9.7.5	Shear modulus	70
10	Stability assessment methods	71
10.1	Hoek and Marinos approach	71
10.2	Panthi and Shresta (2018) approach	73
10.3	FEM numerical modelling - RS2	75

10.3.1	Model setup	76
10.3.2	Loading condition, mesh and convergence criteria	77
10.4	Convegence-confinement method	78
11	Results and some remarks from the stability assessment methods	83
11.1	Hoek-Marinos results	83
11.2	Panthi-Shresta results	86
11.2.1	Panthi and Shresta results indication on support	87
11.3	RS2 results	88
11.3.1	Comparison of RS2 results	91
11.4	CCM results	92
11.5	CCM indication on tunnel support	93
11.6	Comparison of all strain results	95
12	Discussion	99
12.1	The results' indication on tunnel stability	99
12.2	The results indication of arched RRS support	100
12.3	Uncertainties and limitations	102
12.3.1	Input-parameters and sensitivity	102
12.3.2	Nature and basis of the assessment methods	104
13	Conclusion	105
13.1	Recommendations	106
	References	107
	Appendix	i
	A Chart for evaluating the disturbance factor D	i

B Q-system parameters and support chart	iii
C Excel formulae for implementation to CCM	xi
D CCM Characteristic curves for all chainages reviewed	xiii

1 Introduction

1.1 Background and motivation

The required extent of rock support during tunnelling varies greatly, from almost no support for massive, good rock to more comprehensive, heavy support for weakness zones. The rock supporting practice also differs for areas with different traditions and standards. It is common to differ between rock reinforcing support and load-bearing support (Grimstad, 2018; NFF, 2008). Arched ribs of reinforced shotcrete (RRS) is the most common load-bearing support type in Norway today. However, the introduction of shotcrete and RRS implementation has severely and abruptly increased the amount of performed support in Norwegian tunnelling (Høien et al., 2019). If all sections that may be reminiscent of weakness zones are (excessively?) supported with arched RRS, chances are that the need for traditional engineering calculation and judgement may be greatly reduced.

The standard practice for rock support in Norwegian tunnelling today, is largely based on the “observational method” (NFF, 2018). This method consists of state-of-the-art equipment and technology, as well as quick decision making from skilled tunnel workers and engineering geologists. For road tunnels, the rock mass classification and support estimation is quickly and continuously carried out using the Q-system (Barton et al., 1974; NGI, 2015) in combination with the Norwegian Public Roads Administration support table (NPRA, 2021), (given in Table 3). The most noticeable change in support is when the assigned Q-value is lower than 0,2. Implementation of arched RRS as well as spiling bolting to maintain the profile has become a common supporting method of tunnelling through challenging conditions in Norway (NFF, 2018). Recently, it has been questioned whether the rock supporting practice in Norway has become too conservative when it comes to the implementation of load-bearing support, i.e. most often arched RRS (Høien, 2019; Bøgeberg and Skretting, 2021). This hypothesis will be further studied in this thesis, in an attempt to contribute to a possible answer.

In the light of this, two weakness zones in the Ryfylke subsea tunnel are examined. The rock mass consists of weak, highly foliated and schistouse phyllite. Thus, the tunnel may be subjected to plastic deformation and squeezing problems (Panthi, 2006; Hoek and Marinos, 2000). The stability of the tunnel will be investigated by means of empirical methods (Q-system, critical strain (Sakurai, 1981) and Singh et al. (1992)), analytical methods (Carranza-Torres and Fairhurst (2000) and Panthi and Shresta (2018)), semi-analytical methods (Hoek and Marinos (2000)) and numerical methods (RS2). The results from all methods will be interpreted and compared against the actual performed rock support and observed stability in the Ryfylke tunnel. With this methodology, it can be examined whether there are any correlations between analytical calculations and the rock supporting practice utilized in Norwegian road tunnels today. It will also be examined whether the stability assessment methods provide realistic descriptions of the tunnel stability.

1.2 Objectives

With this thesis, the stability in two weakness zones in the Ryfylke tunnel will be assessed. The validity and realism of the results obtained from the various approaches will be discussed and compared. Descriptions from NPRA representatives and their final geological report on the Ryfylke tunnel, as well as the authors engineering geological judgement will be used as a basis for the validity evaluation. Findings may contribute to the discussion of which stability assessment methods are suitable in modern-day tunnelling, and which may be rejected.

Further, the performed support will be compared with the indications of the analytical, semi-analytical, empirical and numerical methods. This comparison can contribute to the discussion of whether the rock supporting practice in weak rock in Norway today is too conservative.

1.3 Limitations

There are no known data available on rock stress magnitude or intact rock properties for the Ryfylke tunnel weakness zones. Therefore, the input parameters utilized in the presented analyses carry some uncertainty. Concludingly, it might be that the analyses carried out are not sufficient to give a quantitatively accurate description of the total tunnel stability. Additional investigation may be needed.

1.4 Outline

This thesis is divided into 13 main sections. Sections 2 through 7 consists of selected background theory and introduction to various concepts that are relevant for the study carried out. In Section 8, the case in the Ryfylke tunnel is presented. In Section 9, the assesment and evaluation of input parameters which will be used in the main stability assessment methods are reviewed. The main stability assessment methods are presented in section 10. Section 11 belongs to the obtained results and brief comments, while Section 12 makes up a broader discussion about the results which will be implemented to the research questions. Finally, Section 13 presents the selected conclusions and recommendations.

2 Rock masses and their properties

In this section, generally well known basic theory on rock masses and their properties will be reviewed. This includes geological variations, discontinuities, strength, deformation modulus, anisotropy, continuity and rock mass classification. Rock mass will be described generally, but not very comprehensively, as this is out of the range of this thesis. Several important aspects may not be included.

2.1 Rock mass

Rock mass is the building material in which underground openings are constructed. The rock masses are comprised of two main features; the rock and their discontinuities, and the mechanical processes acting on the rock mass (Panthi, 2006). The quality and competence of a rock mass is related to strength, deformability, anisotropy, discontinuity and weathering and alteration, as illustrated in Figure 1.

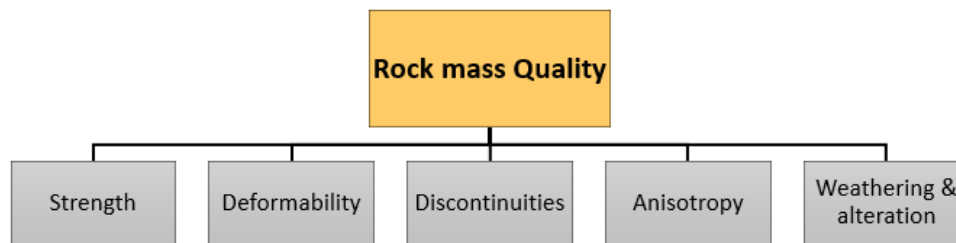


Figure 1: Rock mass quality. Modified after: Panthi (2006).

Several well known estimates for rock mass strength are available, e.g. those presented in Section 9.6. The estimations are often correlated to rock mass classification values, such as the Q-system (Barton et al., 1974) or the Geological Strength Index (GSI) (Hoek and Brown, 1997). These are reviewed in Section 4.1 and 2.6.1. Rock mass strength is also dependent on the strength of intact rock, which is commonly tested in the laboratory or in-situ. The rock mass deformability will give qualitative and quantitative indications of how the rock mass will behave and deform when subject to disturbance and stresses. Some estimates of the rock mass strength and deformation modulus are reviewed in Section 9.6 and 9.7.

The shortest distance between adjacent discontinuities is denoted as 'spacing', while the extension of it is named 'persistence'. Further, the discontinuities are either rough and irregular or smooth and plane. They can be filled with friction-reducing and swelling coatings, not filled, or filled with hard minerals which increases the friction. The degree of jointing and their properties should provide good indications of both rock mass strength, and its mechanisms. This is the reason why the most common rock-mass classification systems places great emphasis on discontinuities.

2.2 Continuous and discontinuous rock masses

The concept of continuous and discontinuous rock masses is an important one regarding stability and the stabilizing factors. As well as the nature of the rock mass, it is dependent on the size scale. The size of the underground opening compared to the structure in question and size of the rock blocks can give a good indication of how the system will behave (NBG, 2000). Usually, the larger the scale of rock or rock mass, the weaker the system will be. This is due to the increased number of dominating discontinuities and irregularities which will decrease the overall strength. This concept can also be downscaled to intact rock specimen, as Hoek (2006) showed, Figure 2.

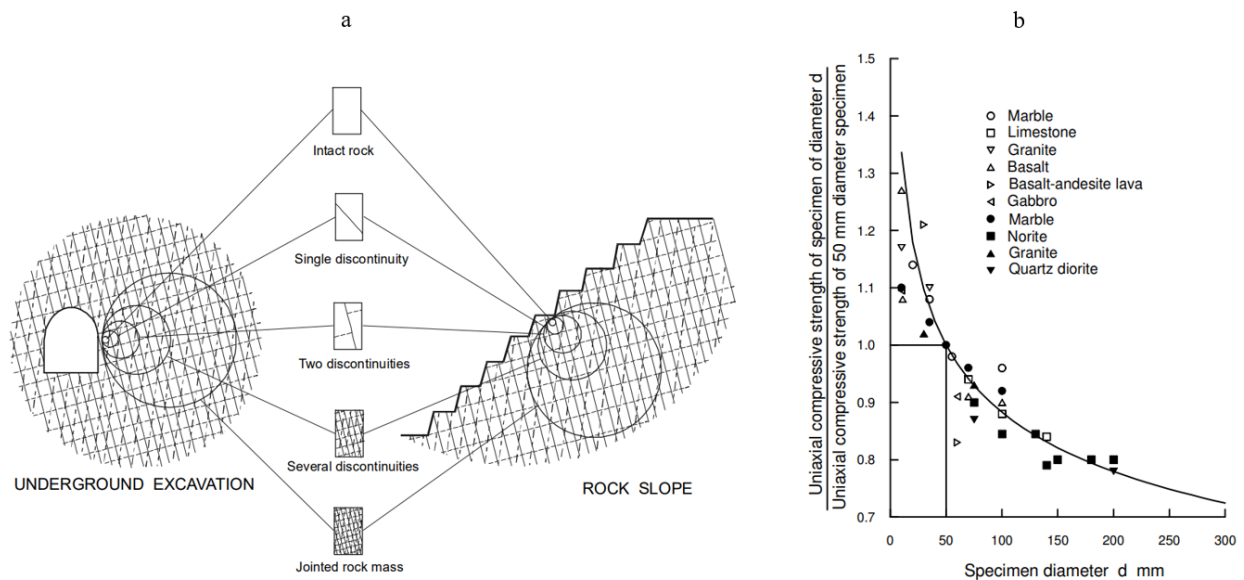


Figure 2: a: Scale effect of continuous/discontinuous behaviour of the rock mass. b: Sample size effect on the uniaxial compressive strength of intact rock specimen. From: Hoek (2006).

Palmström (1995) proposed the following classification for continuous and discontinuous rock mass:

1. If the tunnel diameter is 5-100 times larger than the diameter of the rock blocks. the ground is discontinuous. The behaviour of the system is likely to be highly anisotropic and dominated by the discontinuities and their properties.
2. The ground is continuous and behaves like a bulk material if:
 - Tunnel diameter is less than 5 times the block diameter in massive rock.
 - The ground is highly jointed and the tunnel diameter is more than 100 times the block diameter. The material will now behave similarly as a soil.

An illustration of the difference is given in Figure 3. The generalized Hoek-Brown failure criteria is only suitable for continuous rock masses, see section 2.6.

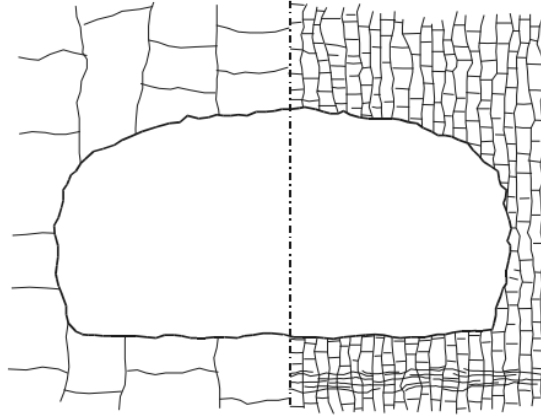


Figure 3: Illustrative difference between discontinuous (left) and continuous (right) rock mass. From: NBG (2000).

2.3 Plasticity and plastic deformation

Very weak rock mass is often assumed to exhibit an “elasto-plastic” material behaviour (Li, 2018). The models of the behaviour is given in Figure 4. The model is comprised of an elastic spring in series with a plastic friction element. The stress-strain curve shows that the material undergoes elastic deformation until a certain yield load is reached. After this yield load is reached, the material only undergoes “flow”, with no change in applied load. Unlike the plastic behaviour, hard and brittle rocks such as Basalt will deform elastically until a yield load is reached. Then, brittle failure will happen in the rock, and it will be destressed almost immediately. This may be given as the main conceptual difference between elastic/brittle and plastic/weak rock and rock mass. The elasto-plastic material behaviour is the one in which several stability assessment solutions are based, e.g. Convergence-Confinement Method (Carranza-Torres and Fairhurst, 2000), Hoek-Marinos approach (Hoek and Marinos, 2000) and RS2 plastic numerical simulation. These methods are reviewed later in this thesis, Section 10 and 11.

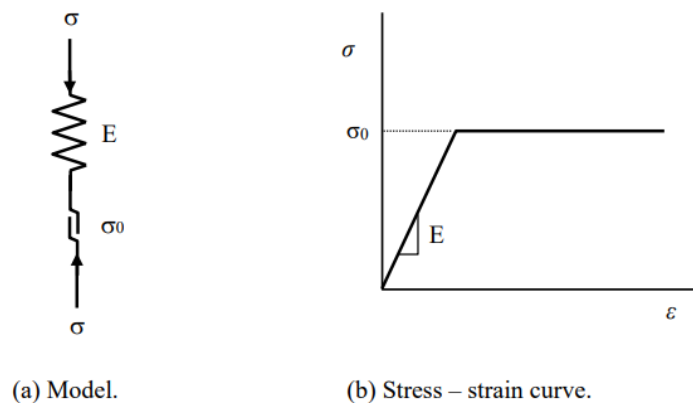


Figure 4: Model for perfectly elasto-plastic material. From: Li (2018).

Some times, the elasto-plastic material behaviour does not describe weak rock mass with realistic accuracy. Often, the rock mass will undergo a time-dependent weakening once the yield load is reached, at the same time as it undergoes deformation. When a residual strength is reached, the material may undergo “flow”. This behaviour is often referred to as “strain-softening” (Hoek, 2006). Thus, it is important to be aware that some stability assessment methods which utilizes elasto-plastic material behaviour may overestimate the long-term stability of the materials, and correspondingly underestimate the creep-deformation effect.

Due to the rock stresses induced and concentrated around the underground opening, weak rock mass in the vicinity of the opening may undergo failure. If this is the case, a plastic zone will form around the tunnel opening, as shown in Figure 5. This zone will be de-stressed, and may deform plastically over time, leading to tunnel collapse if support measures are not taken. Typical rock mass which exhibits this behaviour is comprised of e.g. phyllite, shale and slates.

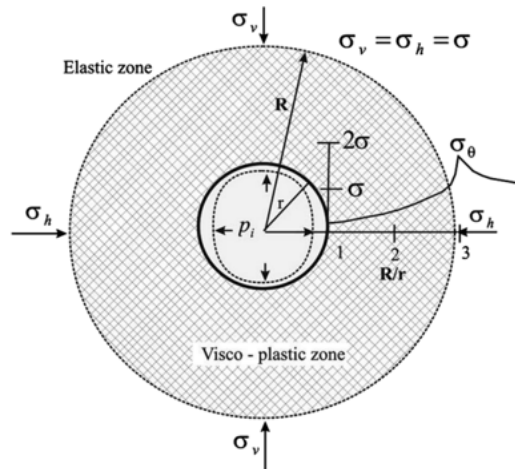


Figure 5: Plastic zone forming around the underground opening. In this figure, isostatic in-situ stress and a circular tunnel opening is represented. This is seldom the case in reality, and therefore, the form of the plastic zone may deviate from the one illustrated. From: Panthi (2006).

2.4 Strength anisotropy

Often in rock mass systems or even intact rock, there is a smaller or larger degree of strength anisotropy. For intact rock, this can be due to the orientation of foliation for sedimentary and metamorphic rocks. For rock mass systems, dominating sets of discontinuities and weakness will provide strength anisotropy. The degree of anisotropy may be determined by the arrangement and amount of certain elastic and anisotropic minerals such as mica, chlorite, amphiboles, and some pyroxenes (NBSG, 2000). In the weaker rocks such as phyllite and schist, their mechanical characteristics are weak and their nature is highly schistose. Therefore, these weak rocks lack sufficient bonding/friction and have reduced self-supporting capability. As a result severe stability problems may be faced during tunnelling (Panthi, 2006). Figure 6 shows the effect of the loading direction to foliation/schistosity on the rock strength.

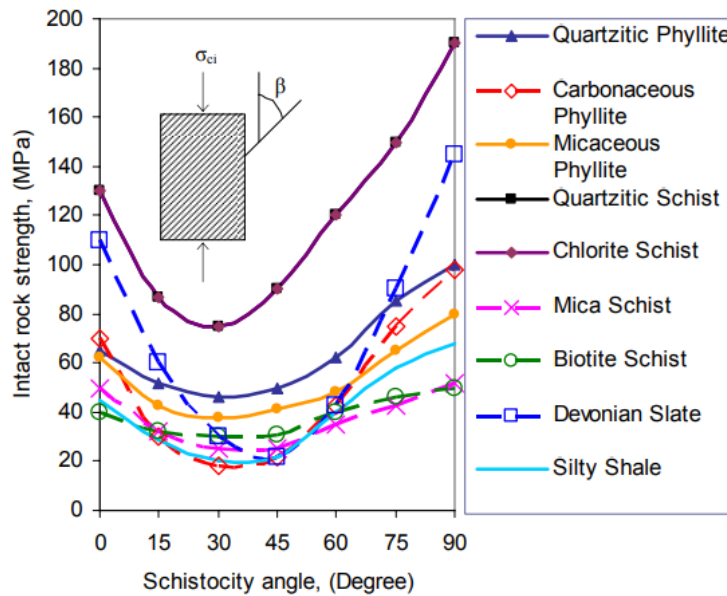


Figure 6: Effect of loading direction on strength of schistose rock. From: Panthi (2006).

As can be seen, the rock strength is lowest when the loading direction angle is approximately 30° to the foliation, and the rock is strongest when loaded perpendicular to the foliation. If a rock mass in addition to being foliated is highly folded due to tectonics, the local directions of highest rock strength may vary greatly over small distances. This makes for very complex tunnelling conditions. The author argues that the orientational strength of the Ryfylke phyllite further defends the intact strength-reduction carried out in Section 9.3, on the σ_{ci} which is tested perpendicular to the foliation (Panthi, 2006).

2.5 Weakness zones

Weakness zones normally occur along only 1 - 15% of a tunnel (Palmström and Berthelsen, 1988). Still, they form an important feature in rock tunnelling since they can be vital for the safe completion of a project. Regarding subsea tunnels, the deepest part of the fjord often coincides with major faults or weakness zones (Nilsen, 2014). Therefore, emphasis needs to be put on detecting these zones during the pre-construction investigations, as well as a suitable construction and rock stabilizing strategy when tunnelling through the zone. An unexpected encounter with a weakness zone of adverse conditions may be an expensive regret for all parties of the tunnelling project.

It is common to distinguish between two main types of weakness zones (NBG, 2000):

1. Weakness zones which are formed from tectonic events. These include the various types of faults and shears.
2. Weakness zones consisting of weak materials formed by other processes such as weathering, hydrothermal activity or alteration.

According to NBG (2000), a *weakness zone* is a part of the rock mass where the mechanical properties are significantly lower than those of the surrounding rock mass. Weakness zones can be faults, shear zones, thrust zones and weak mineral or rock layers. Of course, such zones will usually require a larger extent of rock support compared to the rest of the tunnel.

Defined in NBG (2000), a *fault* is a "Major rupture zone ranging in width from a decimetre to more than a hundred metres, occasionally more than a thousand metres. The walls are often striated and polished (slickensided) as a result of shear displacement. Frequently rock on both sides of a fault is shattered and altered or weathered, resulting in fillings such as breccia and gouge. In order to be characterised as "fault", there must be proof of movement". The gouge material varies greatly, dependent on the host rock and the conditions taking place during the fault processes.

For subsea tunnels, Kim et al. (2022) has defined four different types of weakness zones:

- Depression due to erosion of bedrock.
- Fault or weakness zone formed by tectonic activity.
- Fractured zone at contact area between intrusive dyke and rock mass.
- Flat and weak sedimentary or meta-sedimentary rock mass.

It should be noted that the weakness zones presented in Section 8.3 in the Ryfylke tunnel consists of the fourth type for zone 1, and a combination of the second and the fourth type for zone 2.

2.6 The generalized Hoek-Brown failure criteria and GSI

In 1980 Hoek and Brown developed the well known non-linear failure criteria for intact rock specimens, tested in the laboratory with the triaxial loading method (Hoek and Brown, 2019). The empirical equation to fit the results of triaxial tests on a wide range of intact rock samples, proposed by Hoek and Brown, is given by Equation 1:

$$\sigma_1 = \sigma_3 + \sigma_{ci} \sqrt{m_i \frac{\sigma_3}{\sigma_{ci}} + 1} \quad (1)$$

where σ_1 and σ_3 are the major and minor principle stresses, σ_{ci} is the unconfined compressive strength of the intact rock specimen and m_i is a material constant for the intact rock specimen.

Revisions and developments of the Hoek-Brown criteria eventually lead to the Generalized Hoek-Brown criteria which is an estimation of rock mass strength. Hoek (1994) proposed the expression in Equation 2 for the rock mass strength:

$$\sigma'_1 = \sigma'_3 + \sigma_{ci} \left(m_b \frac{\sigma'_3}{\sigma_{ci}} + s \right)^a \quad (2)$$

where m_b , s and a are rock mass constants given by Equation 3, 4 and 5.

$$m_b = m_i \exp[(GSI - 100) / (28 - 14D)] \quad (3)$$

$$s = \exp[(GSI - 100) / (9 - 3D)] \quad (4)$$

$$a = 1/2 + 1/6 \left(e^{-GSI/15} - e^{-20/3} \right) \quad (5)$$

D is a factor of disturbance that a rock mass has been subjected to due to blasting. The value ranges from 0 to 1.0, where a more disturbed area of the rock mass is assigned a higher D-value. A chart for the estimation of the disturbance factor D is reproduced after Hoek and Brown (2019) in Appendix A. The chart is based on experience and on analysis of results from a number of papers on GSI-application from the system's early days. It is pointed out that a large number of factors can influence the degree of disturbance and that it may never be possible to quantify these factors precisely (Hoek et al., 2002). The inclusion of the disturbance factor into the Hoek-Brown equations (3 and 4) is based on back-analysis of excavated tunnels and slopes (Marinos et al., 2005).

The disturbance of the rock mass will vary with distance from a free face due to blast damage and stress relief and, in some cases, to stress induced fracturing (Hoek and Diederichs, 2006). It is therefore important to not assign a D-value to the entire rock mass in question. As for numerical modelling, very few models allow this variation to be incorporated directly into the model but it is generally possible to include a number of concentric rings around the excavation and to assign a lower value of D to each successive ring (Hoek and Diederichs, 2006). This is partly done in the numerical model case from the Ryfylke tunnel in Section 10.3.

The constants m_b , s and a were meant to deal with rock masses where failure occurs as a result of rock blocks sliding on discontinuities or rotation of rock blocks, rather than internal rock compression failure (Hoek and Brown, 2019). Therefore, the criteria is best suited for rock mass consisting of interlocking angular blocks, but with a continuum approach.

2.6.1 GSI

For rock masses in which the generalized Hoek-Brown criteria is applicable, the GSI- Geological Strength Index- classification system was developed for rock mass classification. The GSI classification is meant to deal with the parameters m_b , s and a in Equation 3-5 in the generalized Hoek-Brown criteria. The chart for estimating GSI is reproduced in Figure 7. The quantification process of the GSI chart is related to the orientation and frequency of discontinuities and it is limited to rock masses in which this classification is applicable. Hence, a GSI quantification of a rock mass must be applied with caution.

The basis for the classification system is that the strength of a jointed rock mass depends on the properties of the intact rock pieces and also upon the freedom of these pieces to slide and rotate under different stress conditions (Hoek, 2006). This freedom is controlled by the geometrical shape of the intact rock pieces as well as the condition of the surfaces separating the pieces. Angular rock pieces with clean, rough discontinuity surfaces will result in a much stronger rock mass than one which contains rounded particles surrounded by

weathered and altered material (Hoek, 2006). The GSI value is included into calculations to estimate the rock mass strength reduction relative to the strength of the intact rock components. According to Nilsen (2016), GSI "classes" can be divided roughly as shown in Table 1.

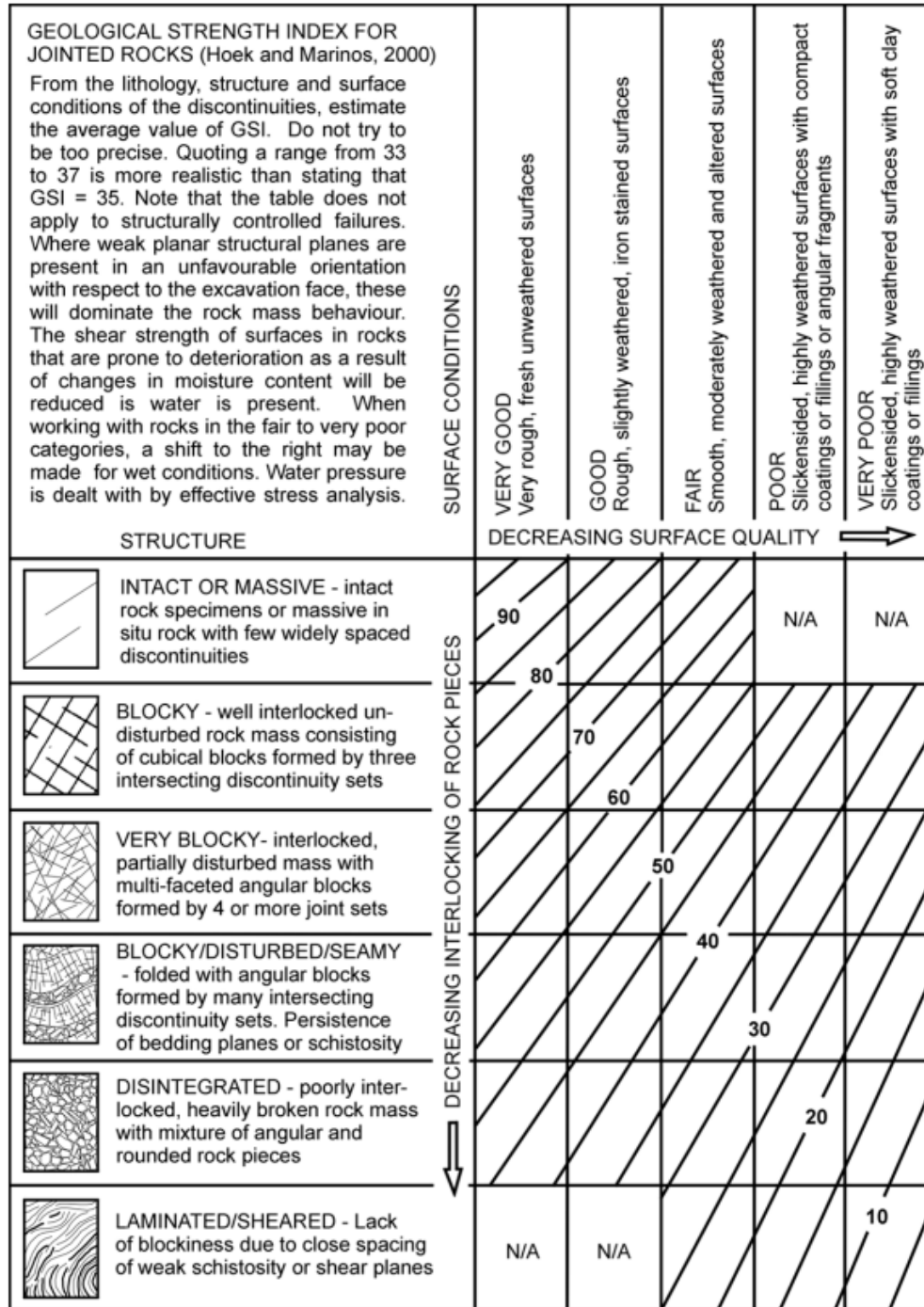


Figure 7: Chart for deciding GSI. From: (Hoek, 2006).

Table 1: GSI-classes as suggested in Nilsen (2016).

GSI- classes				
Very good	Good	Medium	Poor	Very poor
>75	56-75	36-55	21-35	≤20

2.6.2 GSI- strengths and limitations

During the increase of usage of the RMR and the Q-system in the earlier days, it became evident that the classification systems were difficult to apply for rock masses of very poor quality (Marinos et al., 2005). It is argued that both systems are very dependent on the RQD-parameter, and this is certainly not suitable in very weak, disintegrated-like rock masses. The GSI system does not include RQD, and puts greater emphasis on geological observations. This does make for a more practical approach. Also, the sole purpose of GSI is to estimate rock mass properties, whereas the Q-system and RMR includes rock reinforcement and support design. Thus, parameters like acting stresses (J_w/SRF in the Q-system) and water and orientation conditions (R_w and R_θ in the RMR-system) were eliminated. Of course, one of the major strengths of the GSI system is the connection with the parameters included in the Hoek (1994) (Hoek-brown) estimation of rock mass strength (σ_{cm}) and the associated parameters (m_b , s and a), as well as the Hoek and Diederichs (2006) estimation of rock mass modulus (E_{rm}) (see next section).

The GSI quantification is not suitable to tectonically disturbed rock masses where the structural fabric has been destroyed (Marinos et al., 2005). GSI is not suitable to rock masses in which there is a clear dominant structural direction, i.e. highly anisotropic. An example of these conditions is undisturbed slate, in which the bedding represents the dominant structural direction. Another example of inappropriate conditions is hard rock masses with few discontinuities with large spacing. In such cases, stability is largely controlled by structure geometry and the properties of the discontinuities (Marinos et al., 2005). As is the case for many other rock-mass classification systems, GSI suffers from subjectivity, especially because the estimation is based on non-measurable parameters.

It is argued that for a rock mass with a single well-defined shear or fault-zone, it may sometimes be appropriate to apply the Hoek-Brown failure criteria for rock mass. Then, the GSI value is assigned to the rock mass, ignoring the single discontinuity. The discontinuity is treated as a significantly weaker element (Marinos et al., 2005).

3 In-situ and induced rock stress

Rock stresses are the stresses (force per unit area) which exists inside the rock mass. They may be quantified by their magnitude (often *MPa*) and direction. The in-situ rock stresses are vital parameters regarding the stability of tunnelling projects. The most important stress-related parameters are the orientations and magnitudes of the major and minor principle stresses. It is well known that high in-situ stresses combined with high stress anisotropy causes great induced stress concentrations, as well as tensile stresses around tunnel openings. This gives adverse stability conditions. However, also low rock stresses may give stability problems, as the confining pressure on rock blocks defined by intersecting discontinuities are low. This may lead to rock fall under gravity and tunnel collapse, especially relevant for tunnels with low overburden. For the latter conditions, the shear strength of discontinuities and clamping on rock blocks are the most important aspects of stability.

Rock stresses are mainly caused by 4 factors (Li, 2018; Panthi, 2006):

- Weight of the overlying strata (gravitational)
- Tectonic movement
- Residual factors
- Topographic influence

It is well known that in-situ stresses generally increases with depth. The gravitational stresses due to the overlying strata are commonly derived from Equation 6, where σ_v is the vertical stress, γ is the gravity density of the overlying strata and z is depth or overburden. Rocks usually have densities around $2700\text{kg}/\text{m}^3$. Thus, an example of vertical in-situ rock stress at a depth of 200 meters is $5,4\text{MPa}$.

$$\sigma_v = \gamma z \quad (6)$$

The horizontal stress induced by the gravitational stress has commonly been derived from Equation 7, where ν is the Poisson's ratio.

$$\sigma_h = \frac{\nu}{1 - \nu} \sigma_v \quad (7)$$

Hoek (2006) states that the relation in Equation 7 is inaccurate for the total horizontal stress, and seldom used today. Hoek suggests the total horizontal stress is related to the vertical stress by a complex factor k , a stress-anisotropy constant. The horizontal stress is then derived by Equation 8

$$\sigma_h = k \sigma_v \quad (8)$$

Sheory (1994) and Hoek (2006) presents the factor k for different deformation moduli and depth levels with the graph presented in Figure 8. It is evident that the factor k generally decreases with depth below surface z . The stress conditions converges to an isotropic state at great depths. Horizontal stresses at depths that

are not great may be several times the magnitude of the vertical stress in Norway, e.g. due to the tectonic and topographic influence (Myrvang, 2001).

Tectonic stresses are also responsible for incidents such as faulting and folding (NBG, 2000). The mechanism behind the tectonic stresses are plate tectonics, which are results of warm streams of masses in the underlying asthenosphere.

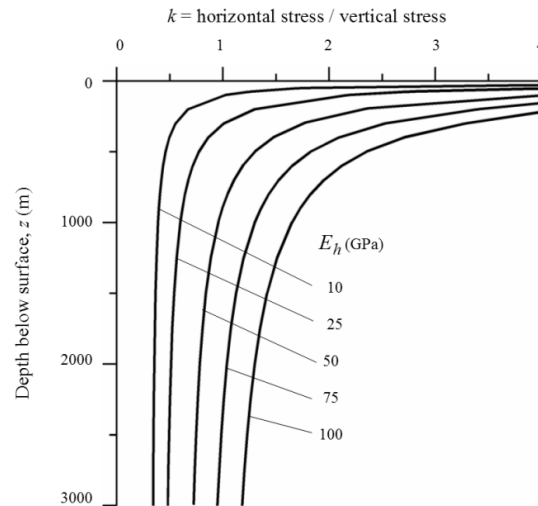


Figure 8: Stress factor k for various depth and deformation moduli. From: Hoek (2006).

Conclusively, the horizontal in-situ stress levels are one of the hardest initial parameters to estimate in the field of engineering geology and rock mechanics to be implemented in further analyses. However, there have been comprehensive studies carried out for large scale horizontal stresses. One of them was carried out by Myrvang (2001), who proposed the large-scale map of horizontal stresses in Norway, shown in Figure 9. This map may be used as an initial, crude estimation of horizontal stresses and stress direction in a large-scale area. Of course, local varieties may have significant deviations.

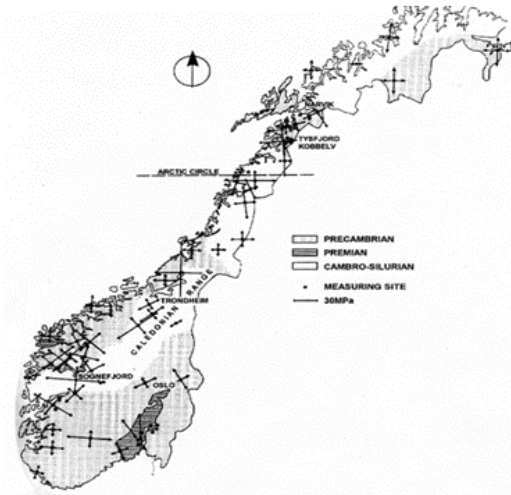


Figure 9: Large scale map of the distribution of horizontal in-situ stresses in Norway. From: Myrvang (2001).

3.1 Stresses induced after opening of excavations

After the excavation of an underground opening, the in-situ stresses are disturbed and redistributed. The area with the most redistributed stress is along the tunnel periphery, as well as in the vicinity of it. According to Kirsch theory of induced stresses, the stress distribution around an underground opening may be illustrated as shown in Figure 10. The magnitude of the redistributed stresses in a homogeneous and isotropic rock mass may be calculated, as Kirsch proposed, by Equation 9 and 10.

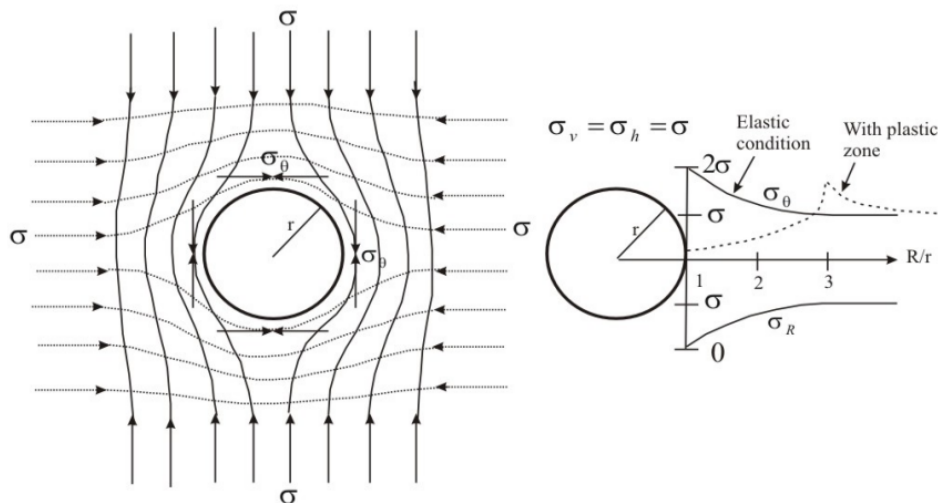


Figure 10: Stress redistribution around a tunnel opening. From: Panthi (2006).

$$\sigma_{\theta} = \sigma \times \left(1 + \frac{r^2}{R^2}\right) \quad (9)$$

$$\sigma_R = \sigma \times \left(1 - \frac{r^2}{R^2}\right) \quad (10)$$

Where r is the opening radius and R is the radial distance from the opening center. σ_{θ} is the tangential stress around the opening, while σ_R is the radial stress. One can see that the tangential stress will be two times the in-situ stress on the tunnel periphery, while the radial stress will be zero. However, the in-situ stresses are rarely isotropic. If one has obtained the magnitudes of the major and minor principle stresses, the maximum and minimum tangential stresses around a tunnel periphery can be found by Equation 11 and 12, according to Kirsch's solution.

$$\sigma_{\theta_{max}} = 3\sigma_1 - \sigma_3 \quad (11)$$

$$\sigma_{\theta_{min}} = 3\sigma_3 - \sigma_1 \quad (12)$$

Most often, the rock mass in the vicinity of an underground opening has undergone disturbances and failure, due to high stress concentrations, tensile stresses and other factors. Therefore, the stresses of the rock mass could be better described by plasticity theory (Panthi, 2006). It can be seen from Figure 10 that the stresses in the plastic stress plot is decreased due to rock failure. The maximum tangential stress is then located some distance away from the tunnel periphery, in the area of more intact, elastic rock.

3.2 Stability problems due to rock stresses

Stability problems for the tunnelling project may occur either if the stresses are very high or unfavourably low. This may delay and complicate the construction process. Examples of stability problems associated with high rock stresses are floor heaving, spalling, squeezing, wall bulging and rock burst (Li, 2018; Panthi, 2006).

Weak rock and rock masses are more exposed to floor heaving, squeezing and wall bulging due to the decreasing $\frac{UCS}{\sigma}$ relationship. Hoek and Marinos (2000) proposed a classification of squeezing problems from the strain of the rock mass and the ratio between rock mass strength and in-situ stress, presented in Figure 11. The graph is for unsupported rock. The Hoek-Marinos method will be further reviewed in Section 10.1.

Hard rock and rock masses may be exposed to rock spalling and rock burst if the principal in-situ or induced stress reaches up to 40-60% of the UCS of an intact rock sample tested in the laboratory. Spalling and rock burst makes tunnel construction a very dangerous process. As for Norwegian road tunnels, the alignments are rarely located in areas with such excessive overburden, so that they are rarely exposed to these conditions.

Swelling clay, however, may cause significant stress on the rock mass at the tunnel periphery. This was found to be the main reason for the Hanekleiven tunnel failure, which has become an infamous case in the Norwegian tunnelling society.

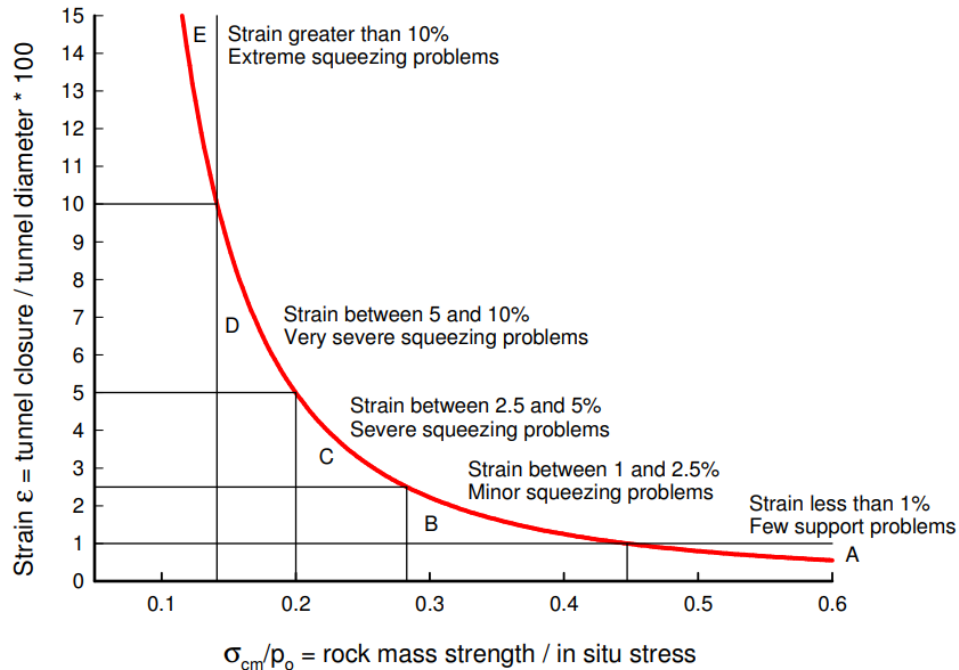


Figure 11: Classification of squeezing problem. From: Hoek and Marinos (2000).

What may just be more relevant for the Norwegian road tunnels is the occurrence of stability problems due to low stress, with various types of rock fall and difficulties of maintaining the tunnel profile during excavation. Of course, weakness zones intersecting the tunnel alignment is also a concern of main importance. The rock mass within weakness zones are generally destressed and can be described as having low-stress stability problems (Panthi, 2022a).

A large extent of the Norwegian rock mass consists of either Precambrian gneisses of relatively high quality or Cambrian-Silurian rock of various quality, as shown in Figure 12. The rock mass have generally high self-bearing capacity, and supporting strategies in Norway is to to a large extent make use of this capability (Høien, 2019). The challenge of tunnelling in the high quality gneisses, other than weakness zones, are often the occurrence of joints and planes, especially the ones that intersect with each other.



Figure 12: Regional geology of Norway and Scandinavia. From: Høien et al. (2019).

In tunnels excavated in jointed rock masses at relatively shallow depth, the most common types of failure are those involving wedges falling from the roof or sliding out of the sidewalls of the tunnels (Hoek, 2006). If the horizontal stress in the rock mass is low, the clamping effect on these wedges may not be sufficient to prevent the wedges from falling under gravity. The fall of one wedge may in turn cause larger rock fall due to the reduction in rock mass restraint.

3.3 Shear strength of discontinuities

The shear strength of discontinuities is important for both rock slope stability and the stability of tunnel wedges, as the tunnel wall will appear as a steep rock slope after excavation. The shear strength of a single joint is dependent on both the properties of the rock material and the surface condition of the rock joint (Li, 2018).

A widespread estimation of joint shear strength is the Barton-Bandis criteria (Barton and Choubey, 1977). The peak shear strength of the rock joint is expressed as Equation 13, where τ_p is the peak shear strength of the joint, σ_n is the normal stress acting on the joint, ϕ_r is the residual friction angle, JRC is the joint roughness coefficient and JCS is the joint wall compressive strength. The residual friction angle ϕ_r is further derived from Equation 14, where ϕ_b is the basic friction angle, r is the Schmidt rebound number for wet and weathered surfaces and R is the Schmidt rebound number for dry and unweathered surfaces.

$$\tau_p = \sigma_n \tan \left[\phi_r + JRC \log_{10} \left(\frac{JCS}{\sigma_n} \right) \right] \quad (13)$$

$$\phi_r = (\phi_b - 20) + 20 \left(\frac{r}{R} \right) \quad (14)$$

The JRC is the unevenness and waviness of the joint, varying in value from 0-20 and can be found by matching the joint with the profiles given in Figure 13. The JCS is found in field by using a Schmidt-hammer. The basic friction angle ϕ_b is a material constant and values for various rock types can be found in Barton and Choubey (1977).

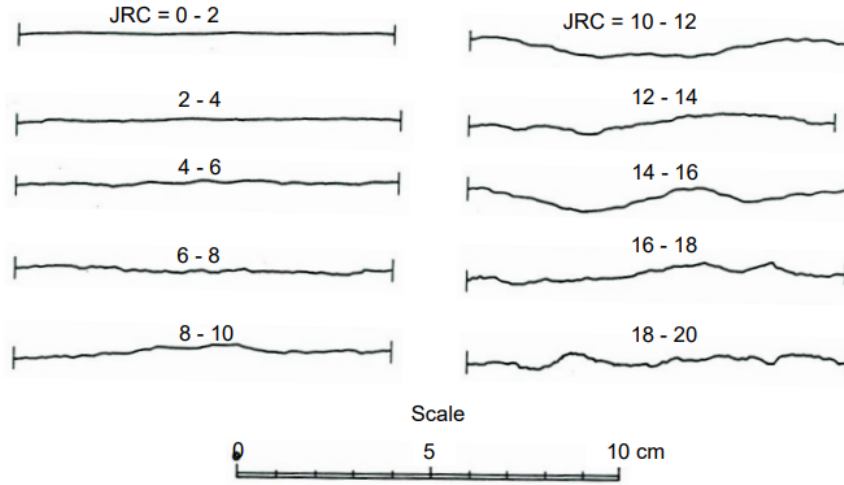


Figure 13: Typical roughness profiles. From: Barton and Choubey (1977).

The above relations are dealing with shear strength of discontinuities in which rock wall contact occurs over the full length of the discontinuity (Hoek, 2006). The shear strength may be drastically reduced if it is covered by filling material, depending on type and thickness of the filling. This material may contain swelling clay that may cause excessive stress on the rock mass and blocks. Therefore, it is common to collect some samples of the filling material in fault planes for further laboratory testing. When water pressure is present and significant, σ_n in the relation above may be replaced by the effective normal stress σ'_n , which is equal to $\sigma_n - u$, where u is the water pressure (Hoek, 2006). The shear strength of discontinuities is a key component of several rock mass classification systems, e.g the Q-system, see Section 4.1.

3.4 Critical strain

Sakurai (1981) introduced the concept of critical strain, which can be described as the strain of a rock or rock mass at yield load. The critical strain may be described by Equation 3.4:

$$\epsilon_0 = \frac{\sigma_c}{E} \quad (15)$$

The critical strain tends to decrease with increasing intact uniaxial compressive strength, and generally varies between 0,1-1% for both intact rocks and rock masses (Sakurai, 1981). However, the critical strain does not seem to correlate clearly with the rock mass strength. The concept carries the advantage that no knowledge is required on the stress levels, which as mentioned can be tedious to estimate or back-calculate without direct measurements. Sakurai (1981) states that the critical strain generally differs from the strain at failure. However, for linear-elastic material, the critical strain is assumed to be approximately the same as the failure strain. The concept is shown in Figure 14.

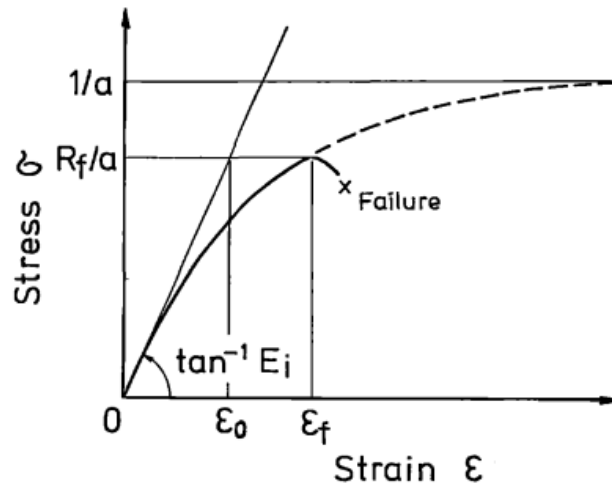


Figure 14: Hyperbolic stress-strain curve for non-linear material. From: Sakurai (1981).

Sakurai (1981) further states, as a result of the aforementioned, that the critical strain for rock masses may be estimated from the basis of laboratory testing on intact rock specimen. If the measured strain at an underground construction site exceeds the maximum allowable strain, Sakurai proposes actions such as changing the excavation scheme by increasing the number of rock bolts, sprayed concrete thickness together with the installment of steel ribs.

Further, critical strain for rock types tested in the SINTEF rock mechanics laboratory is presented in Figure 15. Phyllite is highlighted, as it is the dominating rock type of the weakness zones which will be presented in Section 8. One can see that the interval for critical strain for phyllite ranges approximately from 0,1-0,25 %.

It can be seen that the critical strain values are not very high, and typical unsupported rock mass surrounding an underground opening in weak rocks may easily exceed the critical strain value, as will be shown in Section 11.

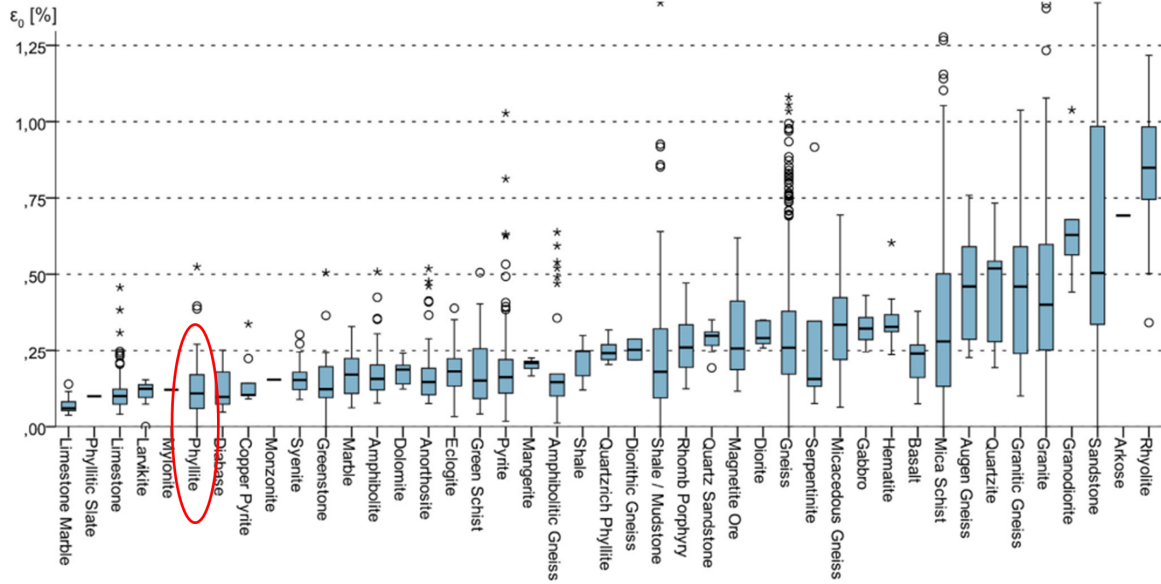


Figure 15: Critical strain for Norwegian rock types. Reproduced from SINTEF in Høien et al. (2019). Phyllite highlighted.

3.5 Singh et al. prediction of tunnel squeezing

One well known empirical method for the prediction of potential tunnel squeezing is the one developed by Singh et al. (1992). The results are based on deformation measurements, observed support pressure and the rock mass quality, with the main classification from the study being the Q-system. Out of the studied cases, a clear line of demarcation can be found in Figure 16. This line is given by:

$$H = 350 \times Q^{1/3} \quad (16)$$

That is, rock squeezing can be expected if the depth is greater than $350 \times Q^{1/3}$ (Fatemi Aghda et al., 2016).

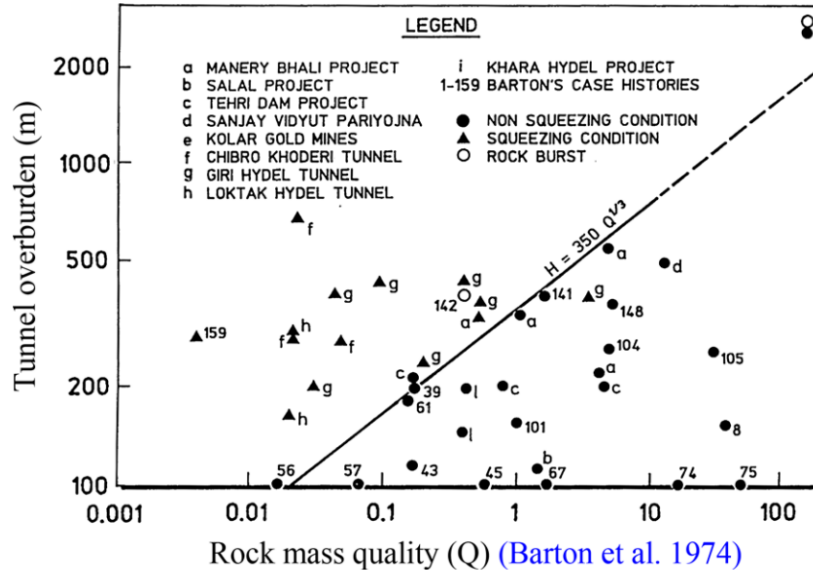


Figure 16: Case studies and approach for predicting rock squeezing. Reproduced from Singh et al. (1992) in Fatemi Aghda et al. (2016).

A weakness of this method is that it may be very difficult to estimate the Q-value for the very weak rock mass. Furthermore, the depth influence on in-situ stress conditions is counted twice with both SRF and H. Accordingly, it is very difficult to estimate SRF and Q-value for use in this squeezing prediction method (Fatemi Aghda et al., 2016).

4 Estimation of rock support

For Norwegian road tunnels, the common practice is to have controlling engineers and engineering geologists on site during construction to consecutively estimate and classify the rock mass quality. The rock mass classification is performed in accordance with the Q-system developed by Barton et al. (1974). The tunnel mapping during construction should include information on type of rock, structures, orientation of joint systems, type of discontinuity, water leakage and description and orientation of any type of weakness zones. In Norwegian tunnelling today, it is common to allocate a special item for this in the tender specifications, popularly called "the owners half hour" (NFF, 2018). The rock mass character must be assessed quickly after the blast, so that temporary and/or permanent support can be installed quickly for the safety of the tunnel workers. It is common to cover the tunnel face and recently blasted section with shotcrete, and of course, rock mass characterization must take place before this.

4.1 Q-system

The following subsection is largely reproduced from the Specialization project from the author (Torgersen, 2021).

The Q-system is a rock mass classification system which is empirically based on an evaluation of a large number of case histories of underground excavations. The Q-value is derived by Equation 17 (Barton et al., 1974):

$$Q = \frac{RQD}{J_n} \times \frac{J_r}{J_a} \times \frac{J_w}{SRF} \quad (17)$$

The six parameters are:

- RQD = Rock Quality Designation, degree of jointing
- J_n = Joint set number
- J_r = Joint roughness number
- J_a = Joint alteration number
- J_w = Joint water reduction factor
- SRF = Stress Reduction Factor

The quotient $\frac{RQD}{J_n}$ represents block size or degree of fracturing, $\frac{J_r}{J_a}$ represents inter-block shear strength, and $\frac{J_w}{SRF}$ makes up the active stress condition. The Q-value is logarithmic and spans from 0.001 (exceptionally poor) to 1000 (exceptionally good). A more competent and stable rock mass will have a higher Q-value. The rock mass is then divided into 7 quality grades, shown in Table 2. The corresponding Q-system support chart and derivation of input-parameters can be found in Appendix B.

Table 2: Classes of rock mass quality from the Q-value (NGI, 2015).

		Q-system classes					
Class	Exceptionally poor	Extremely poor	Very Poor	Poor	Fair	Good	Very-excep. good
Q-value	0.001-0.01	0.01-0.1	0.1-1	1-4	4-10	10-40	40-

It is generally realized, and well described in Palmström and Broch (2006), among others, that the most realistic and practical application of the Q-system is for rock masses within the interval Very poor to Good (Q: 0.1-40), marked in blue in Table 2. This is also the quality for which most of the empirical data is acquired, and a very large part of Norwegian bedrock is within this interval. The RQD-parameter is especially hard to quantify for very poor rock mass quality (Hoek, 2006).

These quality grades, along with the largest span of the underground opening and the safety demands for the type of excavation (ESR), derives a support category class in which the required extent of rock support is estimated. See NGI (2015) for a full description of how to use the Q-system for rock mass classification and support estimation.

Mapping of the Q-value and in-situ rock conditions is usually done in the pre-construction phase investigations and during construction of the tunnel. Although it being a useful tool for the stability and support estimation of the construction, Nilsen et al. (2003) and Carter and Marinos (2020) states that complimentary investigation methods should be used along with the Q-system. Other rock mass classification systems should also be applied.

4.2 NPRA support classes

The methodology for estimating support in Norwegian road tunnels is by using the support chart from the Norwegian Public Roads Administration (NPRA, 2021). It is valid for tunnels of cross section T8,5 - T12,5, and determines the permanent support of the tunnel. The support chart is based on the Q-system and differs a little bit from the Q-support chart. For example, the NPRA support chart suggests only six support classes while the Q-system suggests nine. Another quite important difference is that NPRA recommends the utilization of ribs of reinforced shotcrete (RRS) if the Q-value is lower than 0.2, while the Q-system utilizes RRS from $Q = 0.4$. Also, NPRA only suggests rebars of $\varnothing 20\text{mm}$ in its RRS. The NPRA support chart is reproduced in Table 3.

Table 3: Support classes. From: NPRA (2021).

Rock mass class	Rock conditions Q-value	Support class Permanent support
A/B	Weakly jointed rock mass	Support class I
	Average joint spacing: >1m Q = 10-100	- Scattered bolting - Sprayed concrete B35 E700, thickness 80mm
C	Moderately jointed rock mass	Support class II
	Average joint spacing: 0.3-1 m Q = 4-10	- Systematic bolting, c/c 2m - Sprayed concrete B35 E700, thickness 80mm
D	Strongly jointed rock mass or bedded schistose rock	Support class III
	Average joint spacing: <0.3m Q = 1-4	- Systematic bolting, c/c 1.75m - Sprayed concrete B35 E1000, thickness 100mm
E	Very poor rock mass Q = 0.2-1	Support class IVa - Systematic bolting, c/c 1.5m - Sprayed concrete B35 E1000, thickness 150mm
		Support class IVb - Systematic bolting, c/c 1.5m - Sprayed concrete B35 E1000, thickness 150mm - RRS: - Rib dimension S30/6 Ø20mm, c/c 2-3m - Bolting with arch c/c 1.5m, length 3-4m - Invert cast concrete to be evaluated
F	Extremely poor rock mass Q = 0.01-1	Support class V -Systematic bolting, c/c 1-1.5m -Sprayed concrete B35 E1000, thickness 150-250mm - RRS: - Rib dimension D60/6+4 Ø20mm, c/c 1.5-2m - Bolting with arch c/c 1.0m, length 3-6m - May be replaced by lattice girders - Cast concrete invert, pitch min. 10% of tunnel width
		Support class IV - Excavation and support to be evaluated specifically
G	Exceptionally poor rock mass Q <0.01	

It is further stated that additional, adapted rock support may be added to the support-class table recommendations. The amount of support is increased compared to the Q-system. This is due to the dimensioning life service time and traffic safety (NPRA, 2021). One can see that the most substantial increase in rock

support happens in the transition from support class E1 - E2. In addition to increasing the bolting density, it is suggested to install ribs of reinforced shotcrete, with additional steel for construction and shotcrete to cover the rib. Studying this abrupt increase in utilized support elements, it can be argued that more gradual support increase should be considered (Høien, 2019; Bøgeberg and Skretting, 2021). A small, subjective evaluation difference from engineering geologists on the Q-value could well be the difference of arched RRS utilization and general systematic bolting.

4.2.1 The need for load-bearing support and Ribs of Reinforced Shotcrete (RRS)

While bolts and shotcrete acts as rock mass reinforcement, arched RRS works as a load-bearing structure which ensures an even load distribution and preferably long-term tunnel stability. The need for load bearing support can be decided based on analytical (statical), numerical or empirical methods. The extent of permanent support is decided from engineering geological mapping and evaluation at the tunnel face (NFF, 2008). Based on this, it is evident that an experienced engineering geologist is vital for every underground construction process.

NFF (2008) indicates that when the Young's modulus of the majority of the rock mass of an area is too low to obtain sufficient stability with local rock mass reinforcement, the rock mass will not be able to carry much load. If the Young's modulus of the rock mass is low, the rock stresses will eventually lead to excessive rock deformation. Then, the elements left carrying load is not the rock mass, but the installed support. The objective then is to achieve a solid construction with a geometry which allows the stresses to distribute evenly.

When constructing the RRS, radial bolts may be installed first. A surveyour may measure the theoretical levelled profile, and the radial bolts are marked accordingly. To ensure an evenly distributed load and creation of a load-bearing arch, the blasted-out tunnel profile is levelled with shotcrete. See Figure 17 lower left. 6 rebars of diameter $\text{Ø}20\text{mm}$ (following NPRA approach) is mounted on steel joints of 40-60cm length and set up along the levelled profile. The steel joints are again attached to the tunnel wall with radial bolts c/c 1-1.5m of length 3-6m. See Figure 17 upper left. The radial bolts attaching the joints should be grouted rebar bolts or combination bolts with at least $\text{Ø}20\text{mm}$ diameter. The number of spliced rebars should not exceed 3 rebars per joint. The tangential rebars along the profile making up the RRS is usually 6m long (NFF, 2008). When the arched RRS is subjected to great loads, the rebar will begin to absorb load as the deformation increases. The rebars should prevent further deformation. For the shotcrete to be able to withstand some deformation, the shotcrete must have an energy-absorption capability of E700 or more.

The current practice regarding the use of arched RRS in Norway is largely based on experience and empiricism (Høien, 2019). Grimstad et al. (2002) states that RRS is very similar in shape and support to lattice girders, but are more flexible in application because RRS is not prefabricated. This information is useful because lattice girders are default support elements which are incorporated in the Hoek and Marinos (2000) classification table, see Section 10.1. In most cases, RRS have been installed without any measurements of support pressure, deformation or calculations of the capacity of the RRS. Therefore, the support can often be excessive with a waste of resources (Grimstad et al., 2002).

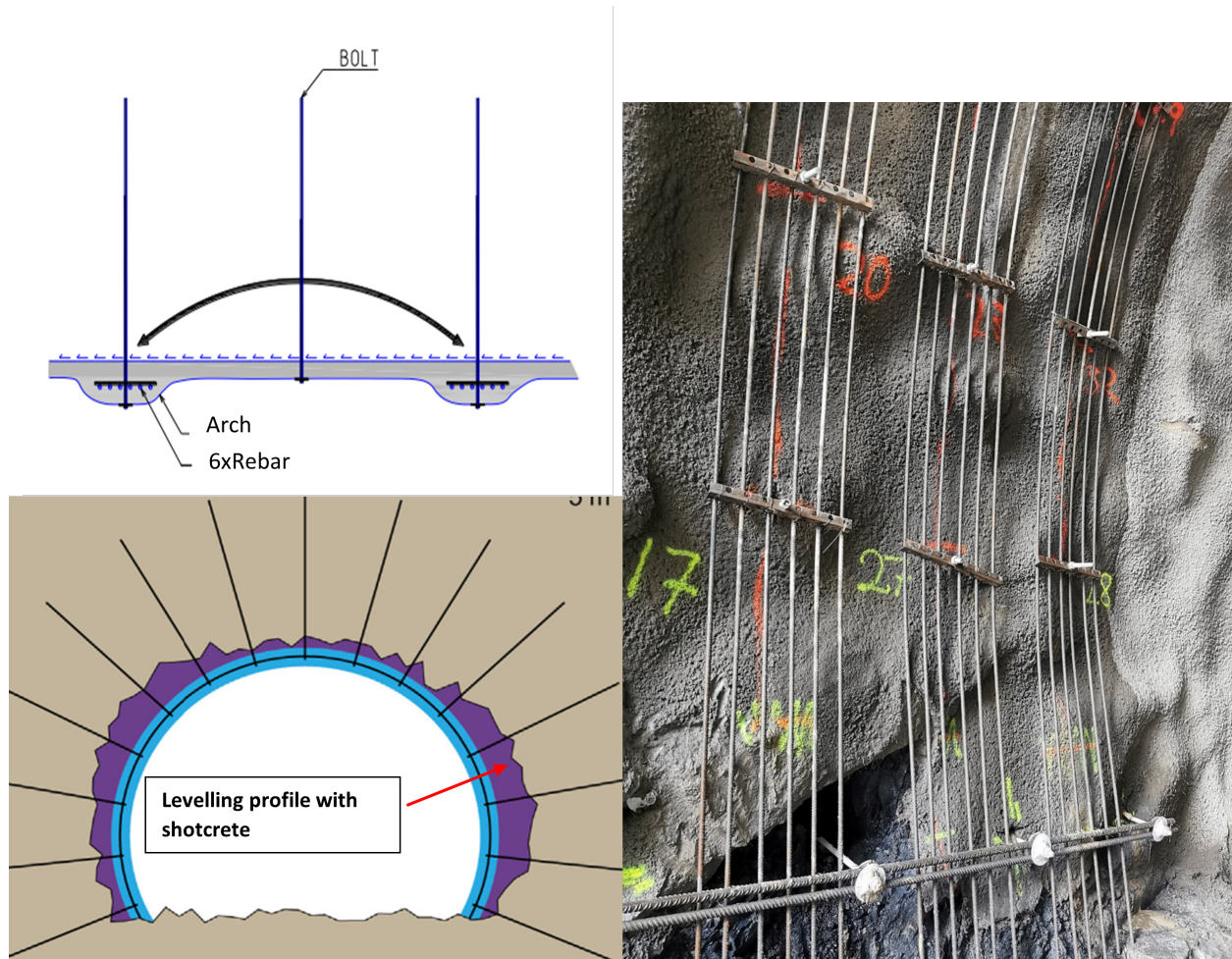


Figure 17: Upper left: principle of single-rebar RRS. From: NFF (2008). Lower left: Levelling of blasted-out tunnel profile. Modified after: Høien et al. (2019). Right: Ribs of rebars c/c 1m at tunnel cut section at Fornebubanen, ready for covering with shotcrete. Photo: Espen Torgersen.

Grimstad et al. (2002) states that when deformations are 2-10cm or more in an underground opening with a span of 10m, it is of utmost importance that flexible primary layers of sprayed concrete in combination with rock bolts are used to control the deformation of the rock mass without collapse. This is, of course, in accordance with the current practice for rock support in Norway. Shotcrete is almost always added to the tunnel face after surveying and rock mass classification is done.

4.3 Conversion between Q, RMR and GSI

Often, one does not have direct information of the mapped GSI values for e.g. a tunnel section. At least, this is the case for Norwegian tunnelling projects, where the standard classification system for tunnel mapping is the Q-system. Therefore, when in need for the GSI as an input value, one may have to estimate it indirectly.

Hoek and Brown (1997) have previously proposed the relations presented in Equation 18 and 19 for the

estimation of GSI based from the Q- and RMR- values. If your initial information is RMR from Bieniawski (1989), the simple relation in Equation 18 was proposed under the condition that $RMR' > 23$, RMR's groundwater rating is set to 15 and adjustment for joint orientation is set to zero. Hoek and Brown found that for very poor rock masses the value of RMR is very difficult to estimate. Therefore, the GSI value should not be derived based on RMR if $RMR < 23$. Because of this, the GSI would be derived from the modified Q-value (Q'), where $Q' = RQD/J_n * J_r/J_a$ and $GSI > 18$. Later, Hoek et al. (2013) proposed a new simple linear equation which related the GSI value to RMR's $JCond_{89}$ and RQD, presented in Equation 20.

$$GSI = RMR'_{89} - 5 \quad (18)$$

$$GSI = 9 \ln Q' + 44 \quad (19)$$

$$GSI = 1.5 JCond_{89} + RQD/2 \quad (20)$$

The latter equation was further processed by Hoek et al. (2013), with the RMR parameters converted to the Q-systems' jointing parameters. It was found that $1.5 JCond_{89}$ can be converted to $35 J_r/J_a / (1 + J_r/J_a)$. Substituting this into Equation 20 yields the relation presented in Equation 21:

$$GSI = \frac{52 J_r/J_a}{1 + J_r/J_a} + RQD/2 \quad (21)$$

Some comparisons were made of GSI-values visually mapped at tunnel face and the relations obtained by Equation 20 and 21, see Figure 18. As can be seen, the relations present some deviations, but the fit is an acceptable approximations for engineering applications (Hoek et al., 2013).

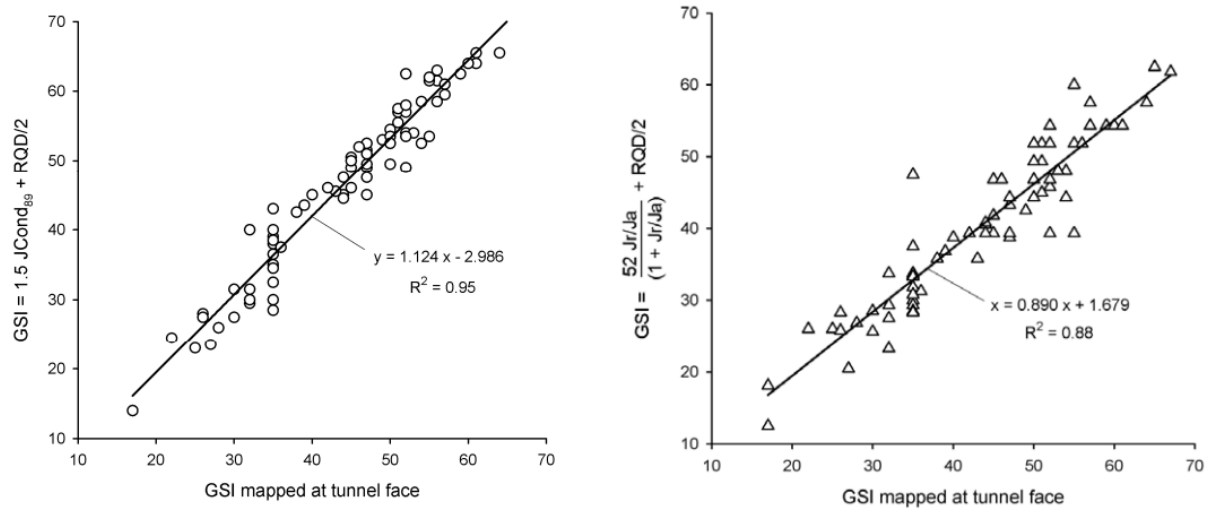


Figure 18: Comparison of GSI mapped at tunnel face and the GSI relations from $JCond_{89}$ and RQD, and J_r/J_a and RQD, respectively. From: Hoek et al. (2013).

5 Engineering geological investigation for road tunnel projects

The main goal of engineering geological planning and design of underground excavations is to achieve an optimum techno-economical result based on engineering geological knowledge (Nilsen, 2017). It is widely known that to predict adverse ground conditions is a vital part of every tunnelling project (Palmström et al., 2003; Nilsen, 2016). A main principle is that the extent of ground investigation should represent the type and complexity of the project (NBG, 2000). If surprising ground conditions are encountered, projects may suffer from great delays. One of the most expensive regrets for contractors is down-time when expensive construction equipment and crew are up and running (Paraskevopoulou and Boutsis, 2020). As a result, the project may end up in court due to twists. This twist is often referred to as differing ground conditions (DOC). In this section, some of the main aspects of engineering geological investigation for road tunnel projects will be reviewed. Some of the content in this section is reproduced from the authors specialization project, Torgersen (2021).

As it is road tunnels that are reviewed, the Norwegian Public Roads Administration (NPRA) is the main responsible authority for safe operation and construction of roads and road tunnels. The handbook "N500 Road Tunnels" (NPRA, 2021) and "V521 Tunnel guidance" (NPRA, 2022) (both in Norwegian) serves as standards and guidance for project owners, consultants and contractors as for which requirements are connected for stages from pre-construction investigation to tunnel construction and the finished product.

5.1 Standards and requirements for pre-construction investigation in Norway

The pre-construction investigation is usually divided into 3 main stages, presented in Table 4.

Table 4: Terminology for the different stages of pre-construction investigation. Note that the terminology may vary across the field of engineering geology.

Stages of pre-construction investigation	
Pre-feasibility	Tidlig planfase
Feasibility	Kommunedelplan
Design phase	Reguleringsplan

From the handbook N500 Road Tunnels (NPRA, 2021), the requirements for the Pre-feasibility stage are given in Table 5. Further, the investigation in the later stages are based on the investigation results from previous stages, which is an important principle. The requirements for the feasibility stage is given in Table 6, and the for the design phase in Table 7. It can be noticed that, naturally, the detail of the obtained information is increasing for the design phase. When all investigation phases pre-construction are done, a detailed engineering geological report should be available as part of the project tendering documentation.

Table 5: Pre-feasibility stage, NPRA (2021).

Requirements for the Pre-feasibility stage	
Evaluations	Investigation
Localize the most suitable tunnel alignments.	Complete desk study.
Map and evaluate critical areas for cost and safety of the project.	Geological mapping.
Plan and design of tunnel portals.	Examination of areas specifically sensible to the tunnel construction.
Evaluation of uncertainty regarding rock cover.	
Report requirements	
Map overview of the area with relevant tunnel profiles and profile numbers.	
Geological map of scale 1:1000 - 1:5000.	
Geological profiles for the relevant tunnel alignments, including executed core drilling.	
Overview of areas that requires further investigation.	
Description of geological conditions for the tunnel alignments and feasibility. Recommendation for further investigation, especially the needed extent of core drilling, geophysical investigation and laboratory testing and analyzes.	

Table 6: Feasibility stage, NPRA (2021).

Requirements for the feasibility stage	
Evaluation	Investigation
Investigations should form the basis of the decision of tunnel alignment	Mapping in scale 1:1000, including soil and rock conditions, fractures and fracture properties
Evaluate the need for detailed investigation regarding environmentally hazardous rock	Field investigation, localization of rock boundaries, bedding and foliation, fracturing, weakness zones, deep weathering.
Evaluate the quality of the rock regarding potential reuse.	Soil type and extent
Evaluate possibilities for tunnel portals and cuts.	Register variations of groundwater level
Evaluate sensitivity of flora and fauna	
Report requirements	
Overview map with selected tunnel alignment and profile numbers.	
Geological map in scale 1:1000 in A3 format. Shall include data from field mapping and observation, joint measurements, rock mass classification, estimates of rock support, performed ground- and core drilling, performed seismic measurements and other investigation results.	
Geological profile for decided tunnel alignment.	
An overview of the local geology of the area, with structural, hydrological and environmental geological conditions.	
Overview of areas that require special measures, such as weakness zones.	
Updated proposal of further investigation needed. Estimates of extent of ground and core drilling, seismic measurements, core sampling and laboratory analyzes.	

Table 7: Requirements in design phase (NPRA, 2021).

Requirements for the design phase	
Evaluation	Investigation
Review of results from previous investigation	All investigations have been carried out at the end of this stage.
Evaluate groundwater level, pore pressure, subductions and contamination.	Carry out remaining investigation
For subsea tunnels: Rock cover less than 50 meters to be approved by the road authorities.	Soil type and extent
Create a dedicated geological report for the project, based on previous investigation and investigation carried out at this stage.	Register variations in level of groundwater level
Report requirements	
Overview map with selected tunnel alignment and profile numbers.	
Geological map in scale 1:1000 in A3 format. Shall include all obtained data from field mapping and observation, joint measurements, rock mass classification, estimates of rock support, performed ground- and core drilling, performed seismic measurements and other investigation results.	
Geological profile for decided tunnel alignment.	
Description of rock, structures, foliations and other geological observations. Analysis of degree of fracturing, properties and orientation. Joint rosette and contour plot.	
Results from all performed investigation.	
Special local considerations and conclusions.	
Report requirements: Interpretive part	
Interpretation of geological conditions along tunnel: rock boundaries, failure structures, weakness zones and their probable interference with the tunnel alignment.	
Uncertainties regarding rock cover and tunnel cut. Rock mass classification along tunnel alignment (Q-values).	
Geotechnical and hydro-geological conditions. Soils and their properties. Consequences of landslides and subductions.	
Estimation of extent of injection grouting. Estimated leakage criteria. Probability of facing highly water bearing zones which will complicate construction.	
Point out conditions that may complicate drilling and blasting. Evaluate possibilities of encountering high or low rock stresses.	
Suggest staffing for the construction.	

From NBG (2011) interpretation and guidance to Eurocode 7, the requirements for the different stages are as follows, also mentioned in Torgersen (2021):

1. The pre-feasibility stage is for providing the geological basis for evaluating the feasibility of the project. Examination of possible tunnel alignments and potentially critical areas for cost and safety should be included.
2. The feasibility stage is for providing the basis for geological selection of alignment alternatives. Cost

estimation is to be evaluated within an accuracy of $\pm 25\%$. The document should as a minimum include a 1:1000 scale map of soil, rock, weakness zones and discontinuity orientations, as well as field and ground investigations carried out.

3. The design phase, or zoning plan, is for providing the basis for planning of the final alternative and the basis for estimating quantities and cost. Cost estimation should be within an accuracy of $\pm 10\%$. All pre-construction phase investigations are concluded at the end of this phase.

5.2 Investigation methods used

To obtain the information needed for planning and design of the tunnel, various investigations have to be carried out. Investigation methods commonly used in the different stages of a tunnelling project are shown in Table 8, modified after NFF (2009a). A more thorough review of the methods, their strengths and limitations are covered in Torgersen (2021). It is an important principle in engineering geological planning and design that the investigations are carried out step wise. The execution of each step is based on the results from the previous step (Palmström et al., 2003; Nilsen, 2016). Naturally, all methods are not applicable for every type of construction project. For example, for subsea tunnels, it is impossible to carry out traditional engineering geological mapping pre-construction. Here, geophysical methods have to be utilized to obtain information.

Table 8: Investigation methods for different stages, modified after NFF (2009a), and reproduced from Torgersen (2021).

Pre-construction			During construction	During operation
Pre-feasibility	Feasibility study	Design phase		
	- Desk study of maps, aerial photos, reports	- Eng.geol.mapping (detailed)	- Face mapping - Probe drilling - Monitoring (rock stress, convergence)	- Monitoring (Extencometer etc.)
- Basic knowledge of ground conditions	- Field investigation of key points	- Geophysical investigations	- Sampling	
- Eng.geol.mapping	- Visit to nearby excavations	- Drilling - Sampling - Lab. testing	- Lab. testing - MWD - TSP	- Quality control
	- Eng.geol.mapping			
>Recognition of major challenges	>Preliminary design	>Final design	>Modification of design	>Maintenance

6 Subsea tunnels and special requirements

When dealing with subsea tunnels, there are some aspects that make them stand out from "standard" road tunnels. The most important in an engineering geological aspect are (Nilsen, 2014):

- Increased difficulty in investigating the rock mass in the subsea sections. Special methods are required. Increased difficulty in interpreting the investigation results.
- The deepest parts of the fjords and straits in most cases coincide with major faults or weakness zones, making this a very critical part of the tunnel construction.
- The potential of water inflow is indefinite, and hydraulic pressure may be high. All leakage water has to be pumped out of the declining tunnel.
- Saline water give more corrosion on tunnelling equipment and rock support materials.

In the stability analysis carried out in this thesis, both weakness zone sections are subsea (see Section 8). The most unstable conditions in subsea sections often include gouge with active swelling clay. Combined with the indefinite potential of water leakage, this may cause great swelling pressures on the rock mass and rock support. Thus, the tunnel stand-up time may be drastically decreased.

As a result of the increased technical complexity of the tunnel, the investment in pre-construction phase investigations should also be higher. Nilsen (2014) gives a proposed approximation for the investigation cost of 8-12% of excavation cost for subsea tunnels, compared to 1-5 % for land tunnels. The investment in pre-construction phase investigation is also dependent on the geotechnical category (GC) of the project.

Because of the difficulty in attaining reliable and sufficiently detailed information about the rock mass, construction-phase investigations serve a more important role. Thus, continuous investigation by methods like probe-drilling, MWD and TSP are vital. This is extensively covered in Torgersen (2021). In addition to this, after successful implementation at the Frøya subsea tunnel, an external team of experts providing an independent risk assessment is recommended for all subsea tunnels being constructed in the future (NFF, 2018).

6.1 Minimum rock cover

Optimization of the minimum rock cover is a key factor for the planning of subsea tunnels. The requirements for maximum inclination of the road tunnel is $\leq 5\%$. It is also required that the subsea tunnel is to be planned with a minimum overburden of 50 meters (NPRA, 2021). The combination of these requirements may make it tricky to construct the tunnel in an economically viable way in practice. Because of this and the narrow fjords, the requirement for rock covers will to a big extent decide the length of the tunnel, and therefore the tunnelling costs. Excessive rock cover will make the tunnel unnecessarily long, but insufficient rock cover may cause severe stability problems and unacceptable risk during excavation (NFF, 2009b). Because of this, there is in principle a relation between tunnelling cost and minimum rock cover as presented in Figure 19.

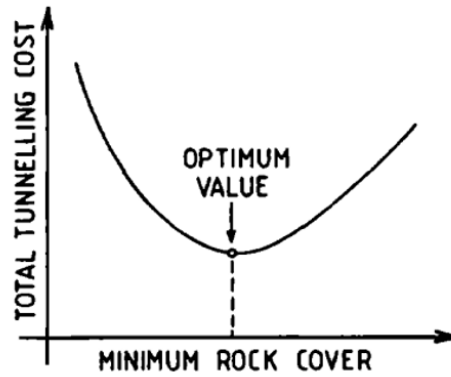


Figure 19: In-principle relation of tunnelling cost and minimum rock cover. After: Nilsen (1990).

A rock cover of less than 50 meters can only be accepted if advantageous rock mass conditions can be well documented. A rock cover less than 50 meters has to be carefully examined and approved by the Directorate of Public Roads. The conditions also have to be checked by independent review (NFF, 2018). Nevertheless, almost all of the subsea tunnels constructed in Norway up until 2009 have areas of overburden lower than 50 meters (NFF, 2009b). Figure 20 shows the Norwegian subsea tunnel's respective minimum overburden and measured seismic velocity at the respective area. It can be seen that the required minimum rock cover increases with depth to bedrock and decreasing seismic velocity.

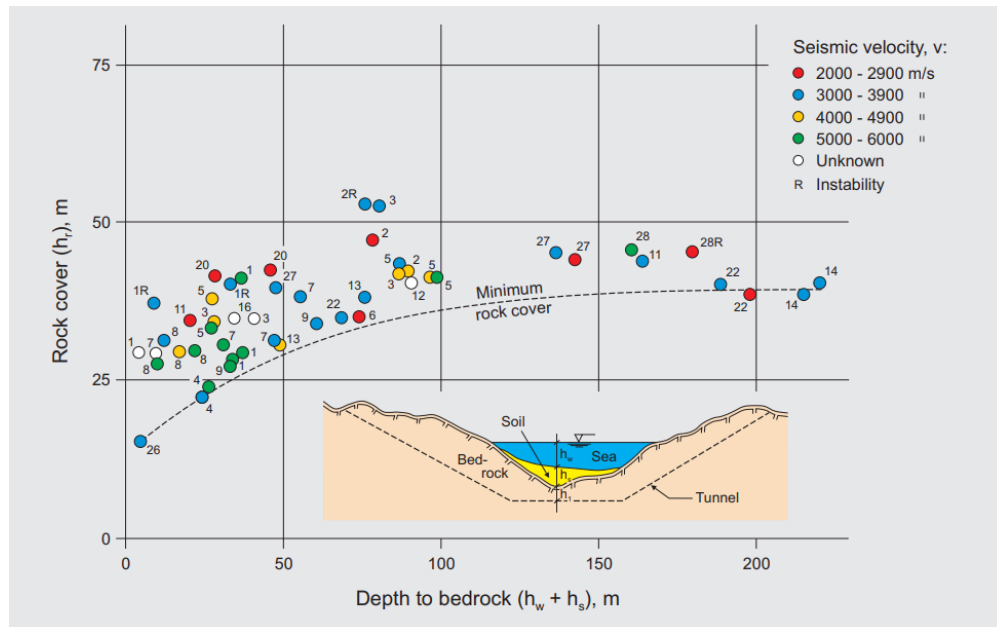


Figure 20: Minimum rock cover and seismic velocities for Norwegian subsea tunnels up until 2009. From: NFF (2009b).

6.2 Some challenging conditions and cases in subsea tunnels

One of the most challenging conditions in tunnelling is when the gouge material of the occurred weakness zone contains swelling clay, smectite (Nilsen, 2011). Other than swelling minerals, clay-fillings which include minerals that reduce the inter-block shear strength, e.g. mica minerals, will worsen the rock mass stability. Some incidents of cave-ins due to swelling clay have occurred long after the completion of the respective project. Therefore, this is a somewhat unpredictable issue that may be very hard to detect in retrospect; The issue must be dealt with right away. For the Oslofjord tunnel, a deep eroded zone caused by glaciation meant that a short section of the tunnel was constructed with no rock cover. The method implemented to complete this was ground freezing, causing a substantial delay of the tunnel project. The clay gouge of the Oslofjord tunnel was found to be highly active and gave a swelling pressure up to 0.55 MPa. The rock mass in the cave-in area which broke through the inner lining was practically without bolts and was only sprayed with a 4-6cm layer of shotcrete (Nilsen, 2011).

For the Atlanterhavs Tunnel, instability happened during construction. The incident happened in a highly crushed zone which had an estimated seismic velocity of 2.8 km/sec from refraction seismic at pre-construction investigations, shown in Figure 21. The area was exposed to large water ingress with pressure up to 23 bars. A 10 meter high cave-in which covered the full tunnel roof came down (Nilsen, 2011). The void was filled with a large concrete plug. Extremely time-consuming construction and heavy rock support had to be carried out the rest of the 25m wide zone.

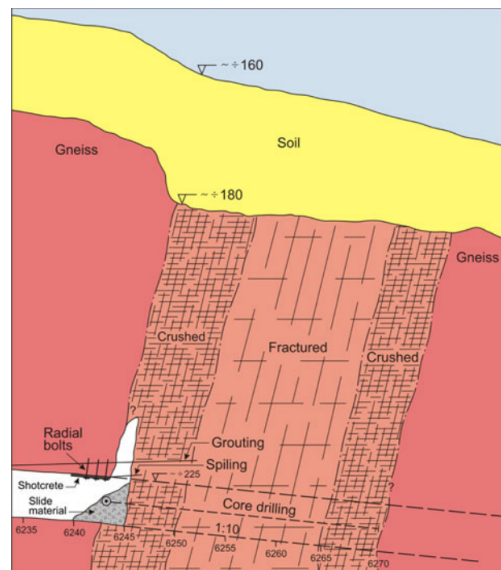


Figure 21: Cave-in situation in the Atlanterhavs tunnel. From: Nilsen (2011).

At the Bjorøy tunnel, there was a more than 10 meter wide Jurassic, tensional fault filled with clay. This zone was unexpectedly encountered in the Precambrian bedrock, and the permeability was extremely high. A very time-consuming support methodology including extensive grouting, forepoling and arching was required to get through the zone (Nilsen et al., 1999).

A specifically relevant example as compared to the Ryfylke tunnel is the North Cape tunnel. Here, flat lying, weak sedimentary rocks caused very poor stability. Comprehensive shotcrete and concrete lining was added at the tunnel face, making for a time-consuming tunnelling process (Nilsen et al., 1999)

7 Numerical analysis

Numerical analysis and software are tools to solve various engineering issues, geomechanical issues among them, which can not be solved solely from empirical or analytical approaches (NBG, 2000).

The primary classification of geomechanical models relies on the distinction between two groups, continuum and discontinuum models. Continuum models may be applied for more homogeneous rock masses, i.e. intact, massive rock or homogeneously heavily jointed rock mass, see e.g. Figure 3. The continuum codes model the rock mass as continuum medium, suitable for only a few numbers of distinctive joints. Among these codes are the RS2 program.

Discontinuum models may be used when one or more discontinuities, along with their geometrical structure, largely controls the stability of the rock mass. The discontinuum codes model the rock mass as a system of individual blocks acting along their respective boundaries. Discontinuum codes may utilize e.g. the Barton-Bandis joint model, as reviewed in section 3.3. UDEC and 3DEC are common discrete-element methods. It may be argued that these types of codes are more realistic, as the rock mass is naturally penetrated by more or less stability-dominating discontinuities. An illustration of when to use the different numerical codes is shown in Figure 22 (Barton, 2021).

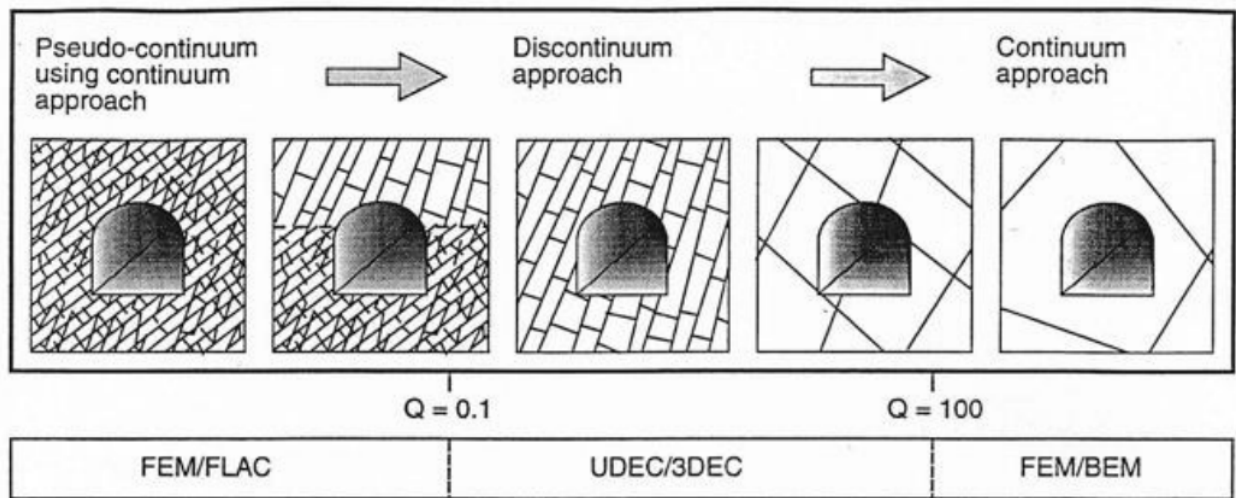


Figure 22: Rough estimation on when the different types of models are suitable. From: Barton (2021).

7.1 Finite element method- FEM

The advantages of the FEM method is that it is easy to understand, easy to model different constitutive behaviour of rock, easy to model complicated geometry and it is currently one of the most popular stress analysis methods in rock mechanics (Lavrov, 2019a). The principles behind the method is the elastic-spring method, in which the spring stiffness and applied load controls most of the results. A given force on the spring yields a given deformation for the nodes based on the spring stiffness. The deformation may also

be effected by boundary conditions, i.e. nodes that are fixed in both or either of the X and Y-direction. The boundary conditions make the system matrices of nodes and springs solvable, and prevents rigid-body motions.

The basic limitation of FEM is that only continuum problems can be modelled, and no rock mass are really continuum. Some modern developments of FEM can attack problems with discontinuities, but the convergence and accuracy of those advanced developments are not always up to expectations (Lavrov, 2019b). This is an area of uncertainty, and the validity of the results from FEM models will be up for discussion. However, some conditions are more continuum than others.

With the application of Discrete Element Models (DEM-models), discontinuities can be modelled with Mohr-Coloumb failure criteria or Barton-Bandis criteria, as is pretty similar to the analytical approach. The joints can further be dry, fluid saturated or coated. A drawback of the DEM-models is that uncertainty and inaccuracy increases when discontinuities are dominating stability, i.e., exactly when using DEM-models are most relevant.

7.2 RS2

RS2, previously Phase 2, is a finite element method numerical program for estimating stresses and deformation in finite element material, developed by RocScience. Being an approximate method, the accuracy of the results is highly dependent on the accuracy of the input parameters. The results will also carry the general limitations and uncertainties of a FEM-model. However, the program is very user friendly and relatively easy to understand and maneuver.

A strength of the program is that the user has several options when it comes to input-parameters such as stress conditions, material definitions and failure criterions. For stress conditions, the user can choose between “gravitaional field stress”, which is suitable for lower overburden, and “constant field stress”, which is more suitable for high overburden where a couple of meters relatively will not impose the field stress much. The user may choose the rock mass deformation modulus according to “Generalized Hoek-Diederichs”, “Simplified Hoek-Diederichs” (both from Hoek and Diederichs (2006)) or “Hoek, Carranza-Torres and Corkum” (from Hoek et al. (2002)). These criteria are reviewed in Section 9. For the failure mechanisms, the user will first choose between elastic or plastic material type. The elastic mode may be sufficient for the purpose of a typical stress-analysis, while the plastic mode also obtains the rock failure and destressing. Further, the user may choose between Mohr-Coulomb, Hoek-Brown, Generalized Hoek-Brown and other failure criteria for the rock mass (Rocscience, n.d.).

8 Introduction to the Ryfylke tunnel project and two weakness zones

The Ryfylke tunnel is a part of the highway 13 Ryfast project in western Norway to establish a mainland connection between Hundvåg and Solbakk, just outside the city of Stavanger, see Figure 23. The tunnel will replace a ferry route of 40 minutes between Stavanger and Tau (NPRA, 2019).



Figure 23: Geographical overview of the Ryfylke tunnel. Modified after Multiconsult (2009).

At completion, the tunnel was the longest and deepest subsea road tunnel in the world, at 14,1km length and reaching 290m depth at its deepest section. The tunnel was constructed as a twin-tube tunnel, with a T8,5 cross section, where the geometrical dimensions are shown in Figure 24. The tunnel was constructed with conventional drilling and blasting, which provides good flexibility with respect to changing geological conditions and widening of the cross section to install heavier rock support.

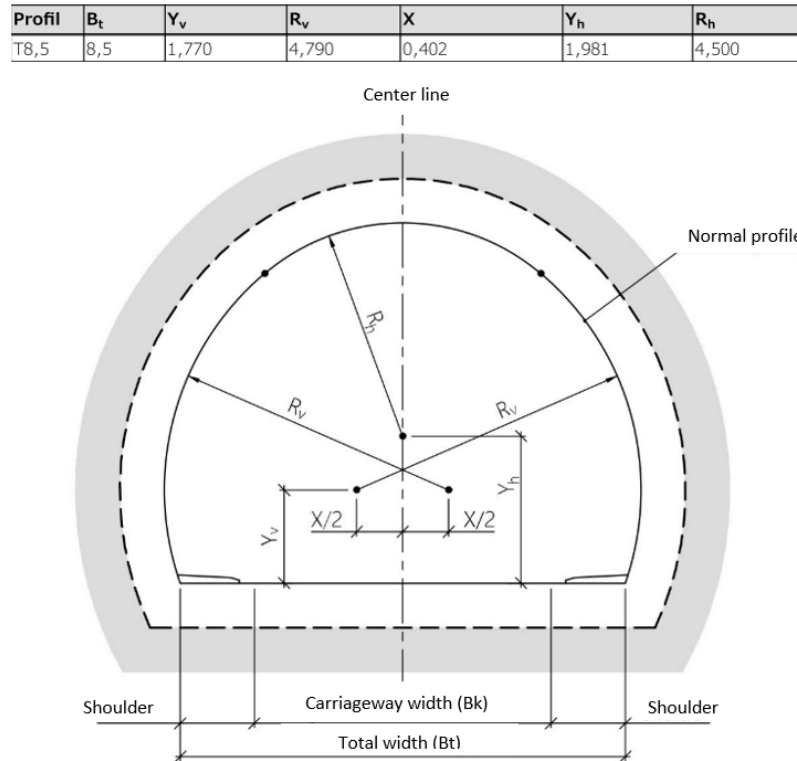


Figure 24: Geometrical dimensions of a T8,5 tunnel profile. Modified after: NPRA (2021).

8.1 Regional Geology

The bedrock geology of this part of western Norway consists of Precambrian indigenous rocks with rocks of the Caledonian sliding deck lying above. The ryfylke tunnel mainly passes through gneisses and phyllites from the Caledonian mountain range formation about 350 million years ago (Multiconsult, 2009; NPRA, 2019). An overview of the regional geology of the area is presented in Figure 25.

Phyllite

Phyllite is a metamorphic rock transformed from clay stone. It is thinly foliated and easily separable along its foliation defined by parallel flakes of mica minerals. It may be described as a weak and schistose rock. Thus, the rock may be subject to plastic deformation if high in-situ stresses are present (Panthi, 2006), and it generally has a low self-bearing capacity.

Experience from the ryfylke tunnel (NPRA, 2019) showed that most of the phyllite had a low quartz content

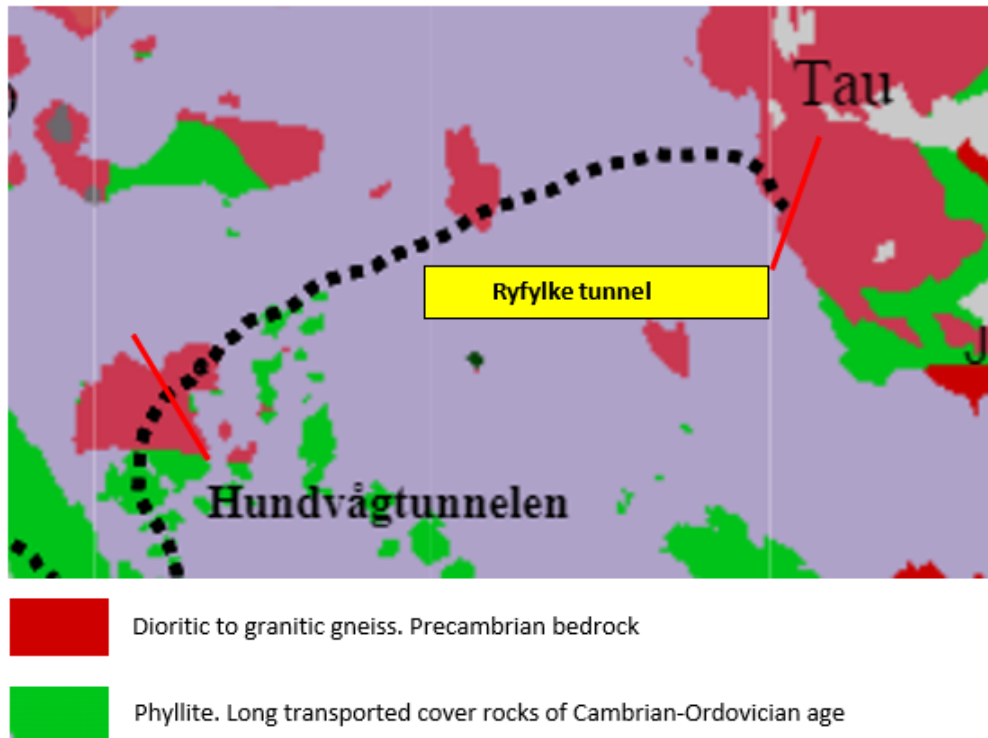


Figure 25: Regional geology of the area of the ryfylke tunnel. Modified after Multiconsult (2009).

and high content of mica, generally decreasing the strength of the rock. The phyllite encountered during tunneling generally had few, random joint sets in addition to the foliation. This made it hard to estimate the number of joint sets with respect to tunnel mapping using the Q-system. Further, it was hard to estimate the strike and dip of the discontinuities (NPRA, 2019).

Gneiss

The gneisses are part of the indigenous Precambrian bedrock. Thus, the rock mass should have relatively high intact strength. Stability problems may be due to weakness/fracture zones or intersecting discontinuities creating sliding blocks. The discontinuities in the gneisses are also often evaluated to be more water-conducting than the discontinuities in the phyllite, due to the nature of the discontinuities. Experience from the Ryfylke tunnel shows that the gneisses come in two main variants. One granitic gneiss with relatively large amount of quartz, and one mica gneiss type. The gneisses encountered usually had 2 joint sets ($J_n = 4$) with a maximum of 3 ($J_n = 9$).

8.2 Geotechnical category

From Torgersen (2021):

“In Eurocode 7 (EC7), a European standard for geotechnical planning and investigation, it is presented a method to categorize geotechnical projects with respect to their complexity and difficulty. The geotechnical

category (GC) is derived from the reliability class and the degree of difficulty, as shown in Table 9.

Table 9: Definition of geotechnical category. Modified after NBG (2011).

Reliability class	Degree of difficulty		
	Low	Medium	High
CC/RC 1	1	1	2
CC/RC 2	1	2	2/3
CC/RC 3	2	2/3	3
CC/RC 4*	*	*	*

* Assessed separately

Reliability in this connection refers to potential personal injury as well as potential economic consequences (NFF, 2018). CC/RC is Consequence Class and Reliability Class, respectively. See EC7 for a more extensive description”.

In the geological pre-construction investigation report from Norconsult (2012), the project is classified as GC3. It was estimated to be a difficult project with complex ground conditions with a great degree of uncertainty, being a subsea tunnel. The ground conditions can only partly be mapped before construction. The degree of difficulty was therefore estimated as ”high”. The consequence class and reliability class was estimated to be CC/RC 3 (Norconsult, 2012). Thus, the investment in pre-construction investigation was relatively high. Geotechnical exploration drilling, refraction seismic surveys on and off shore as well as traditional engineering geological mapping wherever feasible was carried out (Norconsult, 2012).

8.3 Weakness zones at the Ryfylke tunnel

The Ryfylke tunnel lineament was intersected by several weakness zones. Especially two of them caused some stability issues and some tedious construction methods had to be utilized. These two zones will be highlighted further in this section, and used as cases for tunnel stability assessment analysis. Because of confidentiality, the exact location of the zones (tube nr., chainage nr.) will not be specified. The zones will instead be given random chainage numbers, but of course, the length of the zones and the order of the chainage numbers will be the same. Within these weakness zones, the two worst sections with respect to the mapped Q-values will be taken as cases. The chainages of these worst sections are:

- Weakness zone 1: 8437-8463 (26 meters)
- Weakness zone 2: 10629-10651 (22 meters)

8.4 Weakness zone 1

The first weakness zone presented is located entirely in weak phyllite. The phyllite may not have as many distinct joint sets as the gneiss, but it is highly foliated. The discontinuities in the phyllite will typically have low cohesion and friction due to fine material joint fillings, e.g. mica.

The full length of the zone extends from chainage 8416 to 8478 in tube 1, and from chainage 8433 to 8470 in tube 2, see Figure 26. The Q-values, Q-parameters and rock cover for the worst part of the weakness zone ($Q < 1$) is presented in Table 10.

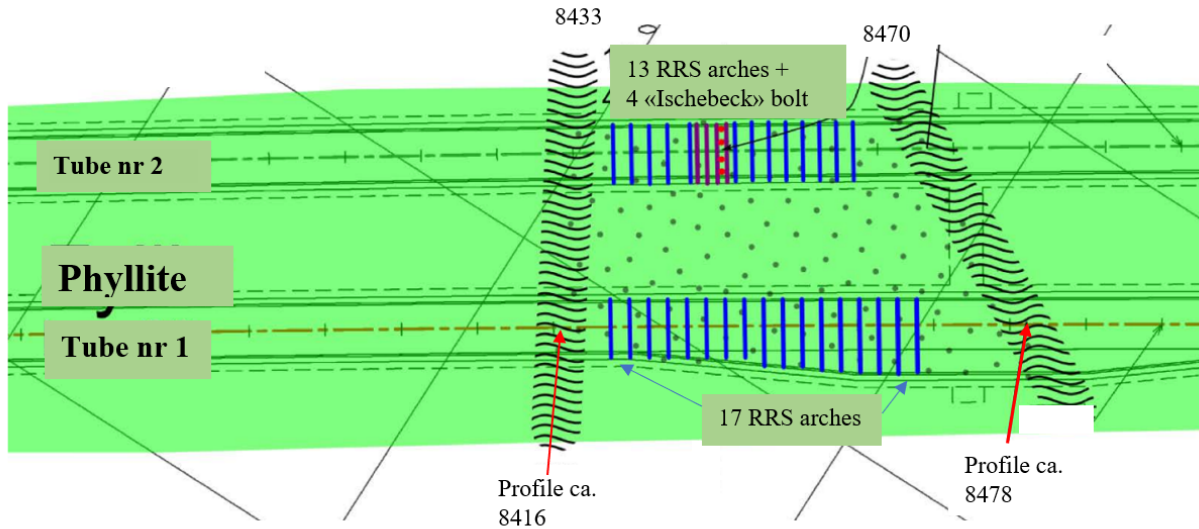


Figure 26: Overview of the first weakness zone located in phyllite. Artificial profile numbers and performed RRS arches included. Modified after: NPRA (2019).

Table 10: Q-values, parameters and rock cover for the worst part of weakness zone 1, tube 2. Q-values and parameters mapped in: NPRA (2019).

Chainage	RQD/Jn	Jr/Ja	Jw/SRF	Q	Rock cover
8437-8441	40/9	1.5/6	0.66/5	0.15	ca 60m
8441-8444	40/9	1.5/6	1.0/5	0.22	ca 61m
8444-8448	45/9	1.5/6	1.0/5	0.25	ca 62m
8448-8452	50/9	1.5/6	1.0/5	0.28	ca 62m
8452-8455	55/9	1.5/5	1.0/5	0.37	ca 63m
8455-8459	55/9	1.5/5	1.0/2.5	0.73	ca 65m
8459-8463	55/9	1.5/4	1.0/2.5	0.92	ca 65m

8.5 Weakness zone 2

The second weakness zone highlighted is mainly located in a transition zone from phyllite to gneiss. It is then affected by the fault from the Precambrian bedrock and the sliding deck. As massive rock, the gneiss will typically be fractured to coarse and blocky material, while the softer phyllite gets more fine material (Nilsen, 2016). The walls are often striated and polished as a result of shear displacement. The main pattern of structural directions often has the same orientation as the joint sets within the structural area due to the stress direction (NBG, 2000).

The full length of the zone extends from chainage number 10472 to 10700, see Figure 27. The Q-values, Q-parameters and rock cover of the worst section is presented in Table 11. To simplify the analysis carried out in the thesis, it is assumed that the rock within the zone is strictly phyllite, as can be seen in Figure 27 is approximately the case. However, the phyllite will still be affected by the adjacent, more competent gneiss, and this fault making up the boundary. The effect of a fault in a weakness zone is very complex to quantify, so this effect will be neglected. Thus, obtained results from stability assessment may deviate somewhat from reality. However, the mapped Q-values should reflect some of the effects of the fault.

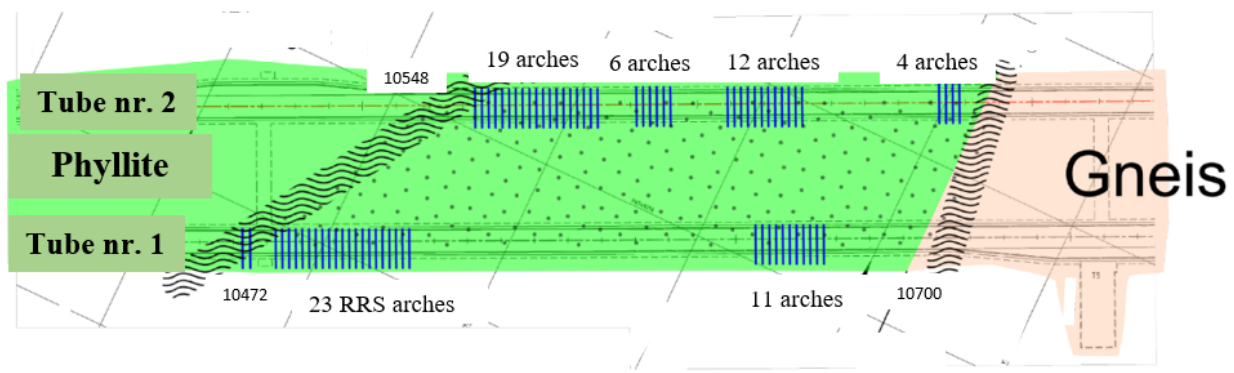


Figure 27: Overview of the second weakness zone located in the transition zone between phyllite and gneiss. Artificial profile numbers and performed RRS arches included. Modified after: NPRA (2019).

8.6 Support methodology and observations during construction

At tunnel face, the weakness zones were relatively heavy supported with spiling bolting c/c 30cm along with 4m radial bolts c/c 1,5m and 15-20cm E1000 shotcrete (NPRA, 2019). The arched RRS was installed considerable distances behind tunnel face. Al-Samarray (2022) informed that in the worst section of weakness zone 2, there was one incident where the face had collapsed up to 2 meters inward within 2 hours when the engineers were away from the tunnel face. Al-Samarray also stated that in some sections, the 15-20cm applied E1000 shotcrete had started to crack before the arched RRS was applied. A photo illustrating the

Table 11: Q-values, parameters and rock cover for the worst part of weakness zone 2, tube 2. Q-values and parameters mapped in: NPRA (2019).

Chainage	RQD/Jn	Jr/Ja	Jw/SRF	Q	Rock cover
10629-10632	35/9	1.5/4	1.0/1.5	0.97	ca 110m
10632-10635	30/9	1.5/4	1.0/1.5	0.83	ca 110m
10635-10638	30/9	1.5/4	1.0/5	0.25	ca 115m
10638-10641	25/9	1.5/4	1.0/5	0.21	ca 115m
10641-10645	20/9	1.5/7	1.0/5	0.095	ca 120m
10645-10648	40/9	1.5/4	1.0/4	0.42	ca 120m
10648-10651	45/9	1.5/4	1.0/4	0.47	ca 120m

poor rock mass quality in weakness zone 2 is given in Figure 28.

Grimstad (2018) states that for a proper dimensioning of rock support, one has to know the induced pressure from the rock mass both immediately and after longer periods of time. Grimstad advises a two-step support methodology for weak rock mass subjected to deforming conditions. He states that the initial controlled deformation should be allowed to happen. Thus, lighter, yieldable support should be installed at tunnel face as the work-support. After the controlled deformation has ceased, heavier, load bearing support should be installed to withstand the secondary, time-dependent deformation. This concept is in relatively good accordance with the support methodology carried out in the Ryfylke tunnel weakness zones. It also has clear similarities to the description of the New Austrian Tunnelling Method (NATM) (NBG, 2000). The concept of secondary, time dependent deformation and support is also in good accordance with the Panthi and Shresta (2018) method, addressed in Section 10. Grimstad further states that for high stress-levels in weak rock, there are no support that can eliminate the tunnel convergence. Early installation of arched RRS or other stiff support will undergo failure due to a massive induced pressure from the converging rock mass if the stresses are high enough. This further backs up the decision to delay the installation of arched RRS in the weakness zones until the face had advanced a considerable distance.

A different question is whether the stress-conditions and rock strength is of such a magnitude that secondary, load-bearing support really is needed to reduce deformation and stop the tunnel from collapsing. This will be addressed in Section 11 and 12.



Figure 28: Photo of the very poor blasted-out rock mass/soil. Photo: Ahmed Al-Samarray.

8.7 Other remarks from the weakness zones

As can be seen from Figure 26 and 27, the areas with the most adverse conditions have been supported by RRS arches, as well as heavy initial support. Contrary to the suggestions from NPRA's support classes shown in table 3, several sections with Q-values over 0.2 still have been supported by RRS arches. Note that almost none of the sections listed in Table 10 and 11 have assigned Q-values lower than 0.2, and these are the sections of tube 2 with the lowest Q-values. This is then decided based on a broader engineering geological evaluation. Further in this thesis, a stability assessment will be carried out to get a better understanding as to e.g. why it was decided to support the tunnel with RRS arches.

Both tunnel sections meets the demand criteria of at least 50m rock cover. It is further mentioned that leakage problems were generally not encountered during tunnel construction (NPRA, 2019). Therefore, leakage is not addressed in this thesis.

9 Assessment of input parameters

Three engineering geological factors which have a direct influence on the stability of tunnels are rock mechanical properties, in-situ stresses and ground waterflow as well as discontinuities, weakness- and fracture zones (Panthi, 2012). When performing a stability analysis, either analytically, empirically or numerically, of course, the input parameters utilized in each method have to reflect the realistic situation as accurately as possible. The best way to decide the input parameters are most often through laboratory or in-situ tests, where one typically finds parameters such as intact rock strength (UCS, σ_{ci}) and the intact modulus (E_i, ν), rock mass strength and modulus (σ_{cm}, E_{rm}) and the in-situ rock stresses ($\sigma_v, \sigma_h etc$). However, no known data of laboratory or field tests are available from the Ryfylke tunnel project. Therefore, in this section, the input-parameters will be estimated by other means.

9.1 Intact rock strength

The assessment of the intact rock strength of the rock types of the two weakness zones presented in Section 8.3 is preferably found by laboratory tests on intact rock specimen. The rock specimen is uniaxially loaded until failure occurs, and the UCS is found. See ISRM (1979) for a detailed description on the suggested method.

In phyllite, which is a naturally anisotropic rock type, the UCS is also dependent on the orientations of the plane of weakness compared to the loading direction (Singh and Goel, 2011). Because of the schistosity, the estimation of the UCS of phyllite carries particular uncertainty. The compressive strength of phyllite from Venezuela studied by Salcedo in 1983 varied with a factor of about 5, depending on the direction of loading, see Figure 29.

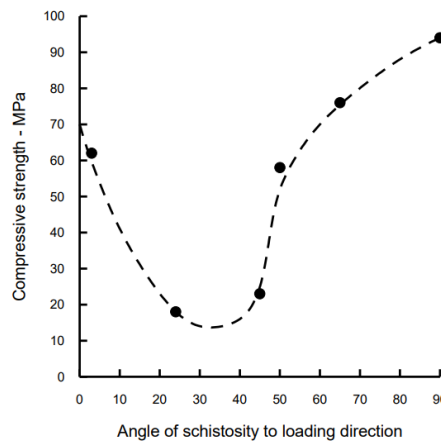


Figure 29: Influence of loading direction to schistosity on compressive strength of Phyllite from Venezuela. Tested by Salcedo (1983), reproduced in Hoek (2006).

Because no rock samples from the Ryfylke tunnel were tested, one will have to give a crude estimation of

the compressive strength of the intact rock by other means. Panthi (2006) found through laboratory testing as aforementioned that the UCS of the “intact” graphitic phyllite from Nepal was 39 MPa. This strength was obtained with loading direction perpendicular to the rock foliation, which gives the highest strength.

Of course, the properties of the Nepali phyllite may deviate somewhat from the phyllite in the Ryfylke tunnel, which is described as mostly mica rich and low in quartz. This should generally make the phyllite weaker than a quartz rich phyllite. However, one can see some UCS intervals and means from different rock types from an outcrop of the Sintef UCS database, see Figure 30. This chart supports the estimation of a phyllite with a UCS of approximately 39 MPa. Thus, this value will be adopted for now for the further stability analysis.

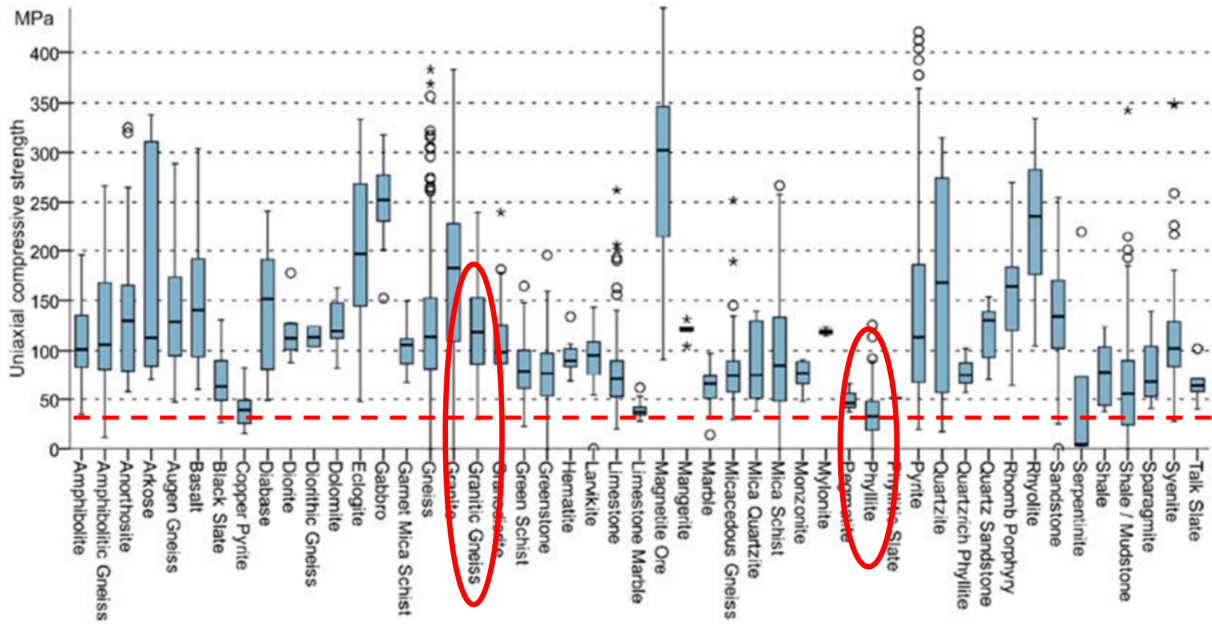


Figure 30: SINTEF database numbers on UCS for different rock types with phyllite and granitic gneiss highlighted. Reproduced from SINTEF in Olsson (2021).

9.2 Intact rock modulus

The intact rock modulus is usually estimated by analyzing the results from laboratory tests. The most significant parameters which describes the intact rock is the Poisson’s ratio ν and the intact deformation modulus E_i .

The intact deformation modulus is defined as the ratio of axial stress change to axial strain produced by the stress change. The intact deformation modulus is usually estimated from the method suggested in ISRM (1979). The tangent deformation modulus is perhaps the most common method. It is generally measured as a fixed percentage of the ultimate strength, usually taken from a level of 50% of the uniaxial compressive strength of the intact rock specimen, see Figure 31. It is important to keep in mind that the degree of moisture may significantly effect the results. Thus, it is of course desirable to replicate the in-situ moisture

conditions as the test is in progress.

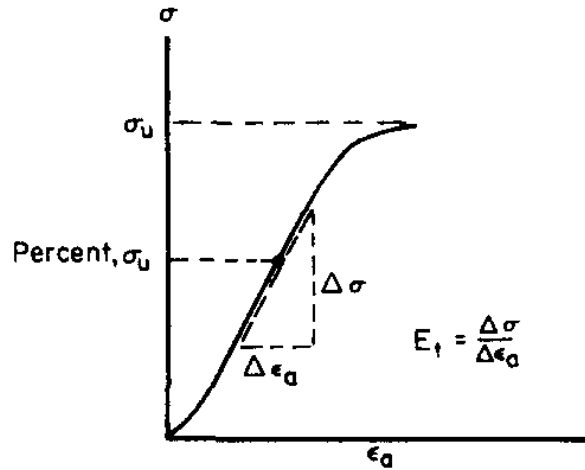


Figure 31: Determination of the Young's modulus (deformation modulus) E of an intact rock specimen by use of the tangent method. From: ISRM (1979).

The Poisson's ratio ν may be calculated as the negative relation between the slope of the axial stress-strain curve to the slope of the diametrical stress-strain curve. The slope of the diametrical curve can also be calculated by e.g. the tangent method. The Poisson's value will be positive since the slope of the diametrical curve will be negative due to the conventions in the procedure (ISRM, 1979).

The author will also here adopt values from Panthi (2006), who derived the respective values from laboratory testing after the suggested ISRM method. The mean Young's modulus obtained on graphitic phyllite from Nepal was 27MPa , while the standard deviation was 2MPa . Poisson's ratio for the graphitic phyllite was found to be 0,10. It is reminded that these are crude estimates for the Ryfylke phyllite, which may deviate in its behaviour.

9.3 Weathering effect on intact rock properties

As a general rule, the weathering process in the rock mass starts from its discontinuities and migrates to the rock minerals (Panthi, 2006). According to Gupta and Rao (2000) there are five main main factors that are important to the contribution of rock weathering; discolouration and staining, change in texture and fabric, disintegration, decomposition and strength reduction. If discontinuity sets become more closely spaced and are open to weathering agents, the degree of weathering increases considerably.

There may be considerable variation in the degree of weathering. ISRM (1978) suggested Table 12 assessing the degree of weathering of the rock mass. The table assesses the variability based on classification into six categories.

Table 12: Weathering classification. From: ISRM (1978).

Term	Description of rock mass conditions	Weathering grade
Fresh rock	No visible sign of rock material weathering; perhaps slight discolouration on major discontinuity surfaces.	I
Slightly weathered	Discolouration indicates weathering of rock material and discontinuity surfaces. All the rock material may be discoloured by weathering and may be somewhat weaker externally than in its fresh condition.	II
Moderately weathered	Less than half of the material is decomposed and/or disintegrated to a soil. Fresh or discoloured rock is present either as a continuou framework or as corestones.	III
Highly weathered	More than half of the rock material is decomposed and/or disintegrated to a soil. Fresh or discoloured rock is present either as a discontinuous framework or as corestones.	IV
Completely weathered	All rock material is decomposed and/or disintegrated to soil. The original mass structure is still largely intact.	V
Residual soil	All the rock material is converted to soil. The mass structure and material fabric are destroyed. There is a large change in volume, but the soil has not been significantly transported	VI

For a case such as the weakness zone in the Ryfylke tunnel, the weathering grade has to be addressed, and it will also contribute to reduce the intact rock strength and modulus (Panthi, 2022b). Figure 32 shows the effect the degree of weathering has on the uniaxial compressive strength reduction. Studying several photos and videos of scaling (without thrusting) of the tunnel face of the Ryfylke tunnel reveals that the exposed phyllite is relatively decomposed and/or disintegrated, as the rock material falls from the face with only a gentle touch from the scaling machine. The author evaluates that these conditions are equivalent to a weathering degree III. Subsequently, the uniaxial compressive strength, σ_{ci} , used as input parameters in the stability assessment is reduced by 50% to 19 MPa.

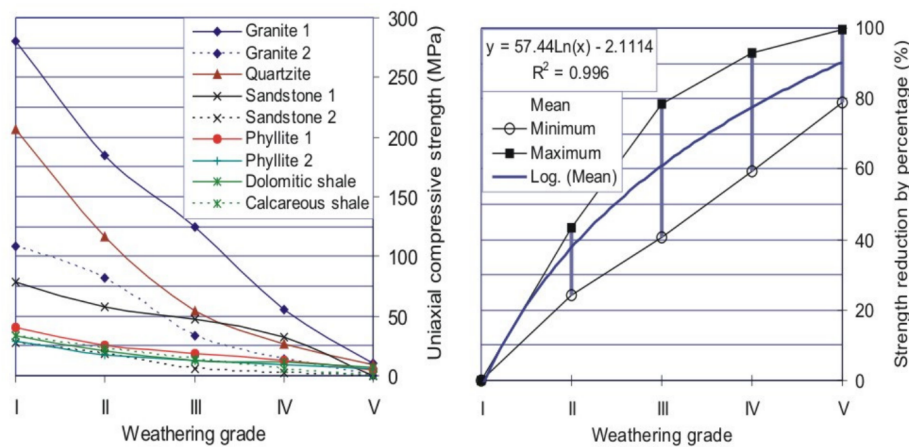


Figure 32: Left: compressive strength of intact rock and Right: strength reduction percentage as a result of the degree of weathering. Reproduced after Gupta and Rao (2000) in Panthi (2006).

It may be tricky to estimate the equivalent reduction of the intact rock modulus E_i without laboratory testing, but it can be stated with some confidence that the reduction of the modulus is roughly equivalent to the reduction of σ_{ci} . Panthi (2006) states that “almost similar trends may be found regarding the elasticity modulus”. Therefore, with weathering effects accounted for, a new intact rock modulus of 13 GPa is obtained.

9.4 GSI

9.4.1 Observational estimation

When obtaining a GSI value from visual observation, one will look at the degree of jointing of the rock mass and the joint surface conditions. The details of the joint surface may be hard to catch up on when examining photographs. It is preferred to observe these conditions in real time during construction. However, in the following subsection, the GSI-values will be visually examined through studying photographs of the tunnel face.

The tunnel sections and corresponding figure numbers are listed in Table 13. The reasoning for GSI estimation can be found in Table 14. Keep in mind that the author has studied more photos than the ones presented here. Also, it should be noticed that the tunnel chainages of the photos are not corresponding exactly to the tunnel chainages listed in Tables 10 and 11. However, this was the listed chainage numbers for the photos the author received from the NPRA. It is unknown whether this is a typing error or that the photos are taken for somewhat different intervals than those where the Q-values and mapping were assigned.

Table 13: Tunnel chainage and corresponding figures.

Tunnel face	8439-8443	8441-8444	8444-8447	8448-8452	8452-8455	8455-8459	8459-8463
Figure(s)	33	34	35	36	37	38	39

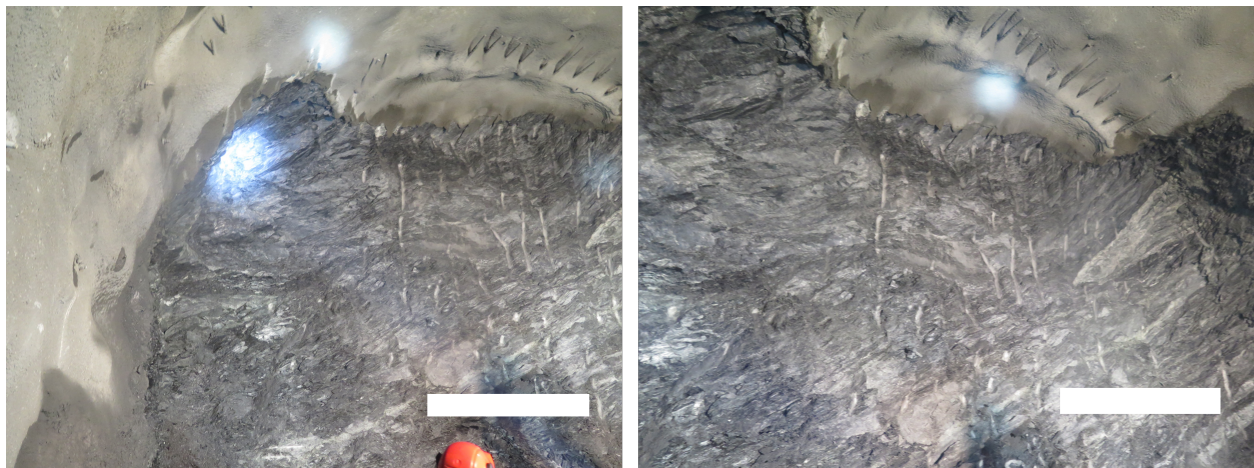


Figure 33: Chainage 8439-8443. Photo: NPRA.

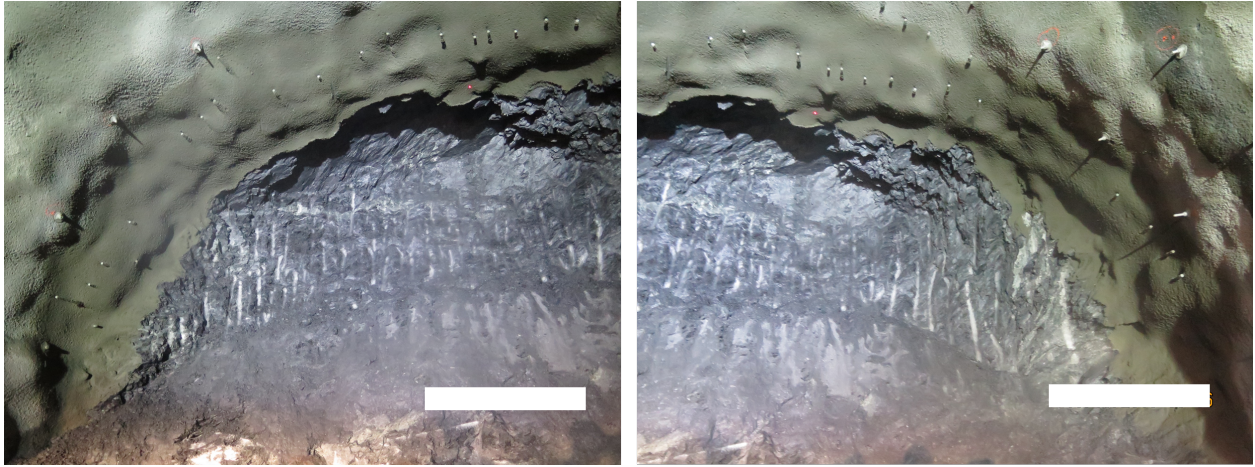


Figure 34: Chainage 8441-8444. Left-middle and middle-right side of tunnel face. Photo: NPRA.

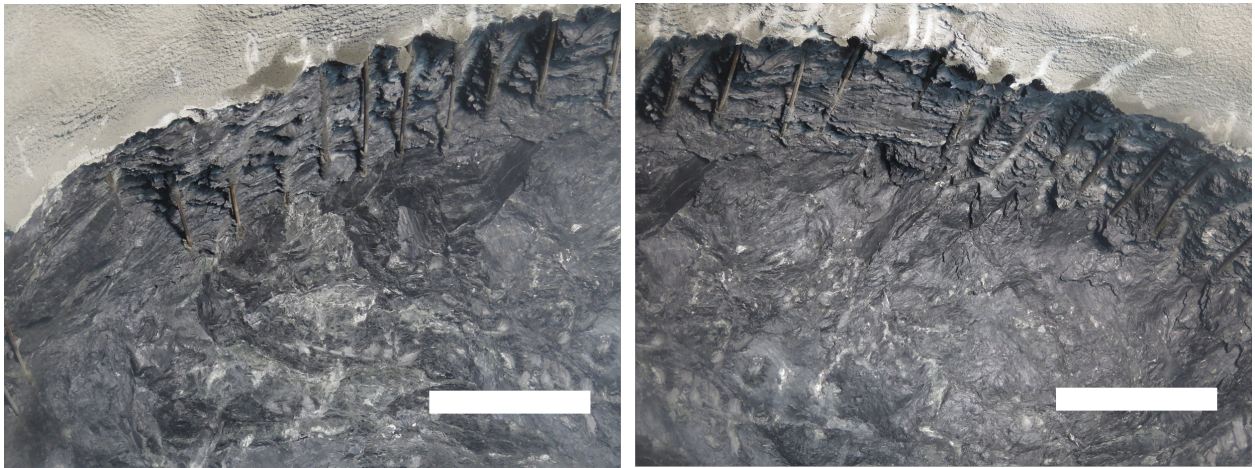


Figure 35: Chainage 8444-8447. Left-middle and middle-right upper part of tunnel face. Photo: NPRA.

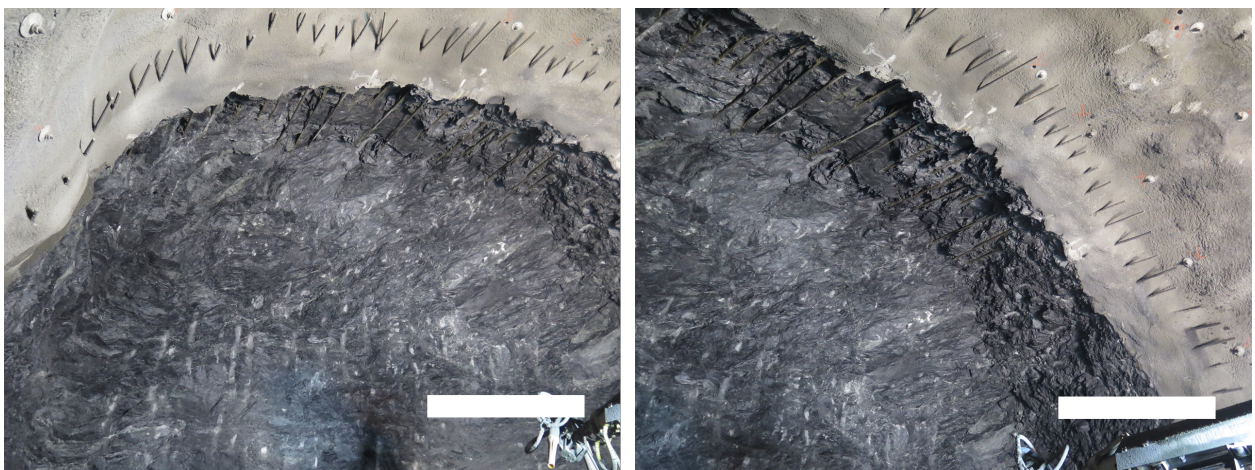


Figure 36: Chainage 8448-8452. Left-middle and upper right side of tunnel face. Photo: NPRA.

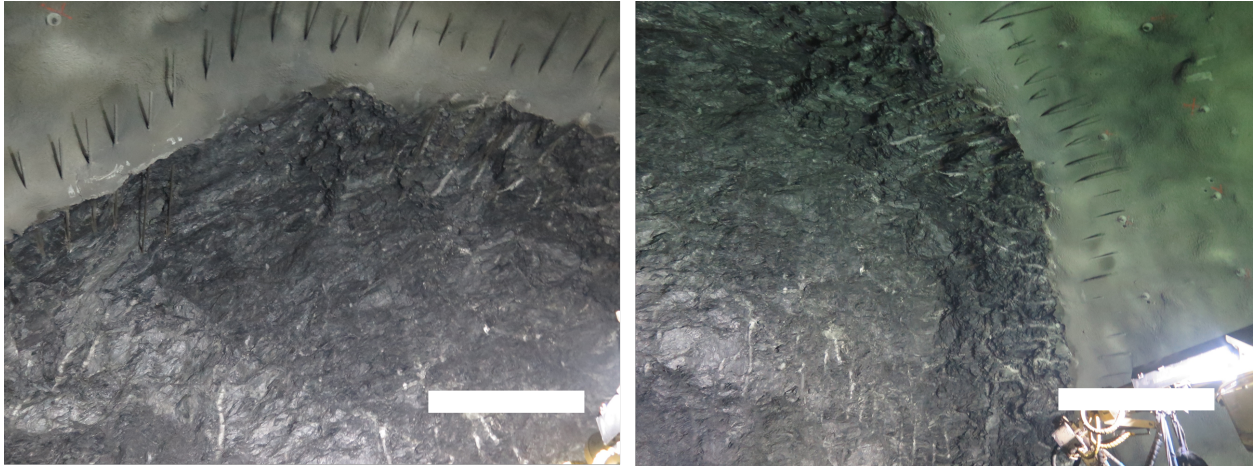


Figure 37: Chainage 8452-8455. Left-middle and right side of tunnel face. Photo: NPRA.

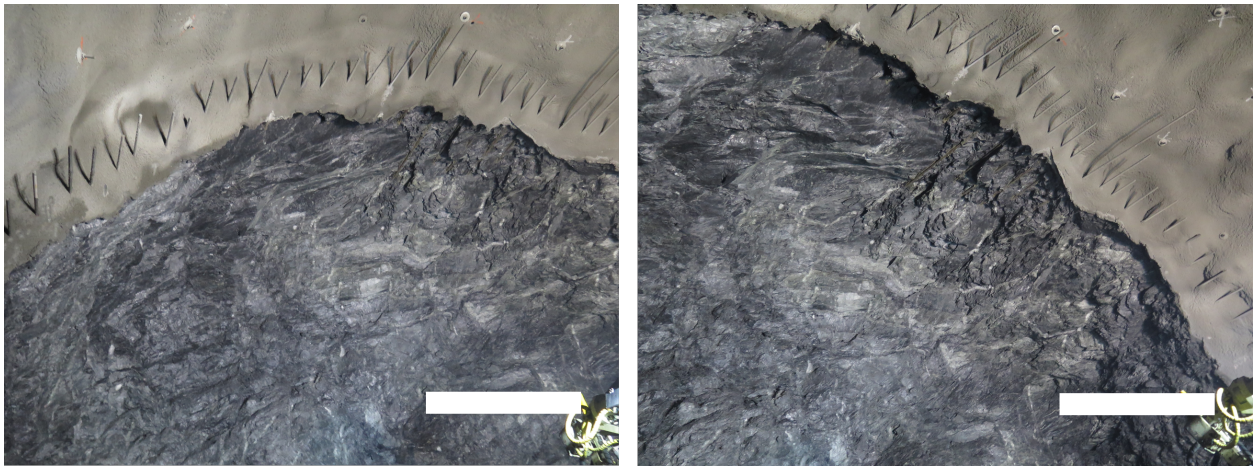


Figure 38: Chainage 8455-8459. Middle-left and right side of tunnel face. Photo: NPRA.

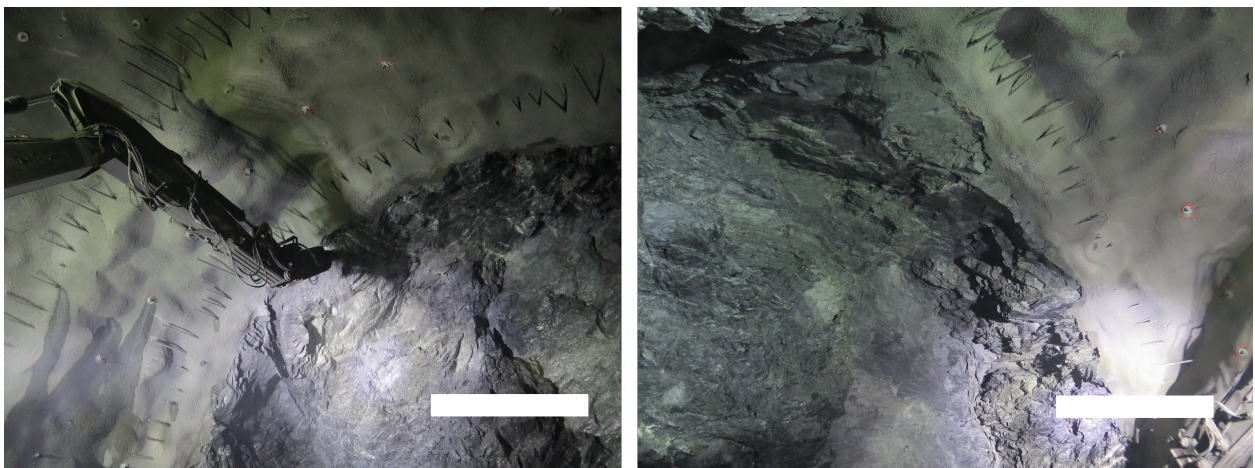


Figure 39: Chainage 8459-8463. Middle-left and right side of tunnel face. Photo: NPRA.

Table 14: Remarks for the observational GSI estimation for weakness zone 1.

Tunnel face	GSI	Remarks for GSI estimation
8437-8441	28	Highly schistouse phyllite in front face. Highly disintegrated in face-walls. Both right and left side. Smooth-slickensided, moderately-highly weathered surface.
8441-8444	30	Highly schistouse phyllite in front face. Moderately disintegrated in face-walls. Smooth-slickensided, moderately-highly weathered surface.
8444-8448	25	Highly schistouse phyllite which appears sheared in front face. Moderately-highly disintegrated in face-walls. Surface appears slickensided and highly weathered and clayey.
8448-8452	28	Highly schistouse phyllite in front face. Less disintegrated in face-walls. Surface appears smooth-slickensided, weathered and clayey.
8452-8455	31	Schistouse phyllite in front face. Less disintegrated in face-walls. Smooth-slickensided, moderately weathered, clayey surface.
8455-8459	33	Schistouse phyllite in front face. Schistouse-disintegrated in face-walls. Smooth, moderately weathered surface.
8459-9463	37	Schistouse phyllite in front face. Schistouse, disturbed face-walls. Smooth, moderately weathered surface.

The observational GSI-values for the Ryfylke tunnel weakness zone 2 are estimated on similar basis as described above. The results from this zone are given in Table 15.

Table 15: Observational GSI-values obtained for weakness zone 2.

Chainage	10629- 10632	10632- 10635	10635- 10638	10638- 10641	10641- 10645	10645- 10648	10648- 10651
GSI	35	33	28	26	25	30	30

9.4.2 Empirical GSI estimation

The estimation of GSI-value based on other rock mass classification systems is discussed in Section 4.3. Barton (1995) proposed the relation between RMR and Q presented in Equation 22 for weak anisotropic rock masses.

$$RMR = 15 \log Q + 50 \quad (22)$$

Utilizing Equation 22, 19 and 21 as well as the Q-parameters presented in Table 10 yields the following rock mass classification values for weakness zone 1 and 2, presented in Table 16 and 17, respectively.

Table 16: Table of conversions from the mapped Q-value in the Ryfylke tunnel weakness zone 1 to RMR and GSI by using empirical relations.

System/ Chainage	Mapped Q-value	RMR (Eq 22) Barton, 1995	GSI (Eq 18) Hoek and Brown, 1997	GSI (Eq 21) Hoek et al., 2013	Mean empirical
8437- 8441	0.15	38	33	30	31.5
8441- 8444	0.22	40	35	30	32.5
8444- 8448	0.25	41	36	33	34.5
8448- 8452	0.28	42	37	35	36
8452- 8455	0.37	44	39	40	39.5
8455- 8459	0.73	48	43	40	41.5
8459- 8463	0.92	49	44	42	43

Table 17: Table of conversions from the mapped Q-value in the Ryfylke tunnel weakness zone 2 to RMR and GSI by using empirical relations.

System/ Chainage	Mapped Q-value	RMR (Eq 22) Barton, 1995	GSI (Eq 18) Hoek and Brown, 1997	GSI (Eq 21) Hoek et al., 2013	Mean empirical
10629- 10632	0.97	50	45	32	38.5
10632- 10635	0.83	49	44	29	36.5
10635- 10638	0.25	41	36	29	32.5
10638- 10641	0.21	40	35	27	31
10641- 10645	0.095	35	30	19	24.5
10645- 10648	0.42	44	39	34	36.5
10648- 10651	0.47	45	40	37	38.5

9.4.3 Correlation and remarks on GSI-values in the Ryfylke phyllite

In the literature from Marinatos and Hoek (2000) it is stated that typical values for “weak schist” (e.g. phyllites), the typical range of GSI values are from 15 to 40, based on their chart. This correlates reasonably well with the GSI values from the Ryfylke tunnel obtained from both empirical and observational approaches. It is important to keep in mind that the GSI and other rock mass classification systems fully or partly based on observations are highly subjective estimations. Two experienced engineering geologists would surely give somewhat different values for the same site, see e.g. Nilsen et al. (2003).

The correlation between the observational and empirical GSI-estimation is shown in Figure 40. It can be seen that the observational estimations are lower than the empirical values throughout the weakness zone. In an attempt to keep a conservative approach, which often is the approach in practice, the observational GSI values are adopted. It should be noted that observational GSI-estimation usually carry an uncertainty of +/- 5-10 GSI.

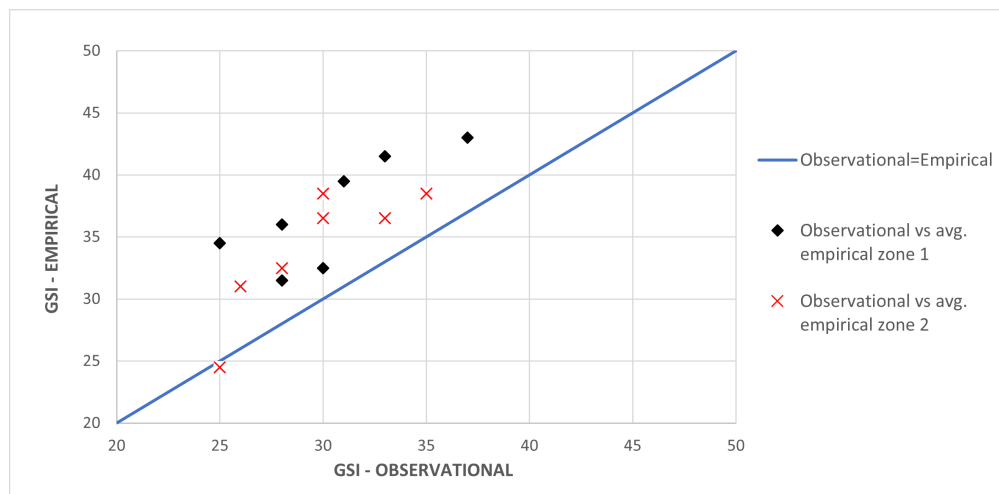


Figure 40: Comparison of observational and empirical estimation of GSI for both Ryfylke tunnel weakness zones.

9.5 In-situ stresses

The section from which the data in Table 10, weakness zone 1, the overburden was 60-65 meters. The vertical stress σ_v can be calculated by Equation 6. Considering a mean rock cover of the area, 62.5 meters, and assuming the overburden is strictly phyllite with a specific weight of $\gamma = 0.027MN/m^3$. This gives a vertical gravitational stress of $\sigma_v = 1.7MPa$.

For weakness zone 2, the overburden of the zone varies from 110-120 meters. Considering a mean rock cover of the area of 115 meters, and assuming the overlying rock is strictly phyllite, the vertical gravitational stress is $\sigma_v = 3.1 MPa$. This stress magnitude is 45% higher than that of weakness zone 1.

The horizontal stress is much more difficult to estimate without in-situ testing, as it typically has more

components than the vertical stress. The horizontal stress is comprised of the gravitationally induced horizontal stress, Equation 7, the stress from tectonic movement, topographic influence and de-glaciation effects. In a simplified case where several stability-assessment methods, e.g. the convergence-confinement method (CCM), see Carranza-Torres and Fairhurst (2000) can be applied, one may assume isostatic stress conditions, i.e. $\sigma_h = \sigma_v$. With the isostatic in situ stress P_o , several solutions to the convergence-confinement method can be implemented, for example that by Vlachopoulos and Diederichs (2009) and Duncan Fama (1993). Note that this is only a simplified estimate to make the solution of the mentioned analytical methods possible. The estimate may deviate from the real horizontal stress, which has to be found by in-situ measurements. Such measurements have not been carried out in this case.

To estimate the influence of in-situ stress anisotropy, such as that carried out in the analysis by Panthi and Shresta (2018), estimations of horizontal stresses that are not equal to the vertical stress needs to be done. The horizontal to vertical stress ratio k can be estimated crudely from Equation 23, based on Sheory (1994).

$$k = 0.25 + 7E \left(0.001 + \frac{1}{H} \right) \quad (23)$$

Where H is the depth below surface and E is the average deformation modulus of the upper part of the earth's crust measured in a horizontal direction. This is important due to the differences in deformation modulus with different directions of measurement in sedimentary and schistouse rock. The solution is reproduced graphically in Hoek (2006), where k can be estimated from Figure 8.

The deformation modulus of the intact, weathered phyllite is described previously to be 13 GPa. Utilizing this value and the relation given in Eq. 23 yields a stress anisotropy value k of 1,8 for weakness zone 1 and 1,1 for weakness zone 2. These values will then be used as the input parameter in the Panthi and Shresta (2018) approach for determining tunnel closure, as well as the RS2 numerical modelling, see Section 10.

9.6 Rock mass strength

In these sub-sections, some estimations of rock mass strengths will be presented, and the results with the given in-put parameters of this thesis will be reviewed and discussed. Keep in mind that there are numerous of other estimations for rock mass strength that is not included in this thesis. Also, when on a real tunnelling project, the in-put parameters should be as accurate as possible, and preferably measured in laboratory or in-situ.

9.6.1 Hoek et al. (2002) rock mass strength

To estimate the rock mass strength by means of the Hoek-Brown failure criteria for rock masses, two basic parameters firstly need to be estimated. These are the intact uniaxial compressive strength and the material constant m_i . The intact uniaxial compressive strength is already accounted for, and estimated to be 19 MPa for the western Norwegian phyllite, with weathering effects accounted for. To determine the m_i for

the phyllite, the estimate in the ' m_i -chart' (see in e.g. Marinos and Hoek (2000)) for different rock types is used directly due to the lack of laboratory testing. This estimation is $m_i = 7 \pm 3$ for phyllites. The mean value of 7 is adopted. Note that the values of the foliated metamorphic rocks in the chart is tested normal to the bedding, and it is stated that the value of m_i may be significantly different if failure occurs along a weakness plane (Marinos and Hoek, 2000). Of course, the phyllites tested for the basis of the chart may also differ from the western Norwegian phyllites.

The disturbance factor D is also a factor that needs to be estimated. It is pretty hard for the author, who were not present during construction, to estimate. In a technical report by NFF (2012), it is highlighted that in Norwegian tunnelling, it is relatively little focus on achieving a smooth blasted profile. The profile may also be more disturbed due to the extensive use of the powerful Slurry-explosives in Norway (Panthi, 2022c). Due to this information, along with the chart presented in Appendix A, a disturbance factor of $D = 0.5$ is adopted.

The 'unconfined compressive strength' of the rock mass according to the Hoek-Brown criteria is then found by inserting $\sigma'_3 = 0$ in Equation 2, obtaining $\sigma_{cm} = \sigma_{ci} \times S^a$. The results are dependent on the GSI value.

The 'unconfined compressive strength' is found to be much lower than both the Panthi (2006) and Barton (2002) estimates for rock mass strength, and it is evaluated that these results are not comparable. However, Hoek et al. (2002) also proposed a relation for estimating 'global rock mass strength', given by Equation 24. This relation is inspired by the traditional Mohr-Coulomb failure criteria based on a cohesion and friction angle value. It is assumed that this estimation is more relevant and comparable for this case.

$$\sigma_{cm} = \sigma_{ci} \times \frac{(m_b + 4s - a(m_b - 8s))(m_b/4 + s)^{a-1}}{2(1+a)(2+a)} \quad (24)$$

9.6.2 Hoek and Marinos (2000) rock mass strength

Hoek and Marinos (2000) presented, along with their approach for tunnel squeezing prediction (see Section 10.1), an empirical equation for calculating the rock mass strength, given in Equation 25.

$$\sigma_{cm} = (0.0034m_i^{0.8})\sigma_{ci} \{1.029 + 0.025e^{-0.1m_i}\}^{GSI} \quad (25)$$

This relation is not as commonly used as the Hoek et al. (2002) estimate, and it can be noticed that this was before the disturbance factor D was introduced. However, it can be seen in the rock mass strength results section that these estimates are very identical.

9.6.3 Panthi (2006) rock mass strength

The Panthi (2006) estimation for rock mass strength is defined by Equation 26. It is based on an analysis of the correlation between rock mass strength and intact rock strength. Panthi (2006) states that the

correlation may be used for an approximate estimation of the ranges of rock mass strength for highly schistose, foliated, thinly bedded metamorphic or sedimented rock with low compressive strength. This description is in good correlation with the phyllite of the Ryfylke tunnel. The estimate is only dependent on the reliable intact unconfined compressive strength parameter found by laboratory testing, whereas the Hoek-Brown rock mass strength criteria is effectively dependent on the unconfined compressive strength, GSI, intact material constant M_i and the disturbance factor D . It is evident that the application of the Panthi (2006) criterion is simple, and the relation excludes subjective parameters. The relation locates in between Barton (2002) estimation and Hoek et al. (2002) conservative estimation of rock mass strength, as can be seen in Figure 41.

$$\sigma_{cm} = \frac{\sigma_{ci}^{1.50}}{60} \quad (26)$$

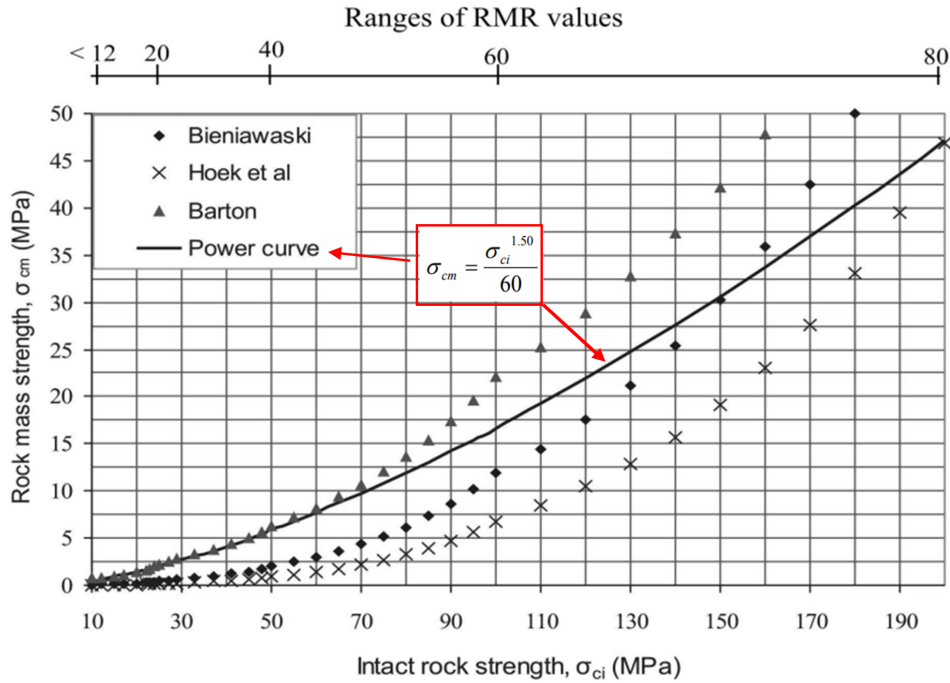


Figure 41: Correlation between rock mass strength σ_{cm} and intact rock strength σ_{ci} . Modified after: Panthi (2006).

The relation yields that for a rock mass comprised of weathered phyllite with an intact compressive strength of 19 MPa, the rock mass unconfined compressive strength is 1.38 MPa. As the intact compressive strength is assumed constant along the weakness zone section, the resulting rock mass strength will also be constant. This separates the Panthi (2006) estimate from the others, which are dependent on varying rock mass classification values.

9.6.4 Barton (2002) rock mass strength

Barton (2002) proposed the relation given in Equation 27 for estimating the rock mass strength. Here, Q_c is the normalized Q-value, i.e. $Q \times \frac{\sigma_{ci}}{100}$. Barton also states that in this Q-calculation, the traditional RQD value is substituted by RQD_0 , which gives the RQD-value in the same orientation as the tunnelling direction. γ is the weight of the overlying rock material in tons per cubic meter, and provides some additional sensitivity to reduced or increased porosity (Barton, 2002). For this to be true, however, the density of rock should be measured in laboratory, and not adopted from empirical tables. It is not clear for the author whether the RQD estimations from the Ryfylke tunnel is adjusted to have the same orientation as the tunnelling direction or not. It is assumed here that the RQD is not adjusted. Thus, this must be taken into consideration as an uncertainty and weakness for utilizing the Barton estimate for rock mass strength in this case.

$$\sigma_{cm} = 5\gamma Q_c^{1/3} = 5\gamma \left(Q \times \frac{\sigma_{ci}}{100} \right)^{1/3} \quad (27)$$

9.6.5 Rock mass strength results and comparison

The summarized results for the two weakness zones are presented in Figure 42 and 43. Input values for the derivation of the rock mass strength can be seen in Tables 18 and 19.

It can be seen that Barton (2002) estimate for rock mass strength is by far the most optimistic. Based on the comparison evident here, it may be argued that this estimate is a little too risky to obtain when predicting rock mass deformation and stability. Panthi (2006) estimate seem reasonable. It fits in well between Barton and the more conservative Hoek (with others) estimate. It can be noted that both Barton and Hoek estimates are dependant and relatively sensitive to the values of their own respective developed classification systems, Q and GSI. It is evident that the Barton-estimate is more sensitive to varying Q-values than the Hoek estimates are for GSI-values, even though the Q system reaches higher orders of magnitude for the different input-parameters (Barton, 2002). Rock mass strength sensitivity with respect to the Q-value for Barton estimate is visualized in Figure 44.

The Panthi approach on the other hand, is, based on Equation 26 only dependent on the intact rock strength, and not on traditional rock mass classification. However, this is not entirely true, as Panthi (2006) states in his doctoral thesis that the relation is developed with highly schistous, thinly bedded rock mass in mind. Thus, a brief description of the rock mass conditions is also given here.

Hoek-Marinos and Hoek et al. estimate are almost identical. It may be argued, based on the different estimates, that for the lower GSI values (and with $D=0.5$ and $m_i=7$), their estimate underestimate the strength of the rock mass. These are very conservative estimates. However, when the GSI-values exceed 37, the Hoek (with others) estimates also exceeds the Panthi (2006) estimate in this case.

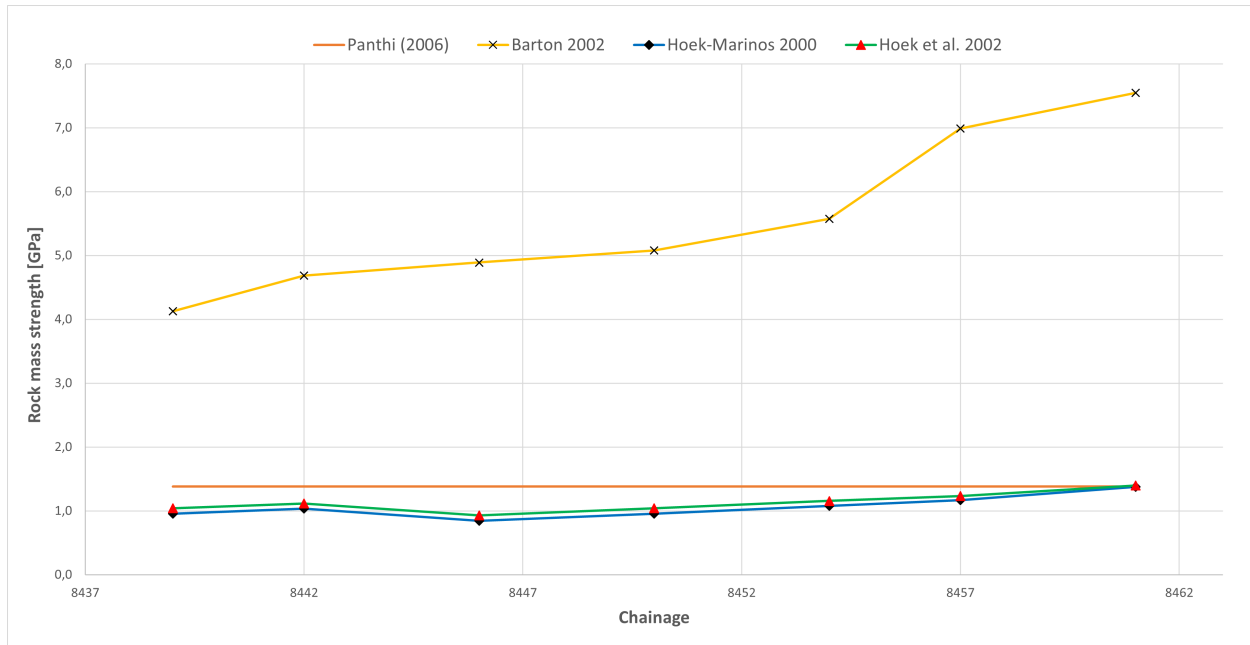


Figure 42: Rock mass strength for weakness zone 1 in the Ryfylke tunnel obtained from various estimates.

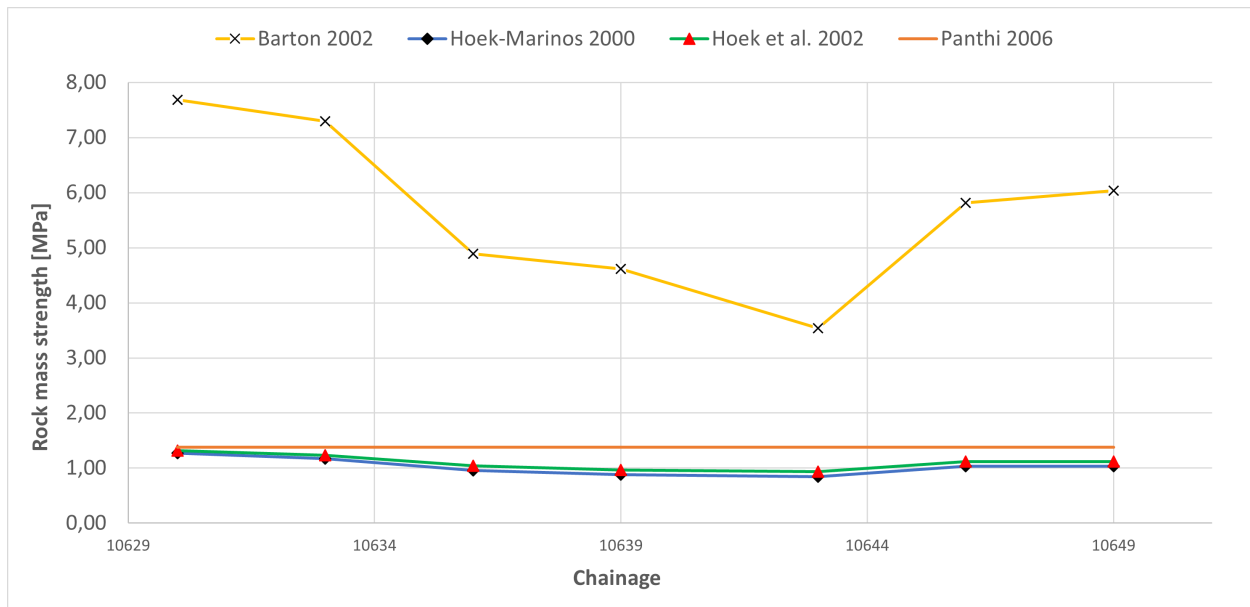


Figure 43: Rock mass strength for weakness zone 2 in the Ryfylke tunnel obtained from various estimates.

By utilizing more than one estimate for the rock mass strength, one may get an idea of the range of the rock mass strength. This is valuable information. The ranges may be used in statistical software such as @Risk to study the probability of different outcomes. The range of values may also be used as different input parameters in numerical software, where one relatively quickly may study the effect of various rock mass strength. If one has available data on tunnel deformation measurements, back calculations and calibrations

Table 18: Summary of the estimation of rock mass strength from chainage 8439-8463.

	Chainage	8437-8441	8441-8444	8444-8448	8448-8452	8452-8455	8455-8459	8459-8463
	GSI		28	30	25	28	31	33
Q		0,15	0,22	0,25	0,28	0,37	0,73	0,92
m.i		7	7	7	7	7	7	7
D		0,5	0,5	0,5	0,5	0,5	0,5	0,5
Sigma.ci		19	19	19	19	19	19	19
a		0,526	0,522	0,531	0,526	0,521	0,518	0,514
s		6,77E-05	8,84E-05	4,54E-05	6,77E-05	1,01E-04	1,32E-04	2,25E-04
m.b		0,227	0,250	0,197	0,227	0,262	0,288	0,349
Hoek et al. 2002, Eq 24		1,04	1,12	0,93	1,04	1,16	1,23	1,40
Panthi 2006, Eq 26		1,38	1,38	1,38	1,38	1,38	1,38	1,38
Hoek-Marinos 2000, Eq 25		0,95	1,04	0,85	0,95	1,08	1,17	1,38
Barton 2002, Eq 27		4,12	4,69	4,89	5,08	5,57	6,99	7,55

Table 19: Summary of the estimation of rock mass strength from chainage 10629-10632.

	Chainage	10629-10632	10632-10635	10635-10638	10638-10641	10641-10645	10645-10648	10648-10651
	GSI		35	33	28	26	25	30
Q-value		0,97	0,83	0,25	0,21	0,095	0,42	0,47
M.i		7	7	7	7	7	7	7
D		0,5	0,5	0,5	0,5	0,5	0,5	0,5
Sigma.ci		19	19	19	19	19	19	19
a		0,516	0,518	0,526	0,529	0,531	0,522	0,522
s		1,72E-04	1,32E-04	6,77E-05	5,19E-05	4,54E-05	8,84E-05	8,84E-05
m.b		0,317	0,288	0,227	0,206	0,197	0,250	0,250
Hoek et al. 2002		1,32	1,23	1,04	0,97	0,93	1,12	1,12
Hoek-Marinos 2000		1,27	1,17	0,95	0,88	0,85	1,04	1,04
Barton 2002		7,68	7,29	4,89	4,61	3,54	5,81	6,03
Panthi 2006		1,38	1,38	1,38	1,38	1,38	1,38	1,38

may be carried out to decide on the more accurate and suitable estimate. Even new rock mass strength estimates may be proposed.

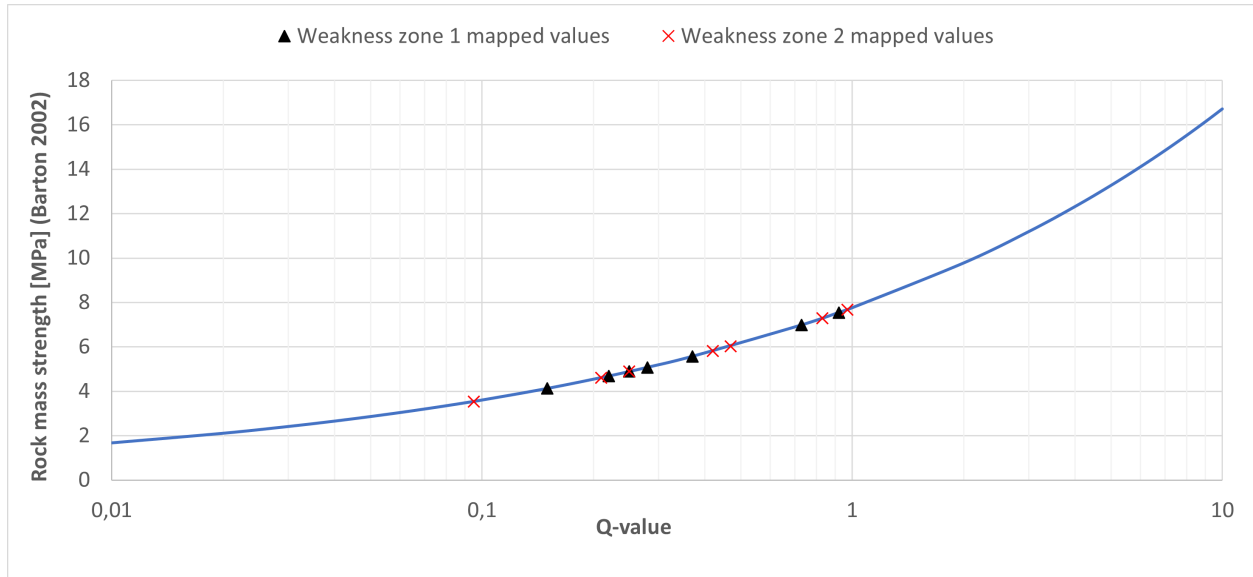


Figure 44: Rock mass strength sensitivity with respect to the Q-value for Barton (2002) estimate.

9.7 Rock mass deformation modulus

One of the main applications for the rock mass deformation modulus today is its use as an input parameter in numerical modelling. It is preferred to carry out field tests to estimate rock mass properties. However, all direct tests such as plate-bearing, dilation-test or hydraulic chamber are time-consuming and imply notable cost and operation difficulties (NBS, 2000). Furthermore, the direct measurements may differ from one another by as much as 100%. One volume of the rock mass will also naturally differ from another volume.

In this section, the rock mass deformation modulus will be estimated for the Ryfylke rock mass by means of empirical approaches. The results will be compared and discussed. There are several empirical approaches developed for this purpose, but the ones reviewed in this section are Hoek and Diederichs (2006) approach, Panthi (2006) approach and Barton (2002).

9.7.1 Hoek and Diederichs (2006) rock mass deformation modulus

To estimate the deformation of a rock mass, Hoek and Diederichs (2006) presented a relation which has gained wide acceptance since. Based on analysis of measured in-situ deformations of several tunnels in China and Taiwan, a best fit equation was derived from the data points, leading to the generalized Hoek-Diederichs Equation 28:

$$E_{rm} = E_i \left(0.02 + \frac{1 - D/2}{1 + e^{((60+15D-GSI)/11)}} \right) \quad (28)$$

where E_i is the deformation modulus of intact rock. The correlation is based on approximately 496 in-situ tests. If measurements of the intact modulus are not obtainable, it is possible to estimate the intact modulus from Equation 29, based on Palmström and Singh (2001) and Deere (1968). Then, the simplified Hoek-Diederichs equation may be utilized, presented in Equation 30.

$$E_i = MR\sigma_{ci} \quad (29)$$

$$E_{rm} = 100,000 \left(0.02 + \frac{1 - D/2}{1 + e^{((75+25D-GSI)/11)}} \right) \quad (30)$$

A critique of the rock mass modulus estimations presented above is that they ignore the depth and stress level factor (Barton, 2021). In practice, it is common that the rock in the surface and at shallow depth is more disturbed by discontinuities and weathering. Accordingly, the rock mass stiffness will logically increase with increased depth.

9.7.2 Panthi (2006) deformation modulus and shear modulus

Panthi (2006) proposed an estimation of the rock mass deformation modulus which is only dependent on the deformation modulus of intact rock E_i , and the compressive strength of intact rock σ_{ci} . The relation is given in Equation 31. Substituting σ_{cm} for the relation given in Equation 26, yields Equation 32:

$$E_{rm} = E_i \times \left(\frac{\sigma_{cm}}{\sigma_{ci}} \right) \quad (31)$$

$$E_{rm} = \frac{1}{60} \times E_{ci} \times \sigma_{ci}^{0.5} \quad (32)$$

During the early design stages of tunnelling projects, the rock mass classifications are usually based on surface observations, which makes them relatively unreliable for the actual conditions at depth. On the other hand, it is more common to collect rock samples for laboratory testing during the early stages (Panthi, 2006). Here, the deformation modulus and rock strength are estimated for the intact rock samples. Therefore, it may be purposeful and advantageous to have an empirical rock mass modulus estimation which does not require an unreliable, subjective rock mass classification value, but rather reliable laboratory-tested parameters. Panthi (2006) further stated that Equation 32 is especially applicable if one is dealing with schistose, foliated and bedded rocks with low unconfined compressive strength, which indeed is the case in the Ryfylke phyllite.

9.7.3 Barton (2002) deformation modulus

The Barton (2002) approach gives a rock mass modulus estimation based on the Q-value and the intact rock strength (i.e. the normalized Q-value). Barton proposed the relation given in Equation 33 for the estimation of rock mass deformation modulus. It can be noted that this estimation is independent of the intact rock modulus. Thus, it may seem like this relation is more suitable for massive, blocky rock mass with competent intact rock. The Q-value neither takes intact rock modulus directly into account. Therefore, this relation will be less suitable for the “homogeneous-like”, weak rock conditions which is attempted to be recreated here.

$$E_{rm} = 10 \times \left(\frac{Q \times \sigma_{ci}}{100} \right)^{1/3} = 10 \times Q_c^{1/3} \quad (33)$$

It can be noted that this estimation is independent of the intact rock modulus. Thus, it may seem like this relation is more suitable for massive, blocky rock mass with competent intact rock. The Q-value neither takes intact rock modulus directly into account. Therefore, this relation will be less suitable for the “homogeneous-like”, weak rock conditions which is attempted to be recreated here. This is supported by the large deviation of results in the upcoming section, which shows that the Barton (2002) approach may overestimate the rock mass strength and modulus if applied to the conditions dealt with in the Ryfylke tunnel weakness zones.

9.7.4 Rock mass deformation modulus results and comparison

The rock mass deformation modulus for the tunnel section of weakness zone 1 and 2 can be seen in Tables 20 and 21, and Figures 45 and 46. The Hoek and Diederichs (2006) approach for weakness zone 1 is plotted with the lowest GSI values (observational values) and the highest GSI values (empirical relation values) for studying of the GSI-sensitivity. For the second weakness zone, only the observational values are used.

Corresponding to the rock mass strength estimation, the deformation modulus estimate proposed by Hoek (with others) gives the most conservative estimate. It may again be argued that these approaches underestimate the competence of the rock mass, based on the comparison with other approaches. It should also be noted that the rock mass deformation modulus proposed by Hoek and Diederichs (2006) is highly sensitive for varying GSI values. This is, in the authors opinion, very much unfortunate because the GSI estimation carries a high degree of uncertainty and subjectivity. A GSI reduction from e.g. 43 to 33, which really is within the range of the GSI uncertainty, reduces the rock mass modulus by 46%. The Hoek-Diederichs approach' sensitivity with respect to GSI is given in Figure 47. It can be seen that for GSI-values exceeding 45-50, the rock mass deformation modulus growth rate is even higher.

Table 20: Input parameters and results from the three estimates for rock mass deformation modulus for the Ryfylke tunnel weakness zone 1.

	Chainage						
	8437-8441	8441-8444	8444-8448	8448-8452	8452-8455	8455-8459	8459-8463
GSI (low)	28	30	25	28	31	33	37
GSI (high)	33	35	36	37	40	43	44
Q-value	0,15	0,22	0,25	0,28	0,37	0,73	0,92
D	0,5	0,5	0,5	0,5	0,5	0,5	0,5
σ_{ci} [MPa]	19	19	19	19	19	19	19
E_i [GPa]	13	13	13	13	13	13	13
H-D 2006 (low GSI), Eq 28	0,52	0,57	0,46	0,52	0,60	0,67	0,83
H-D 2006 (high GSI), Eq 28	0,67	0,74	0,79	0,83	1,00	1,21	1,29
Panthi 2006, Eq 32	0,94	0,94	0,94	0,94	0,94	0,94	0,94
Barton 2002, Eq 33	3,05	3,47	3,62	3,76	4,13	5,18	5,59

Again, the Panthi (2006) estimate does not consider observational factors or changes in the rock mass, other than the intact rock strength and intact deformation modulus. This may be questioned. However, the Panthi estimate sits in well between the two other estimates. Lastly, Barton (2002) is the most “optimistic” estimate, giving very high values compared to the two other estimates. It gives a rock mass modulus of 4-5 times higher than the most conservative Hoek estimate. Even though there are relatively big differences from one approach to another, these estimates provides perhaps a realistic range of rock mass deformation modulus (assuming realistic input parameters) for the section, which would not have been obtained using only one estimate. This range may be utilized in numerical modelling for a simple observation of the effect of the rock mass modulus has on tunnel deformation and convergence.

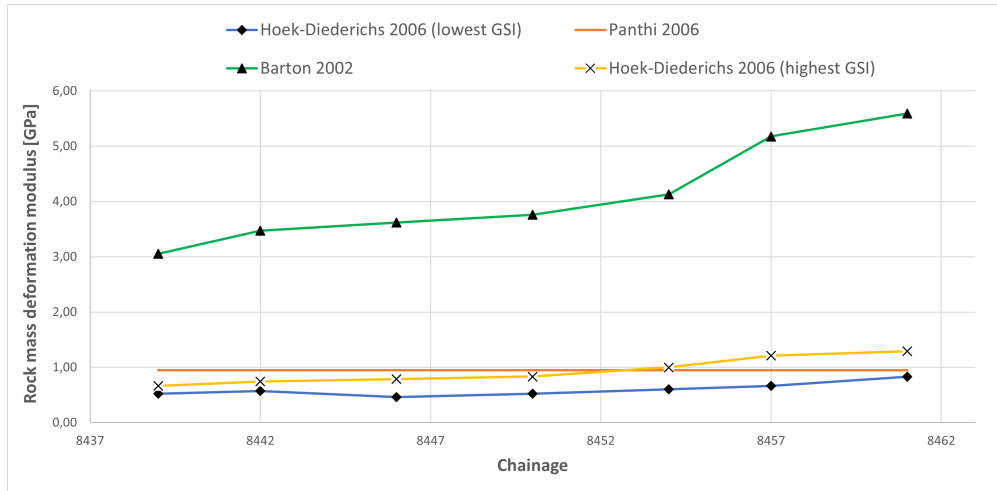


Figure 45: Rock mass modulus obtained for the Ryfylke weakness zone 1 with various estimates.

Table 21: Input parameters and results from the three estimates for rock mass deformation modulus for the Ryfylke tunnel weakness zone 2.

	Chainage							
	10629-10632	10632-10635	10635-10638	10638-10641	10641-10645	10645-10648	10648-10651	
GSI observational	35	33	28	26	25	30	30	
Q-value	0,97	0,83	0,25	0,21	0,095	0,42	0,47	
D	0,5	0,5	0,5	0,5	0,5	0,5	0,5	
σ_{ci} [MPa]	19	19	19	19	19	19	19	
E_i [Gpa]	13	13	13	13	13	13	13	
H-D 2006 (obs. GSI)	0,74	0,67	0,52	0,48	0,46	0,57	0,57	
Panthi 2006	0,94	0,94	0,94	0,94	0,94	0,94	0,94	
Barton 2002	5,69	5,40	3,62	3,42	2,62	4,31	4,47	

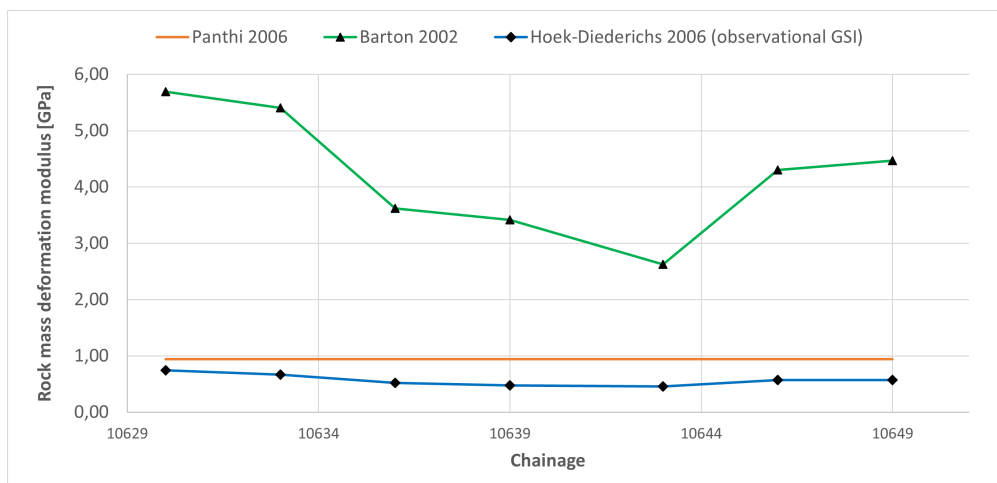


Figure 46: Rock mass modulus obtained for the Ryfylke weakness zone 2 with various estimates. Only observational GSI used.

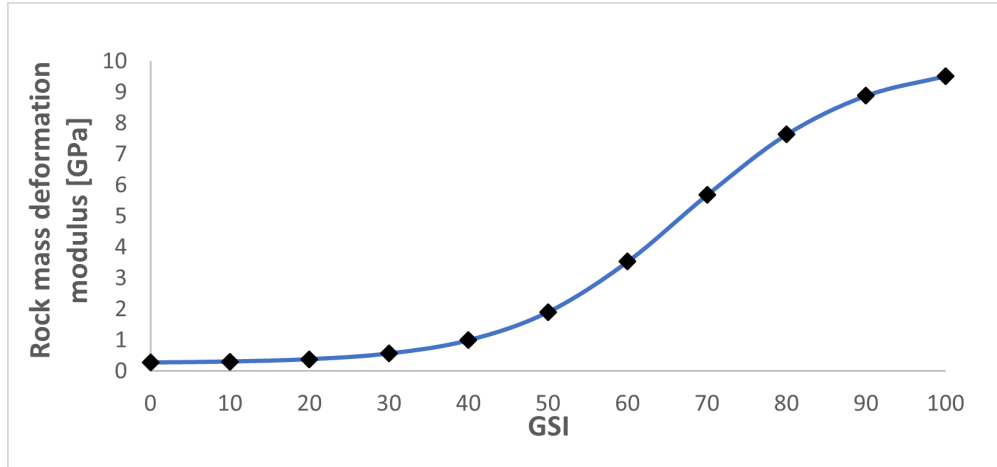


Figure 47: Hoek-Diederichs approach to rock mass modulus sensitivity with respect to GSI.

9.7.5 Shear modulus

From the Panthi estimate for deformation modulus, one may further derive the rock mass shear modulus, which is an input parameter needed for the Panthi and Shresta (2018) approach. Utilizing the Panthi estimate of 0,94 GPa, the Poissons value of 0,1 and the relation given in Equation 39, a rock mass shear modulus of 0,43 GPa is obtained.

10 Stability assessment methods

10.1 Hoek and Marinos approach

Hoek and Marinos (2000) approach is a semi-analytical approach that was established to estimate rock mass squeezing in weak and heterogeneous rock masses. They utilized the Sakurai (1983) approach to estimate the relation of the compressive strength of the rock mass σ_{cm} to the isostatic in-situ stress p_o . Further, this relation is used as an indicator to determine the degree of tunnel deformation and potential squeezing problems. A critical step of the approach is the selection of reliable rock mass properties. This is reviewed in Section 9. In the approach, any realistic criterion for estimating rock mass strength and deformation may be used to estimate the tunnel deformation (Hoek and Marinos, 2000). It should be noted that the Hoek-Brown criteria and many other criterias for estimating rock mass parameters, assumes that the rock mass behaves isotropically. There should be no specific preferred failure orientation. This simplification may deviate due to the anisotropic nature of phyllite.

Hoek and Marinos (2000) utilized Monte Carlo simulations of various conditions with differing parameters such as in-situ stress, (circular) tunnel radius, uniaxial compressive strength of the rock as well as differing Hoek-Brown rock mass parameters (m_i, GSI, D). They utilized the closed form analytical solution for a circular tunnel in an isostatic stress field proposed by Duncan Fama (1993) and Carranza-Torres and Fairhurst (2000) to determine the tunnel strain for the various conditions. The results show that the simulations crudely follow the same relation between tunnel strain, rock mass compressive strength and in-situ stress.

The analysis can be extended to cover tunnels in which an internal pressure is used to simulate the effects of rock support. Hoek and Marinos (2000) found that Equation 34 and 35 could be used to determine the size of the plastic zone and the deformation of a tunnel in squeezing conditions, respectively. Equation 36 gives the strain percentage without support pressure.

$$\frac{d_p}{d_o} = \left(1.25 - 0.625 \frac{p_i}{p_o} \right) \frac{\sigma_{cm} \left(\frac{p_i}{p_o} - 0.57 \right)}{p_o} \quad (34)$$

$$\frac{\delta_i}{d_o} = \left(0.002 - 0.0025 \frac{p_i}{p_o} \right) \frac{\sigma_{cm} \left(2.4 \frac{p_i}{p_o} - 2 \right)}{p_o} \quad (35)$$

$$\epsilon[\%] = 0.2 \times \left(\frac{\sigma_{cm}}{p_o} \right)^{-2} \quad (36)$$

Where d_p is the diameter of the plastic zone surrounding the tunnel, d_o is the original tunnel diameter and δ is the tunnel sidewall deformation. Rock mass strength σ_{cm} can be estimated by empirical relations. Some of the more common equations to estimate rock mass strength were reviewed in Section 9.6.

The classification of the level of squeezing in relation to the tunnel diameter and stress conditions was then concluded. The results can be seen in Figure 48 and Table 22.

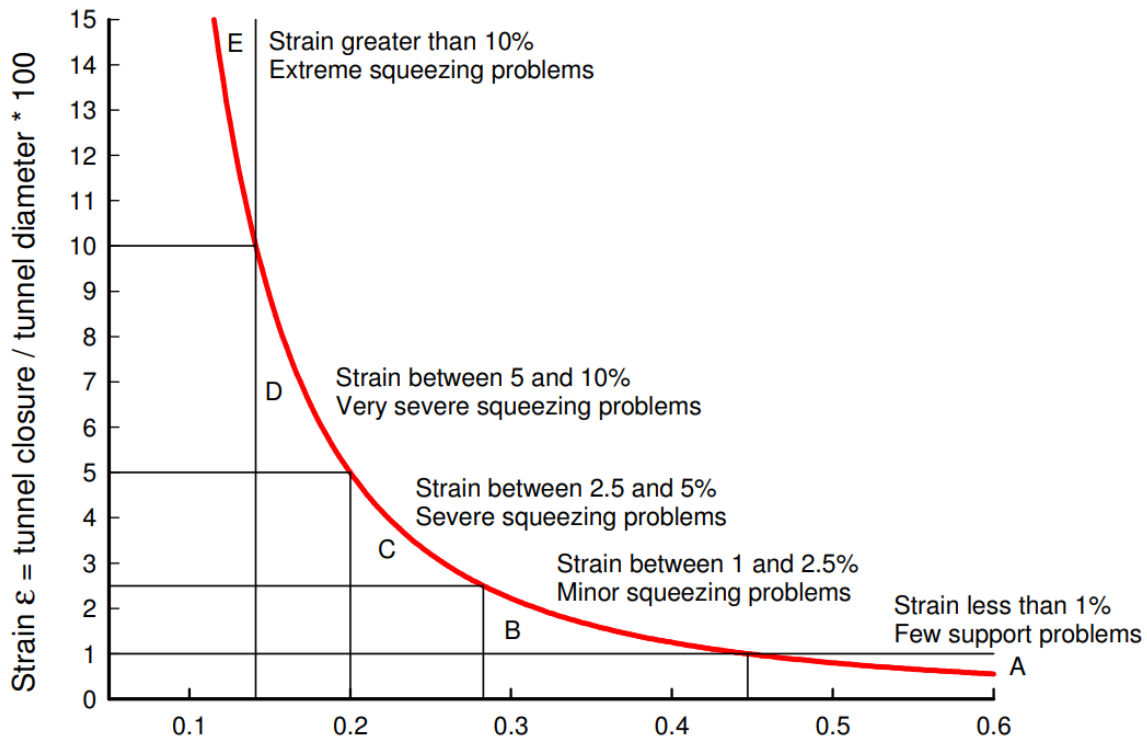


Figure 48: Classification and relation between tunnel strain, tunnel diameter and stress conditions. The plot is for an unsupported tunnel. From: Hoek and Marinos (2000).

It is important to estimate potential tunnel instability as early in a tunnel project as possible. This method gives a preliminary estimate of the tunnel deformation. In this analysis, the Hoek and Marinos method will be used for the two weakness zones reviewed in the Ryfylke tunnel.

The method, however, can not be considered adequate for final design purposes (Hoek and Marinos, 2000). It is important to note that the analysis is based on a simple closed-form solution for a circular tunnel in a hydrostatic stress field and the support is assumed to act uniformly along the tunnel perimeter. It is thus recommended that the tunnel and squeezing analysis should be subjected to numerical analyses (Hoek and Marinos, 2000). Here, one can take into consideration any tunnel shape and several excavation sequences and tunnel supporting elements. Further, the method only considers instantaneous deformation, and no time-dependent deformation (Fatemi Aghda et al., 2016).

Table 22: Degree of difficulty and tunnel support estimation with respect to the tunnel squeezing class. Reproduced from Hoek and Marinos (2000).

	Strain $\epsilon\%$	Geotechnical issues	Support types
A	Less than 1	Few stability problems and very simple tunnel support design methods can be used. Tunnel support recommendations based upon rock mass classifications provide an adequate basis for design.	Very simple tunnelling conditions, with rockbolts and shotcrete typically used for support.
B	1 to 2.5	Convergence confinement methods are used to predict the formation of a 'plastic' zone in the rock mass surrounding a tunnel and of the interaction between the progressive development of this zone and different types of support.	Minor squeezing problems which are generally dealt with by rockbolts and shotcrete; sometimes with light steel sets or lattice girders are added for additional security.
C	2.5 to 5	Two-dimensional finite element analysis, incorporating support elements and excavation sequence, are normally used for this type of problem. Face stability is generally not a major problem.	Severe squeezing problems requiring rapid installation of support and careful control of construction quality. Heavy steel sets embedded in shotcrete are generally required.
D	5 to 10	The design of the tunnel is dominated by face stability issues and, while two-dimensional finite analysis are generally carried out, some estimates of the effects of forepoling and face reinforcement are required.	Very severe squeezing and face stability problems. Forepoling and face reinforcement with steel sets embedded in shotcrete are usually necessary.
E	More than 10	Severe face instability as well as squeezing of the tunnel make this an extremely difficult three-dimensional problem for which no effective design methods are currently available. Most solutions are based on experience.	Extreme squeezing problems. Forepoling and face reinforcement are usually applied and yielding support may be required in extreme cases.

10.2 Panthi and Shresta (2018) approach

Panthi and Shresta (2018) proposed an approach to estimate tunnel squeezing which takes the stress anisotropy into account and distinguishes between the time-dependent and time-independent deformation. If in-situ stress is not isotropic, the degree of squeezing is not only different along the longitudinal alignment but also on the periphery of the tunnel wall. For this research, Panthi and Shresta studied long-term deformation measurements from 24 tunnel sections in 3 tunnels in Nepal, Himalaya, with generally poor rock mass conditions.

Panthi and Shresta (2018) takes the rock mass deformation modulus into account by implementing the related shear modulus for rock mass. The authors found that there was a fairly good correlation between tunnel strain and the shear modulus, support pressure, vertical stress and horizontal-to-vertical stress ratio. The outcome of the analysis is presented in Figure 49.

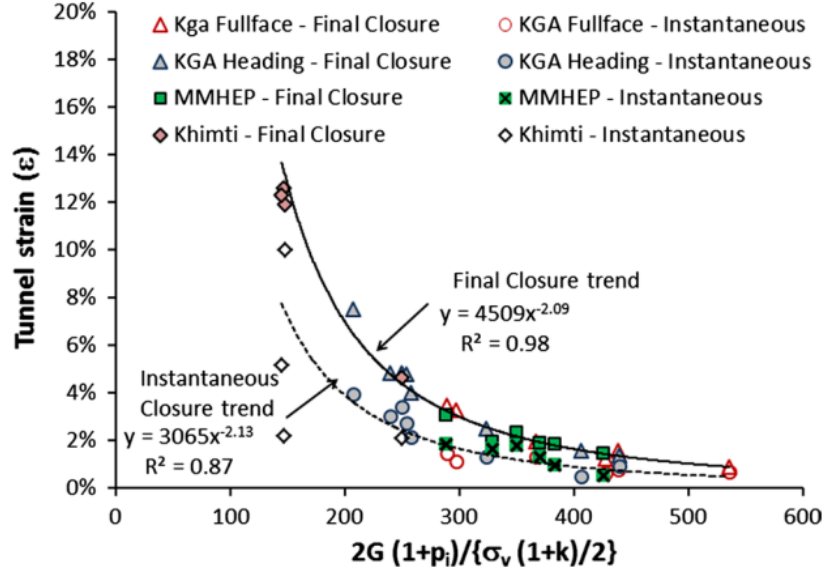


Figure 49: Correlation of instantaneous and final closure with rock mass property, support pressure and in situ stress. From: Panthi and Shrestha (2018).

Panthi and Shrestha applied the Sulem et al. (1987b) and Sulem et al. (1987a) approach for estimating tunnel displacements to their dataset. It was found that the time-independent (instantaneous) tunnel-deformation could be expressed as in Equation 37, and the final closure expressed in Equation 38.

$$\varepsilon_{IC} = 3065 \left(\frac{\sigma_v (1+k) / 2}{2G (1+p_i)} \right)^{2.13} \quad (37)$$

$$\varepsilon_{FC} = 4509 \left(\frac{\sigma_v (1+k) / 2}{2G (1+p_i)} \right)^{2.09} \quad (38)$$

Where ε_{IC} is the instantaneous, time-independent closure, ε_{FC} is the time-dependent final closure, G is the shear modulus of the rock mass, p_i is the internal pressure provided either by face effect or tunnel support and k is the stress anisotropy coefficient. The rock mass shear modulus is related to the rock mass deformation modulus as expressed in Equation 39 (Carranza-Torres and Fairhurst, 2000; Panthi and Shrestha, 2018).

$$G = \frac{E_{rm}}{2(1+\nu)} \quad (39)$$

For their studied tunnel cases, the authors found that the creep deformation included a significant part of the final closure, and it varied with the time span. However, it is highlighted that the time-independent closure is most often dominating and often the crucial part of plastic deformation. This deformation takes place immediately after tunnel excavation and until the tunnel face effect has ceased (Panthi and Shrestha,

2018). Thus, the preliminary tunnel support should be designed with the maximum time-independent deformation in mind (ϵ_{IC}). Correspondingly, the additional tunnel support installed behind tunnel face should be designed with the time-dependent deformation and long term stability of the tunnel taken into consideration (Panthi and Shresta, 2018). Panthi and Shresta (2018) states that traditional 'rock support interaction analysis' assumes that the time-independent maximum deformation takes place after the tunnel face effect has ceased, but this is not representable of the real situation. This distinguishment from time-dependent and time-independent deformation makes the approach unique, and highly useful for the planning of tunnel support and methodology.

As an addition to the Panthi and Shresta (2018) approach, a crude classification table after Panthi (2021) is given in Table 23. Strain levels are given for a tunnel with a span of 10 meters.

Table 23: Classification and action plan based on monitored deformation. After: Panthi (2021).

Classification	Maximum deformation [cm] or strain [%]	Action plan
Minor/insignificant	0-5 (<0,5%)	In principle no action required except in brittle rock mass. Continue long term monitoring.
Alarming	5-15 (0,5-1,5%)	Identify depth of deformation (softening). Action according to depth impact. Continue monitoring.
Serious	15-30 (1,5-3%)	Limited access in the opening. Investigate depth impact. Install reinforcement/repair. Continue monitoring.
Extreme	>30 (>3%)	Restrict access in the opening. Investigate depth impact. Continue monitoring and replace installed reinforcement.

10.3 FEM numerical modelling - RS2

The utilization of numerical modelling has established itself in the industry a long time ago. It is often used in the pre-construction phase, as well as an additional tool to empirical rock mass classification systems when adverse conditions are being dealt with during construction. In this subsection, a 2D RS2 model will be introduced for additional investigation of the tunnel deformation in the Ryfylke tunnel weakness zones.

10.3.1 Model setup

The model created is representing the first tube constructed in the Ryfylke tunnel, which is usually constructed some meters ahead of the second tube. Therefore, the model consists of a single tunnel profile, and not a twin-tube tunnel profile. In addition, this makes for a better comparison with the Hoek-Marinos, Panthi-Shresta and convergence-confinement approach. The model contains only two stages; pre excavation and after excavation stage. At the first stage, the model consists of only phyllite which is not affected by the disturbance factor. At the second stage, the excavation is blasted out and the phyllite in the vicinity of the tunnel profile has been disturbed.

Geometry

The geometry of the excavation can be seen in Figure 50. The purpose of the geometry is to approximately replicate the blasted-out T8,5 tunnel profile, with some additional space for heavy support. Thus, the invert width is taken as 9 meters, and the arc of the tunnel is taken as a 3-point arc with the top at 8 meters above the invert. The resulting widest diameter of the tunnel is 10,5 meters. This is perhaps a little wider than a typical blasted-out T8,5 cross section, but it is deemed satisfactory for the purposes of this study. Further, a section of 1 meter around the tunnel opening is taken as the phyllite which is effected by the blasting. Therefore, this phyllite, presented in green, is assigned the disturbance factor $D=0,5$. At the right side of Figure 50 the average overburden of 62,5 meters can be seen. This is changed to 115 meters when modelling for weakness zone 2. Thus, the model is built up to the surface (or bottom of the ocean), with a free surface here. For this model set-up with relatively shallow depth, the side and bottom boundaries are to have rollers, while the bottom corners are restrained in both X- and Y direction (Lavrov, 2019a).

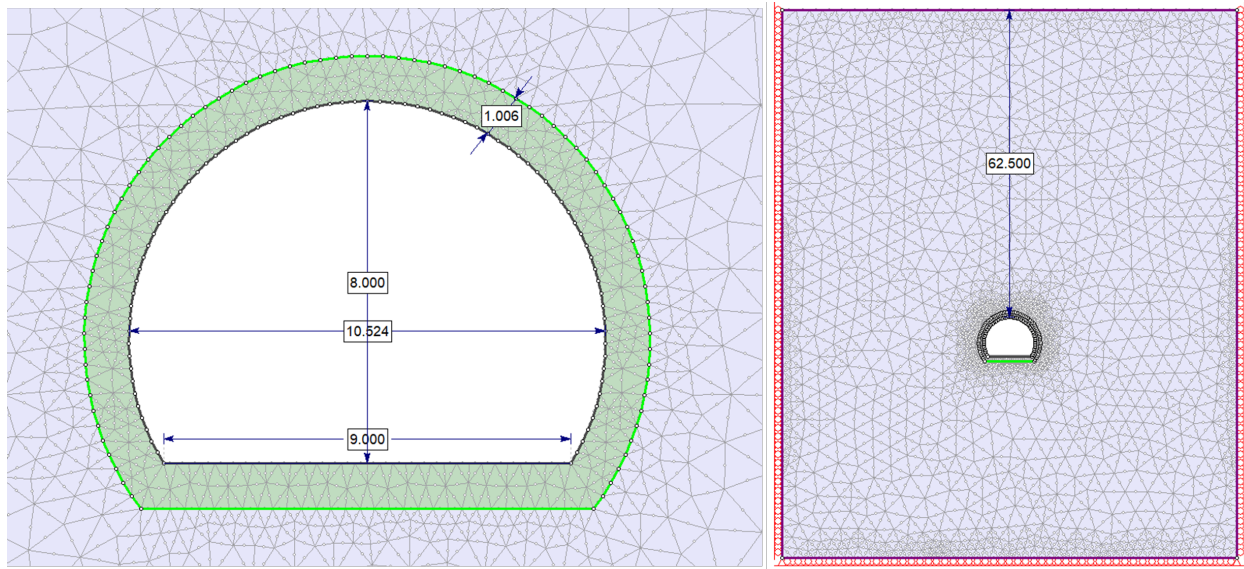


Figure 50: Geometry of the excavated section, approximately replicating the T8,5 tunnel profile.

Material properties and input parameters

The material properties and other input parameters for weakness zone 1 and 2 can be found in Table 24 and 25, respectively. In the software, the generalized Hoek-Brown criteria is used for the rock mass strength for given confining pressure, and the Hoek et al. (2002) equation 24 is used for global rock mass strength. The constant input parameters are an intact UCS of 19 MPa, intact deformation modulus of 13 GPa, an intact material factor m_i of 7 and an in and out-of-plane k value of 1,8. For weakness zone 2, the overburden is 115 meters and $k = 1,1$.

Table 24: Main input parameters for numerical simulation of deformation without support for weakness zone 1.

Chainage	GSI	E_rm [GPa]	m.b	UCS_rm [MPa]	σ_{cm} (global strength) [MPa]
8437-8441	28	0,93	0,535	0,28	1,64
8441-8444	30	1,06	0,575	0,33	1,73
8444-8448	25	0,78	0,481	0,23	1,5
8448-8452	28	0,93	0,535	0,28	1,64
8452-8455	31	1,13	0,595	0,35	1,78
8455-8459	33	1,29	0,64	0,4	1,88
8459-8463	37	1,69	0,738	0,52	2,07
With disturbance factor D= 0,5					
Chainage	GSI	E_rm [GPa]	m.b	UCS_rm [MPa]	σ_{cm} (global strength) [MPa]
8437-8441	28	0,52	0,227	0,12	1,04
8441-8444	30	0,57	0,25	0,15	1,12
8444-8448	25	0,46	0,2	0,09	0,93
8448-8452	28	0,52	0,227	0,12	1,04
8452-8455	31	0,6	0,262	0,16	1,16
8455-8459	33	0,67	0,288	0,19	1,23
8459-8463	37	0,83	0,349	0,25	1,4

10.3.2 Loading condition, mesh and convergence criteria

For a model of this type, which is built up to the surface, the material element loading is put to "field stress and body force". This means that the material is effected by both the loading derived from the field-stress input and the self-weight of the material. When the excavations are at great depths (>800m), only the field stress is chosen, because the effect of the body force is negligible compared to the field stress (Rocscience, n.d.). This is, as mentioned, not the case here.

Due to slow computation and convergence problems, the mesh elements were changed from the default "6 noded triangles" to "3 noded triangles". This decreases the degrees of freedom of the elements (deformation in this case) from 6 to 3. The use of 3 noded triangles greatly decrease the size of the matrix used to solve the problem (Rocscience, n.d.). As a result, the computed estimates may be somewhat less accurate. However, the use of 3 noded triangles is deemed satisfactory for this purpose.

The convergence criteria used for these calculations are "absolute force and energy". When using this criteria, the program checks two conditions at the same time: absolute force and energy. The Rocscience (n.d.)

Table 25: Main input parameters for numerical simulation of deformation without support for weakness zone 2.

Chainage	GSI	E_rm [GPa]	m_b	UCS_rm [MPa]	σ_{cm} (global strength) [MPa]
10629-10632	35	1,47	0,687	0,46	1,97
10632-10635	33	1,29	0,64	0,4	1,88
10635-10638	28	0,93	0,535	0,28	1,64
10638-10641	26	0,83	0,498	0,25	1,55
10641-10645	25	0,78	0,481	0,23	1,5
10645-10648	30	1,06	0,575	0,33	1,73
10648-10651	30	1,06	0,575	0,33	1,73
With disturbance factor D =0,5					
Chainage	GSI	E_rm [GPa]	m_b	UCS_rm [MPa]	σ_{cm} (global strength) [MPa]
10629-10632	35	0,74	0,317	0,22	1,31
10632-10635	33	0,67	0,288	0,19	1,23
10635-10638	28	0,52	0,227	0,12	1,04
10638-10641	26	0,48	0,206	0,1	0,97
10641-10645	25	0,46	0,2	0,09	0,93
10645-10648	30	0,57	0,25	0,15	1,12
10648-10651	30	0,57	0,25	0,15	1,12

documentation recommends the “comprehensive” convergence criteria, which checks for force, displacement and energy at the same time. However, this criteria could not be chosen due to convergence issues.

10.4 Convergence-confinement method

A well-known description and review of the convergence-confinement method (CCM) is that of Carranza-Torres and Fairhurst (2000). The CCM requires input on both ground deformational properties as well as the properties of the supporting materials. In return, one will get an indication of how the installed support interact with the rock mass and their deformation and support pressure. The load on the installed support after the face effect has ceased can be estimated, and checked against the yield capacity of the support. Decisions on timing of the support installation can also be taken. The CCM method is a closed-form analytical solution, and a circular tunnel is assumed. Carranza-Torres and Fairhurst (2000) states, however, that the method gives useful initial estimates if the radius of the widest section of the tunnel opening is used for the calculation. However, with a non-circular cross section there will not be uniform stresses on the support elements, with bending moments occurring.

The CCM method consists of three main elements, with illustrations shown in Figures 51 and 52:

- The Ground Reaction Curve (GRC): This plots the relationship of decreasing internal pressure p_i to radial wall displacements u_r . The support pressure is initially equal to the far-field stress σ_0 some distance before the tunnel section in question has been exposed. Once the tunnel is constructed further away from the tunnel section in question, the load bearing support from the tunnel face (“face effect”)

will decrease and cease. With no support installed, the internal pressure drops to zero and the radial displacement goes to a maximum u_{r-max} .

- The Longitudinal Displacement Profile (LDP): This is a plot of the radial displacement to the distance of tunnel face, or distance to tunnel face divided by tunnel radius (x/R). It is evident that at tunnel face, $x = 0$, the rock mass has already converged approximately 1/3 of the final deformation. Most of the deformation has taken place at approximately 2 tunnel diameters from the tunnel face
- The Support Characteristics Curve (SCC): It is defined as the relationship between the increasing pressure on the installed support p_s and the increasing radial displacement u_r on the installed support.

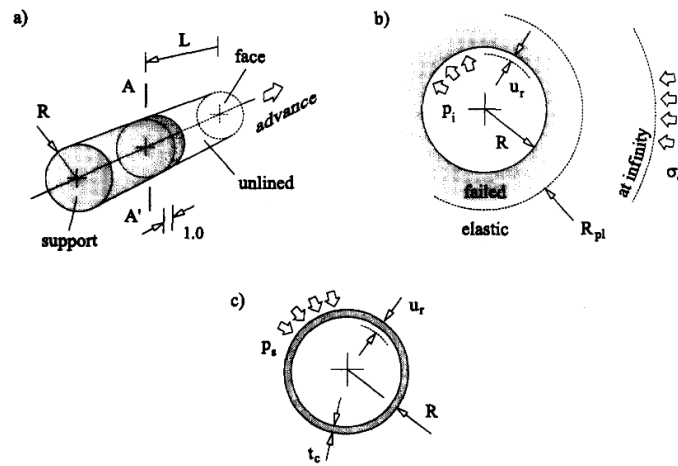


Figure 51: a: Cylindrical tunnel of radius R driven in the rock mass. b: Cross section of the rock mass at Section A-A'. c: Cross section of the circular support installed at section A-A'. From: Carranza-Torres and Fairhurst (2000).

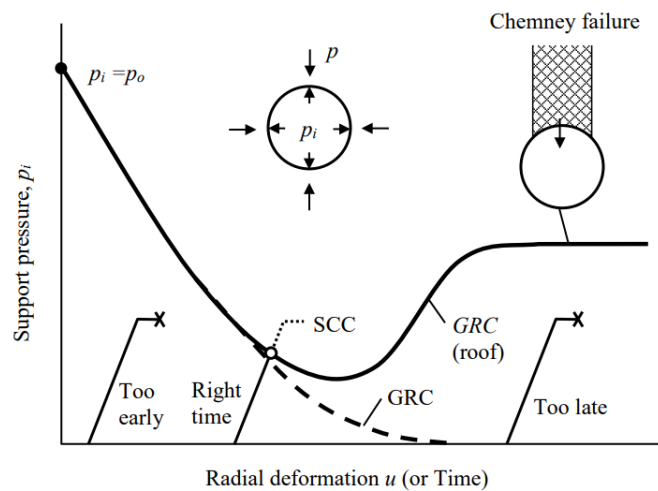


Figure 52: GRC and SCC of the CCM-method, with indication of early, good and late timing of support installation. From: Li (2018).

Due to time constraints and convenience, all the governing equations needed to create the GRC, SCC and LDP will not be presented in the main text of this thesis. An outcrop of the implemented Excel formulae can be found in Appendix C. The plastic part of the GRC is found by the relation in Equation 40.

$$\frac{u_r^{pl}}{R} \frac{2G_{rrm}}{\sigma_0 - p_i^{cr}} = \frac{K_\psi - 1}{K_\psi + 1} + \frac{2}{K_\psi + 1} \left(\frac{R_{pl}}{R} \right)^{K_\psi + 1} + \frac{1 - 2\nu}{4(S_0 - P_i^{cr})} \left[\ln \left(\frac{R_{pl}}{R} \right) \right]^2 - \left[\frac{1 - 2\nu}{K_\psi + 1} \frac{\sqrt{P_i^{cr}}}{S_0 - P_i^{cr}} + \frac{1 - \nu}{2} \frac{K_\psi - 1}{(K_\psi + 1)^2} \frac{1}{S_0 - P_i^{cr}} \right] \times \left[(K_\psi + 1) \ln \left(\frac{R_{pl}}{R} \right) - \left(\frac{R_{pl}}{R} \right)^{K_\psi + 1} + 1 \right] \quad (40)$$

Where u_r^{pl} is the plastic radial wall convergence, K_ψ is the dilation coefficient, R_{pl} and R are the radius of the plastic zone and radius of tunnel, P_i and S_0 are the scaled internal pressure and far-field stress, p_i is the internal pressure and P_i^{cr} is the critical initial support pressure (elastic limit).

The elastic part of the SCC can be plotted by Equation 41.

$$p_s = K_s u_r \quad (41)$$

Where p_s is the support pressure provided by the support and K_s denotes the stiffness of the support system. The plastic part of the SCC is defined by the maximum pressure p_s^{max} that the support can accept before collapse.

The LDP of the Carranza-Torres and Fairhurst (2000) solution to the CCM method is given in Equation 42.

$$\frac{u_r}{u_{r-max}} = 0.25 + 0.75 \left[1 - \left(\frac{0.75}{0.75 + x/R} \right)^2 \right] \quad (42)$$

It should be mentioned that several authors have proposed improved solutions for the LDP, e.g. Unlu and Gercek (2003) and Vlachopoulos and Diederichs (2009). These are not utilized in the calculations.

As with most other methods, the CCM carries its assumptions and limitations. The main assumptions are that the solution is based on a circular tunnel in an isostatic stress field (Carranza-Torres and Fairhurst, 2000). Further, perfectly elasto-plastic material behaviour is assumed, as is not always a good behavioural description of rock mass. However, there have been later revisions of the CCM method, one of which incorporates the strain-softening behaviour (Alejano et al., 2010). This is not applied in this thesis. Oke et al. (2021) summarized the main limitations of the CCM method as follows:

1. The conventional (classical) inclusion of the LDP in the CCM is based on an unsupported approach.
2. There are limited solutions for LDP in supported conditions that consider the stiffness of support and the unsupported span. Those solutions that do exist have their limitations.
3. The CCM does not take into consideration the effect of the overloading of the support systems caused by longitudinal arching.

Further discussion on the CCM method is out of the scope of this thesis, but the author is aware that some critique must be directed at the results obtained from Carranza-Torres and Fairhurst (2000) CCM implementation.

11 Results and some remarks from the stability assessment methods

In this section, the results obtained by utilizing the stability assessment methods presented in Section 10 will be presented, reviewed and commented briefly. The CCM and Panthi-Shrestha results' indication on tunnel support will also be studied. The main findings is that weakness zone 1 is subjected to mostly mild squeezing, while weakness zone 2 is subjected to moderate squeezing with some chainages having severe problems, depending on the various methods. Results also indicate that arched RRS implementation may be a little excessive.

11.1 Hoek-Marinos results

The results obtained for weakness zone 1 by utilizing the Hoek and Marinos (2000) approach are shown in Figure 53 and Table 26. For weakness zone 2, the input-parameters and results are presented in Figure 54 and Table 27. Because the Barton (2002) estimate deviated much from the other estimates and was by far the most optimistic, it is not included in the tunnel strain and deformation results and discussion.

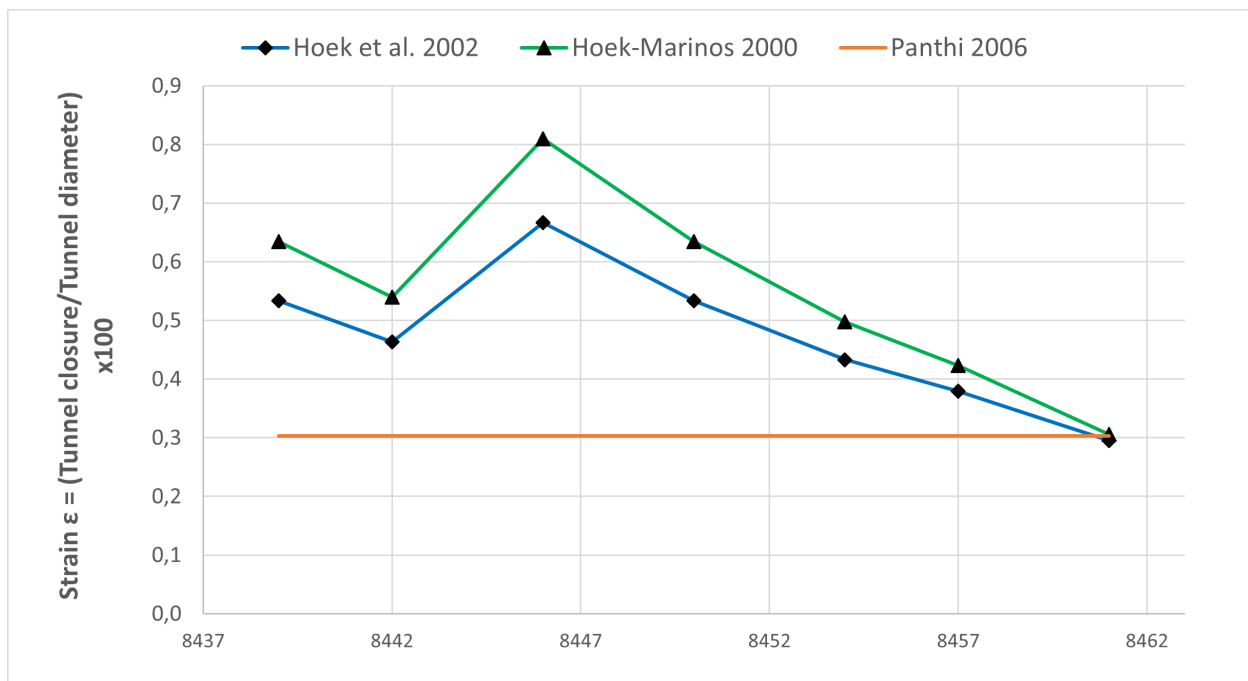
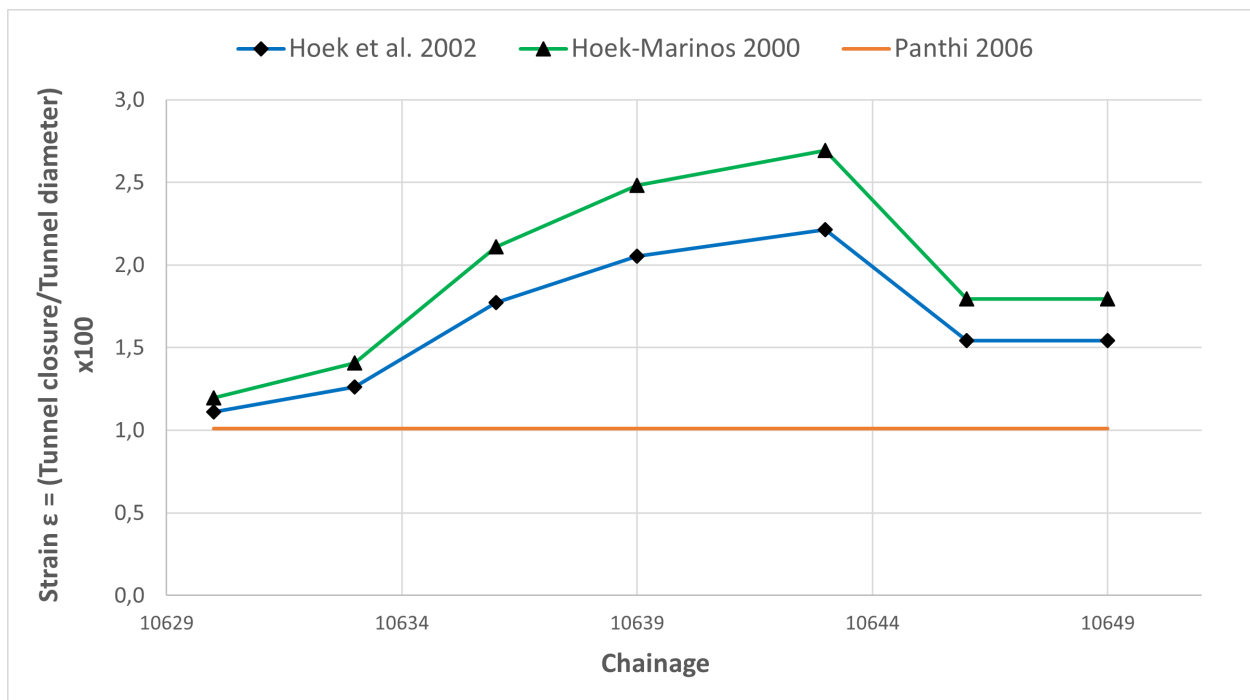


Figure 53: Estimated tunnel strain ϵ without support for weakness zone 1 by implementing Panthi, Hoek et al., and Hoek-Marinos estimate for rock mass strength, respectively.

Table 26: Input parameters and estimated tunnel strainages obtained by the Hoek-Marinos method for weakness zone 1.

	Chainage						
	8437-8441	8441-8444	8444-8448	8448-8452	8452-8455	8455-8459	8459-8463
Field stress P_0	1,7	1,7	1,7	1,7	1,7	1,7	1,7
Rock mass strength σ_{cm} [MPa]							
Panthi 2006	1,38	1,38	1,38	1,38	1,38	1,38	1,38
Hoek et al. 2002	1,04	1,12	0,93	1,04	1,16	1,23	1,40
Hoek-Marinos 2000	0,95	1,04	0,85	0,95	1,08	1,17	1,38
Tunnel strain ϵ [%]							
Panthi 2006	0,30	0,30	0,30	0,30	0,30	0,30	0,30
Hoek et al. 2002	0,53	0,46	0,67	0,53	0,43	0,38	0,30
Hoek-Marinos 2000	0,63	0,54	0,81	0,63	0,50	0,42	0,31

**Figure 54:** Estimated tunnel strain ϵ without support for weakness zone 2 by implementing Panthi, Hoek et al., and Hoek-Marinos estimate for rock mass strength, respectively.

Weakness zone 1

It can be seen that for weakness zone 1, all strain estimations fall under 1%. According to Hoek and Marinos (2000) Table 22, this corresponds to “few stability problems and very simple tunnel support methods can be

Table 27: Input parameters and estimated tunnel strainages obtained by the Hoek-Marinos method for weakness zone 2.

Chainage	Chainage						
	10629-10632	10632-10635	10635-10638	10638-10641	10641-10645	10645-10648	10648-10651
Field stress P_0 [Mpa]	3,1	3,1	3,1	3,1	3,1	3,1	3,1
Rock mass strength σ_{cm} [MPa]							
Panthi 2006	1,38	1,38	1,38	1,38	1,38	1,38	1,38
Hoek et al. 2002	1,32	1,23	1,04	0,97	0,93	1,12	1,12
Hoek-Marinos 2000	1,27	1,17	0,95	0,88	0,85	1,04	1,04
Tunnel strain ϵ [%]							
Panthi 2006	1,01	1,01	1,01	1,01	1,01	1,01	1,01
Hoek et al. 2002	1,11	1,26	1,77	2,05	2,22	1,54	1,54
Hoek-Marinos 2000	1,20	1,41	2,11	2,48	2,69	1,79	1,79

used. Tunnel support recommendations based upon rock mass classifications provide an adequate basis for design”. In practise it is, of course, support implemented on the basis of the Q-system, although the heavier initial support and RRS arches were implemented. Therefore, it is questionable whether the tunnel section is subject to “few stability problems”. The support types from the chart states “Very simple tunnelling conditions, with rockbolt and shotcrete typically used for support”. Although this is not a rigid proposal, it differs greatly from the completed tunnel support. This leaves two hypotheses:

- The completed tunnel support is too conservative.
- The main stability issues are not that of tunnel squeezing, and the use of heavier rock support may be justified by other factors influencing stability.

Regarding the first hypothesis, it is previously stated in the literature that the applied support in Norwegian road tunnels are conservative. The introduction of RRS in the Q-value support chart and the NPRA support table have caused a considerable increase in support in Norwegian road tunnels (Høien et al., 2019). Høien et al. (2019) further states that a downscaling of heavy support would very likely be possible if more studies had been carried out on under which conditions weak rock needed load-bearing support instead of simpler reinforcement. On the other hand, the argument of having an extra safety margin to avoid accidents will always be valid.

Regarding the second hypothesis, it can be argued that for a tunnel section with an overburden of only 60-65 meters, tunnel squeezing will not be the main factor influencing stability. In the section, heavily disturbed, fractured and schistose phyllite was dealt with. This is the description of a rock mass which has a very low self-bearing capacity. Thus, the construction of RRS arches, commonly labelled “load bearing support” may be justified because the rock mass alone could not carry the overburden load. The main question, however, is whether rock reinforcing support such as traditional dense systematic bolting in combination with shotcrete

and spiling bolting would have been sufficient. In this case, the strain and deformation results obtained argues that reinforcing support would have been sufficient.

Weakness zone 2

Studying the results for weakness zone 2, it is evident that the increase in overburden and corresponding stress levels have greatly increased the estimated tunnel strain and deformation. The Panthi (2006) constant estimate just exceeds the 1% level, while Hoek et al. (2002) and Hoek and Marinos (2000) estimates are greater or far greater than the 1% strain level. Hoek and Marinos (2000) states that for the chainages with a strain level from 1-2.5%, “minor squeezing problems occur, which are generally dealt with by implementing traditional support with the occasional light steel sets and lattice girders applied for additional security”. It is again reminded that Grimstad et al. (2002) stated that RRS is similar in its capacity to lattice girders. Therefore, the results for weakness zone 2 are more in accordance to the performed tunnel support.

A couple of meters in weakness zone 2 also exceeds into the Hoek and Marinos strain category C (2,5-5%). Here, it is stated that severe squeezing problems will occur, which requires rapid installation of support and careful control of construction quality. “Heavy steel sets embedded in shotcrete are generally required”. This support description is in reasonably good correspondance to the completed support. The timing of the completed RRS arches, however, is stated to have been when the face was far away from the tunnel section in question (NPRA, 2019). Even though the initial support in the Ryfylke tunnel was installed right away, one might say that this deviates from the proposal of rapid support regarding the delayed RRS installation. In conjunction with the convergence-confinement method and theory (Carranza-Torres and Fairhurst, 2000), the tunnel deformation at this time is mainly completed, with only secondary creep deformation left (see e.g. Panthi and Shresta (2018)). With respect to this theory, it can be questioned why the load bearing support is installed when most of the deformation has ceased. The support structure’s capacity will not be fully utilized, and there will be an increasing risk of smaller or larger collapses and rock failure before the installation of the RRS arches takes place. However, the initial support installed at the Ryfylke tunnel was relatively strong, as reviewed in section 8.6.

11.2 Panthi-Shresta results

When using the Panthi and Shresta (2018) approach, only the Panthi (2006) estimate for rock mass deformation and shear modulus is taken into account. The reason being that the 2006 rock mass strength and deformation modulus estimate and the 2018 tunnel deformation estimate was developed for the same purpose; to be especially applicable to schistouse, highly bedded metamorphic rock, with cases from Nepal, Himalaya.

Keep in mind that the variation of overburden for the two weakness zones are uncertain and varies with a maximum of 10 meters. Thus, the overburden and the vertical stress is given as the average overburden and stress. Correspondingly, the strain and deformation values along the weakness zones are constant. The input parameters and results are given in Table 28.

Table 28: Strain percentage and deformation values obtained from the Panthi and Shresta (2018) approach, with no support pressure applied.

Input parameters				
Parameter	Vertical stress σ_v [MPa]	Shear modulus G [GPa]	k	
Weakness zone 1	1,7	0,43	1,8	
Weakness zone 2	3,1	0,43	1,1	
Results				
	ϵ_{IC} [%]	ϵ_{FC} [%]	Instantaneous deformation [cm]	Final deformation [cm]
Weakness zone 1	1,1	2,0	11	20
Weakness zone 2	2,1	3,9	21	39

One can see from the results that an increase of overburden of just under 100% from weakness zone 1 to 2 gives an increase of strain and deformation of just under 100%. The instantaneous strain makes up 55% and 54% of the final closure. This means that the creep deformation, which the additional tunnel support has to withstand, also here is a considerable part of the final closure. Because the instantaneous closure is starting to take place before support can be applied and deformation can be monitored, it is the deformation range of $\epsilon_{FC} - \epsilon_{IC}$ that is the most interesting regarding support interaction (Panthi, 2022d). This is the deformation which can be detected and effect the installed arched RRS. $\epsilon_{FC} - \epsilon_{IC}$ is equal to 9cm (0,9% strain) for weakness zone 1, and 18cm (1,8% strain) for weakness zone 2. According to Panthi (2022d), these are the values that should be compared with the results obtained from the other methods. Comparing these results with the classification given in Table 23, one can see that the weakness zone 1 strain should cause one to be aware of the squeezing conditions. Action should be taken according to the degree of deformation. For weakness zone 2, a “serious” strain level is encountered. For this strain level, it is recommended to install reinforcement support, i.e., in addition to the preliminary support. Of course, this is in good accordance to the performed support methodology in the Ryfylke tunnel.

11.2.1 Panthi and Shresta results indication on support

When support pressure is applied, the strain rates derived from Equations 37 and 38 decreases quickly. Calculations of instantaneous and final closure with respect to support pressures ranging from 0,0 to 1,5 MPa is shown in Figure 55.

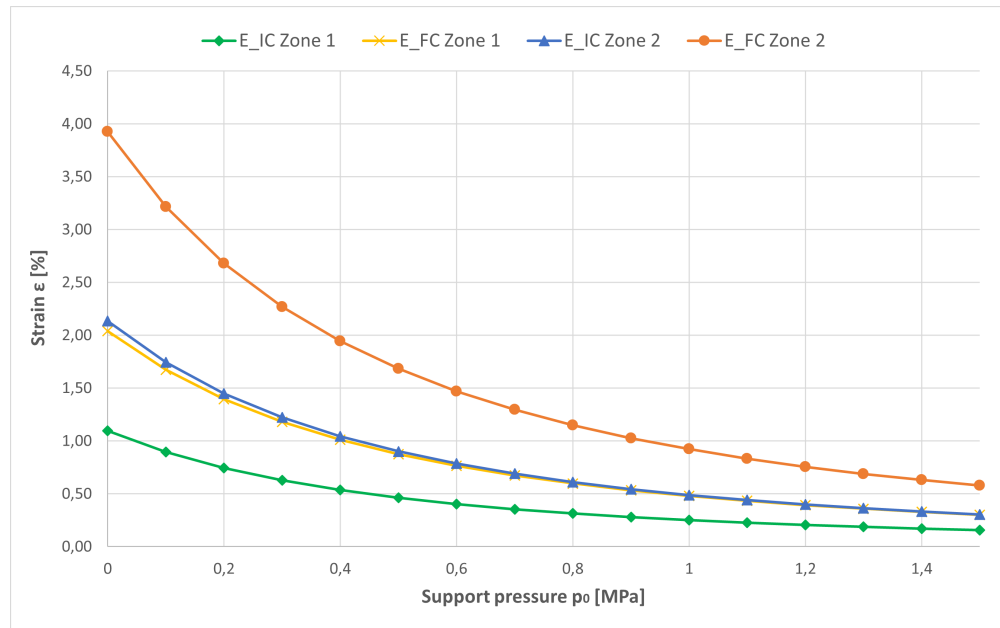


Figure 55: Estimated tunnel strain ϵ with support pressures for weakness zone 1 and 2 by implementing Panthi-Shresta approach.

One can quickly see from the plotted graph that for both weakness zones, there is not a very considerable support pressure that is required to reduce the sum of $\epsilon_{FC} - \epsilon_{IC}$ to under 1% strain. For weakness zone 1, a support pressure of e.g. 0,2 MPa would apparently be sufficient to decrease the $\epsilon_{FC} - \epsilon_{IC}$ strain to well under 1%. For weakness zones 2, approximately 0,4 MPa is required. This is just under the support capacity calculated in Table 32, under the CCM results section. The real cross-section is of course not perfectly circular, and therefore, local stress concentration in the support may exceed its capacity. This low safety-factor indicates that stronger support is needed. Hence, the Panthi and Shresta (2018) results, at least for weakness zone 2, can be said to be more in accordance with the real conditions.

11.3 RS2 results

The results from RS2 are presented in this subsection. In the software, it is easier to explore how the various parameters effect the tunnel deformation. Also, the actual T8,5 tunnel profile could be modelled.

What was checked in the results was the deformation of the mid-wall on both sides, as well as the crown displacement. Invert deformation was ignored, because it is not that big a factor for the tunnel stability. Of course, floor heave is possible in extreme squeezing situations, but deemed as very unlikely for these conditions. To verify the model, the stress levels were checked before excavation in the middle of the crown.

The results from weakness zone 1 can be found in Table 29 and Figure 56. Results from weakness zone 2 is presented in Table 30 and Figure 57. An outcrop from the RS2 result for weakness zone 2, chainage 10641-10644 (GSI 25), which illustrates the measuring points and deformation distribution, is shown in Figure

58.

Table 29: Table of deformation results from RS2 simulations for weakness zone 1, with overburden 62,5 meters.

Deformation [cm]						
Chainage	GSI	Left wall	Right wall	Crown	Wall-convergence	Tolerance
8437-8441	28	7,2	7,2	17	14,4	0,023
8441-8444	30	5,7	5,8	10,2	11,5	0,015
8444-8448	25	9,5	9,3	20	18,8	0,039
8448-8452	28	7,2	7,2	17	14,4	0,023
8452-8455	31	5,1	5,1	9,8	10,2	0,001
8455-8459	33	4,4	4,4	6,7	8,8	0,001
8459-8463	37	2,9	2,9	3,8	5,8	0,001

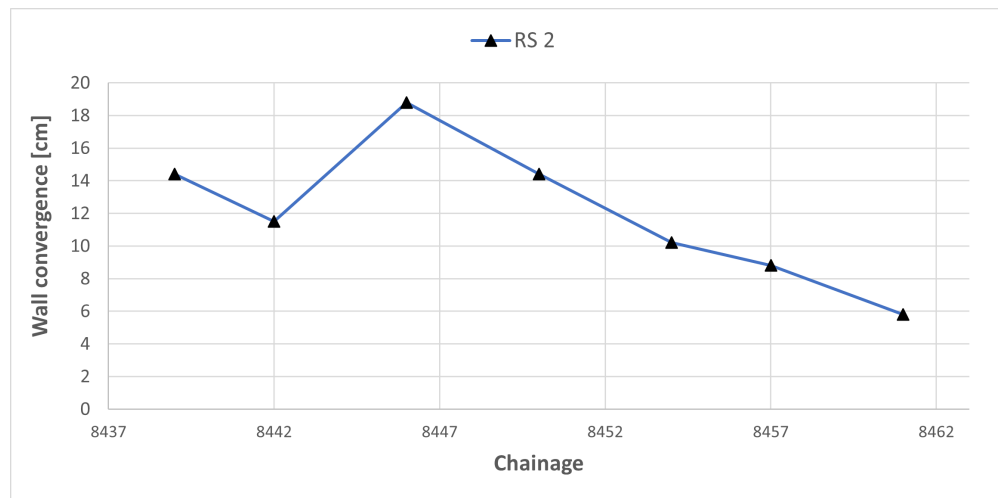


Figure 56: Wall-wall convergence obtained by RS2 simulations for weakness zone 1.

Tolerance

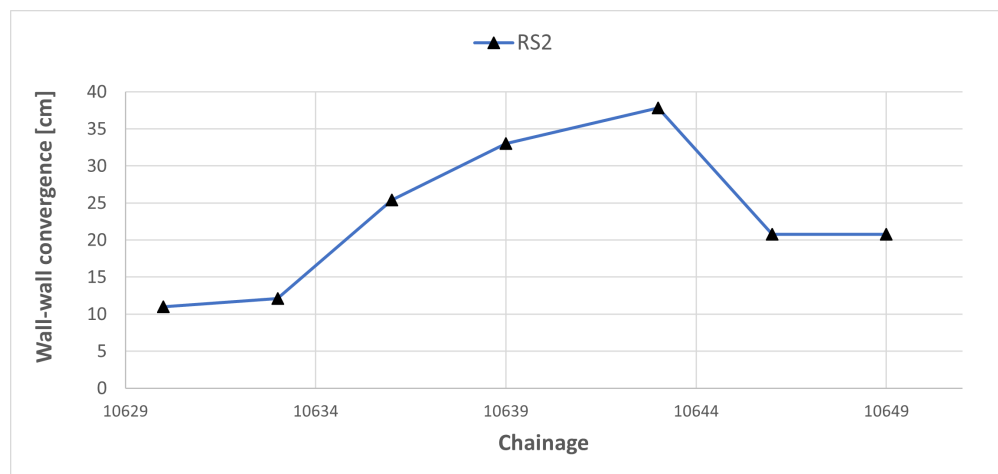
The tolerance value defines the point at which the finite element solution is considered to have converged. The tolerance for the stress analysis is a dimensionless parameter which represents the allowable unbalanced energy in the system, and corresponds to the convergence criteria for a given load step:

- If the energy imbalance of a current state (iteration) is less than the tolerance value, then the solution is considered to have converged, and the iterations are stopped.
- If the tolerance value is not achieved within the specified maximum number of iterations (i.e. energy imbalance remains greater than the tolerance value), then the solution process is deemed not to have converged, for the specified convergence parameters.

The default tolerance is 0,001, and Rocscience (n.d.) gives the recommended tolerance as 0,001-0,01. As can be seen from Tables 29 and 30, the recommended tolerance had to be exceeded to obtain convergence for

Table 30: Table of deformation results from RS2 simulations for weakness zone 2, with overburden 115 meters.

Deformation [cm]						
Chainage	GSI	Left wall	Right wall	Crown	Wall-convergence	Tolerance
10629-10632	35	5,5	5,5	7	11	0,001
10632-10635	33	6,1	6	8,3	12,1	0,001
10635-10638	28	12,7	12,7	21,8	25,4	0,022
10638-10641	26	16,5	16,5	32,3	33	0,028
10641-10645	25	18,9	18,9	42	37,8	0,03
10645-10648	30	10,4	10,4	19	20,8	0,016
10648-10651	30	10,4	10,4	19	20,8	0,016

**Figure 57:** Wall-wall convergence obtained by RS2 simulations for weakness zone 2.

some GSI values. This is because the rock mass material modelled in these cases are very weak, and thus, more elements experience plastic deformation. The results are convergence issues (Lavrov, 2022).

Weakness zone 1

As can be seen from Figure 56, chainage $\sim 8437-8458$ exceeds 10cm wall-wall deformation, and therefore also the 1% tunnel strain percentage class in Hoek and Marinos (2000). Hence, also results from RS2 for this section suggests that squeezing stability problems would occur. The RS2 results are generally higher than the semi-analytical and analytical results. The most deformation is found in the tunnel crown. This is a result of the higher horizontal stress, which creates a stress concentration in the crown. In addition, this is the area of the excavation most affected by the “body force”, as the self-weight of these elements are not supported by underlying elements. The crown deformation values certainly imply that rock fall and/or tunnel collapse would happen if the tunnel is not supported.

Weakness zone 2

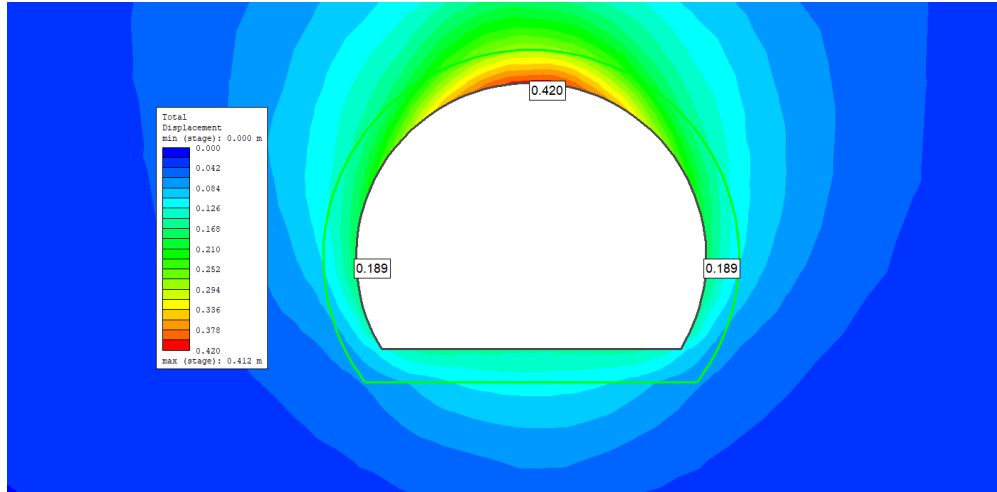


Figure 58: Result from RS2 simulation for chainage 11641-11644, weakness zone 2.

The RS2 deformation results from weakness zone 2 are quite high relative to the previous results, as can be seen in Figure 57. The whole section exceeds the 1% strain rate, with approximately half of the section also exceeding the 2,5 % strain rate. This implies severe squeezing problems and the need for rapid installation of support, according to Hoek and Marinos (2000). In addition, the crown deformation values of 30-40cm gives a clear indication that crown failure and tunnel collapse will happen if adequate support is not added.

11.3.1 Comparison of RS2 results

As previously mentioned, it is possible to study the effect of parameter changes quickly in RS2. One varying parameter is the field stress, which is changed due to the change in overburden from weakness zone 1 to 2. Figure 59 displays the difference in tunnel convergence between the two weakness zones, with respect to the GSI-value. Figure 60 shows the difference in roof displacement.

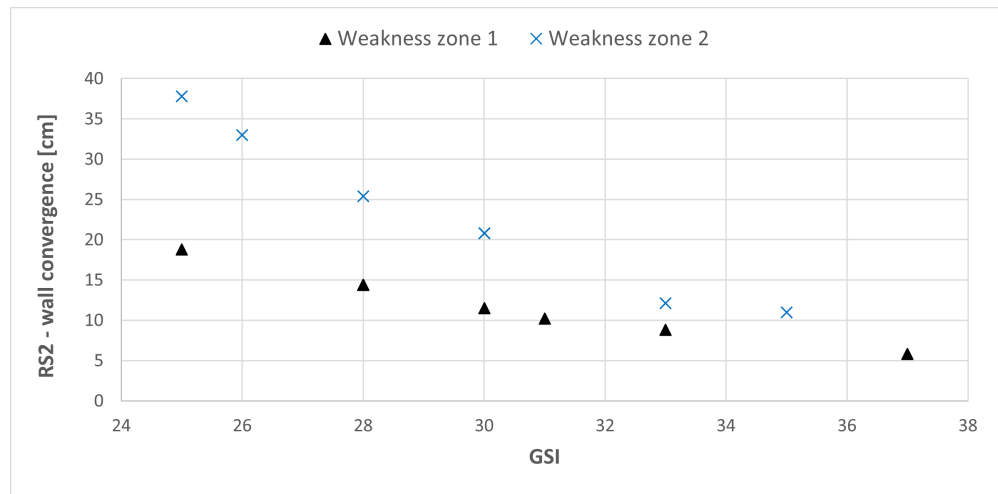


Figure 59: Comparison of wall convergence of weakness zone 1 and 2.

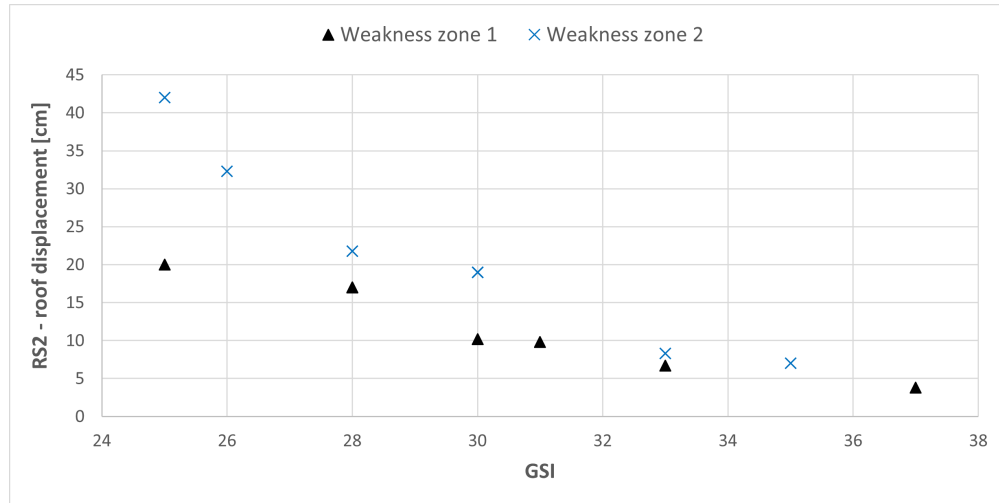


Figure 60: Comparison of roof displacement of weakness zone 1 and 2.

It is not a very clear correlation, but it seems that the differences in deformation due to higher stress-levels increases when lowering the GSI-value. This is deemed realistic, as the stress levels are generally not very high, and the rock mass strength and deformation modulus are more important factors when it comes to the tunnel deformation.

11.4 CCM results

When constructing the GRC, LDP and SCC for the Ryfylke tunnel sections, the Excel formulae in Appendix C, modified from the Carranza-Torres and Fairhurst (2000) paper, has been implemented. Here, for the plastic deformation, the dilation angle should be given according to the condition of the rock mass with which you are dealing with. The dilation angle is said to vary from 0,0-0,5 for soft soils to 30 for hard rocks (Carranza-Torres and Fairhurst, 2000). In this case, a dilation angle of 5 was used. It was also decided to “normalise” the far-field stress σ_0 , because the method assumes an isostatic stress-field. The way this was done was by calculating the far-field stress from Equation 43:

$$\sigma_0 = \frac{\sigma_v + \sigma_h}{2} \quad (43)$$

Utilizing this adjustment gives a far field stress in weakness zone 1 and 2 of 2,38 and 3,26 MPa, respectively. To adjust for this increase of in-situ stress, the intact material parameter m_i is increased to 10, which is still within the range for phyllite. Further, the rock mass strength, deformation and shear modulus were adopted from the Panthi (2006) estimate.

The original formulae contains Hoek-Brown parameters M_b and S without respect to the disturbance factor D . The author quickly discovered that if these formulas were used, the obtained maximum deformation values were very small compared to the other results. When, however, the parameters were substituted by those given in Equations 3 and 4 with $D=0.5$, the obtained maximum displacements were much larger and

fit in well compared with the other results. It can be seen that the CCM and the RS2 results are in good accordance with each other, with the RS2 results generally being a little more conservative. Thus, the results obtained from the CCM method and the Carranza-Torres and Fairhurst (2000) Excel formulae are deemed satisfactory.

The results from weakness zone 1 and 2 with the disturbance factor $D=0,5$ and dilation angle $=5$ are given in Table 31. Keep in mind that the table gives the ultimate tunnel convergence without any support installed. The radial wall displacement output from the CCM construction is multiplied by 2 to obtain total tunnel convergence.

Table 31: Displacement results obtained by utilizing the CCM method without support installed.

Zone 1 ($\sigma_0=2,38$ MPa)		
Chainage	GSI	Total convergence [cm]
8437-8441	28	12,3
8441-8444	30	11,1
8444-8448	25	14,5
8448-8452	28	12,3
8452-8455	31	10,5
8455-8459	33	9,6
8459-8463	37	8,0
Zone 2 ($\sigma_0=3,26$ MPa)		
Chainage	GSI	Total convergence [cm]
10629-10632	35	16,4
10632-10635	33	18,2
10635-10638	28	24,5
10638-10641	26	27,8
10641-10645	25	29,6
10645-10648	30	21,6
10648-10651	30	21,6

From the obtained results, it is evident that the in-situ stress σ_0 is an important factor for the convergence values, as well as the disturbance factor and GSI-value. It can quickly be seen that the increase in far-field stress increases the maximum deformations for the same GSI-values with more than 100%.

11.5 CCM indication on tunnel support

As mentioned, one of the strengths of the CCM-method is that it allows for the initial examination of the installed support interaction with the rock mass and their deformation. There are, of course, additional investigations that need to be carried out to determine a final tunnel design and support system, but the CCM results are said to provide good initial indications (Carranza-Torres and Fairhurst, 2000).

Due to the nature of the results, only the worst case scenario (weakness zone 2 with GSI=25) will be shown

in this section. As is well known, rock bolts and a substantial amount of sprayed concrete usually makes up the preliminary support for work safety in Norway. The table of material properties of support that is supposed to replicate typical preliminary support, is given in Table 32. The values are adopted or adjusted from those listed in Carranza-Torres and Fairhurst (2000).

Table 32: Material properties and some calculated values for the CCM support system comprised of rock bolts and shotcrete.

Material	Property	Value	Unit
Bolts	Width	25	mm
	Length	4	m
	Tensile strength	0,10	MN
	Bending moment	0,03	m/MN
	E-modulus	210	GPa
	spacing	1	m
Shotcrete	Compressive strength	27	MPa
	E-modulus	25	GPa
	Poisson's ratio	0,25	-
	Thickness	8	cm
Computed results			
	Maximum pressure the support can withstand	0,45	MPa
	Maximum displacement of support	4,95	mm
	Actual induced pressure on support system	~0,2	MPa

The plotted characteristic curves of these CCM conditions are shown in Figure 61. In contrast to what was actually carried out in the Ryfylke tunnel, the results clearly indicate that the rock bolting and 8cm layer of shotcrete is sufficient to meet the demanded support pressure, and thus give a stable tunnel. The bolt length of course has to be estimated with respect to the depth of the plastic zone to ensure proper anchoring. However, bolt length does not significantly effect the support capacity. 4 meter length is assumed here. The support capacity is calculated to be 0,45 MPa, but the GRC and SCC intersect at only ~0,2 MPa. This means that in addition to stabilizing the tunnel, the added support is indicated to have a factor of safety of more than 2. At the intersection of the GRC and SCC, the system reaches equilibrium (Carranza-Torres and Fairhurst, 2000). For comparison, Grimstad et al. (2002) claims that for a 10m span tunnel, 12 cm steel-fibre reinforced shotcrete and systematic bolting with 1,5m spacing provides 0,3 MPa support pressure. This is deemed to correspond fairly well to the CCM estimation, with the assumption of evenly distributed loads.

As mentioned, the performed initial support in the weakness zones mainly consisted of 6-8m spiling bolting c/c 30-40cm and 4m radial bolts c/c 1,5m as well as 15-20cm E1000 shotcrete (NPRA, 2019). Obviously, this is way more than the initial support example used for the CCM method. Again, according to the CCM results indication, this performed initial support would be more than sufficient, and it would have a great

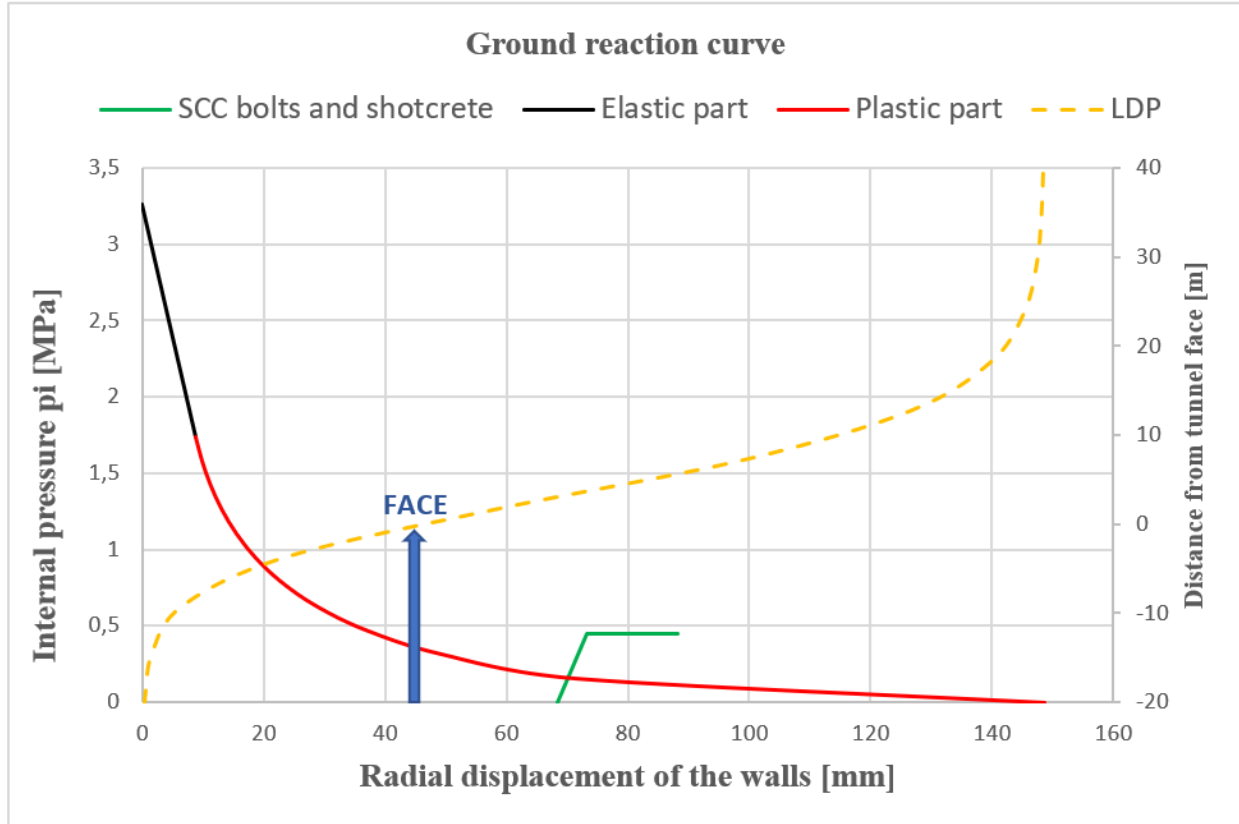


Figure 61: GRC, SCC and LDP for weakness zone 2 chainage 10641-10645. Face position marked.

factor of safety as well.

Because this is the worst case scenario, with the greatest field stress and lowest rock mass strength, it is obvious that the constructed support system would have been sufficient for the other chainages as well, based on the CCM results. In this plot, the support is simulated to have been installed 3m behind tunnel face. This is approximately the equivalent of immediate support after a blast has been carried out. One can see that even for a theoretical support installation right at tunnel face, the support is indicated to meet the demanded support pressure. The calculated characteristic curves for all chainages reviewed can be found in Appendix D.

11.6 Comparison of all strain results

In this section, the results of the tunnel strain and deformation obtained from the different stability assessment methods are compared all together.

Figures 62 and 63 display all tunnel strain results for the two weakness zones in the same system. In the table legend, "HM" represents the Hoek and Marinos (2000) stability assessment method, while the latter names are the rock mass strength estimates incorporated in the method. Again, all Panthi (with others)

estimates are constant, because it is assumed that the intact rock strength and modulus are constant, as well as the in-situ stress.

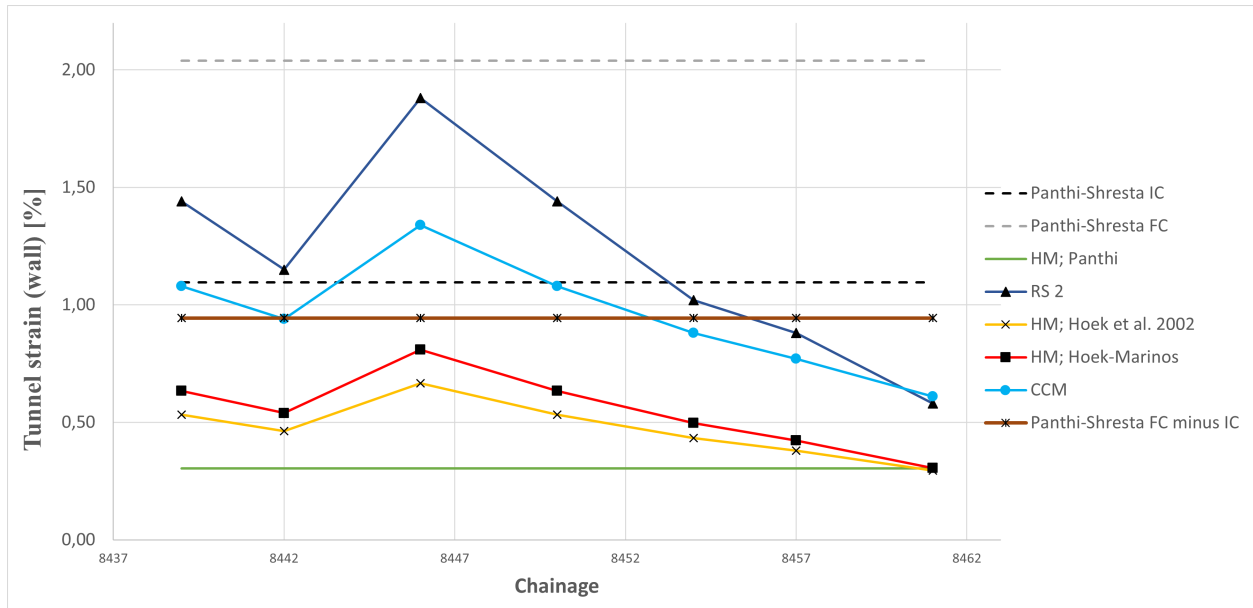


Figure 62: Strainages in weakness zone 1 obtained from different approaches.

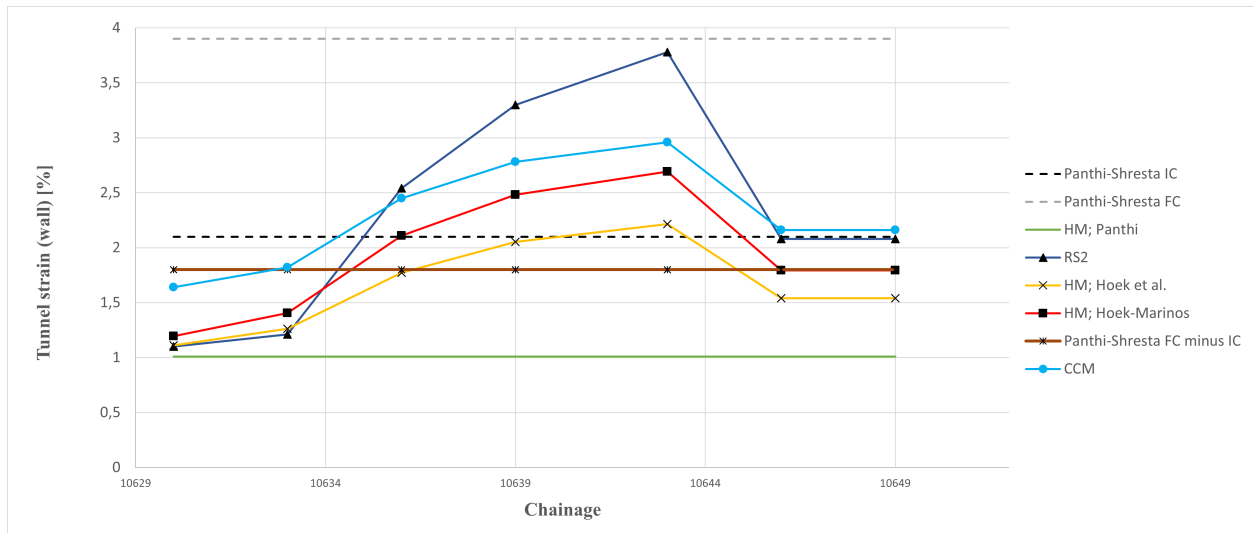


Figure 63: Strainages in weakness zone 2 obtained from different approaches.

It can be seen in these figures that the RS2, CCM and Panthi and Shresta (2018) ($\epsilon_{FC} - \epsilon_{IC}$) are the ones predicting the most tunnel strain for weakness zone 1. RS2 and CCM also give the most conservative results for weakness zone 2, but not by as much. Here, the Hoek (with others) results are exceeding the Panthi-Shresta results for some chainages. Correspondingly, there is particularly one important difference between the RS2 and Panthi-Shresta method, and the Hoek-Marinos method. With the former methods, the stress anisotropy is taken care of, whereas for the latter method, an isostatic stress field is assumed. In the cases from the Ryfylke tunnel, the overburden is not great, so the horizontal stresses are typically of

bigger magnitude than the vertical stress (Myrvang, 2001). With k -values of 1,8 and 1,1 used, the RS2 and Panthi-Shresta method assumes higher stress levels than the Hoek-Marinos method. Hence, it is natural that they estimate more strain for weakness zone 1, where $k=1,8$. The CCM stress-levels are “normalized”, so also these stress levels are higher than the ones incorporated in the Hoek (with others) estimations. In the authors opinion, the inclusion of stress-anisotropy makes for a more realistic approach, even though Hoek (2006) states that for a zone of very weak rock, the local vertical and horizontal stresses tend to be equal. It is evident that the increase of the in-situ stress from zone 1 to 2 has the most effect on the Hoek-Marinos results, as they do not consider stress anisotropy. The effect of the increase of vertical stress is reduced for the other approaches due to the decrease of the k -value.

The RS2, CCM and the Hoek-Marinos results follow the rock mass classification results, which in this case only is the GSI as the Barton results were left out. It is evident that the results are sensitive to the assigned GSI value. This may be described as a weakness, as the results will carry the same limitations as the GSI as a classification system, see Section 2.6.2. It can quickly be seen that the RS2 results are the most sensitive to GSI, as they vary the most for the different chainages. Within the Hoek-Marinos results, it is the Panthi (2006) that is the least conservative estimate, while the Hoek et al. (2002) is the most conservative.

12 Discussion

In this section, the research objectives mentioned in the introduction will be discussed by studying the results presented in the former section. The results' indication on tunnel stability will be discussed. The results from the analytical, semi-analytical and empirical methods will be compared and discussed. It will be discussed whether the utilization of load-bearing support with arched RRS can be justified. Lastly, some uncertainties and assumptions will be considered.

12.1 The results' indication on tunnel stability

On the critical strain theory

As reviewed, the tunnel strain for weakness zone 1 ranges from under 0,5 to 1,5%, while for weakness zone 2 strain is estimated to range from 1 to 3,5%. The first thing which can be concluded is that according to the Sakurai (1981) critical strain theory, all tunnel chainages from the weakness zones will undergo failure if not supported. The phyllite critical strain value obtained from SINTEF is approximately 0,1-0,25%, and all strain results exceed this value. This is to be expected, as the sections are classified as weakness zones, and the tunnel opening of a T8,5 tunnel section is big. Therefore, the rock mass alone would not have sufficient self-bearing capacity to withstand the induced stresses and deformation. This indication is deemed very realistic.

On the crown-displacement in RS2

Another result which clearly backs up rock mass failure is the crown displacement results from the numerical modelling. The numerical modelling is the only method that takes the actual tunnel geometry into account, and the magnitude of the simulated crown displacement results clearly indicate failure and rock fall or tunnel collapse. This too, is deemed very realistic.

On the Hoek-Marinos classification table

It should be mentioned that the Hoek and Marinos (2000) classification given in Table 22 gives very crude and general proposals of geotechnical issues and support types. Hoek and Marinos states that for strain levels under 1%, generally very simple tunnelling conditions are encountered. It is obvious that this description does not fit the conditions in weakness zone 1, although all strain values obtained by the Hoek-Marinos approach are under 1%. To their defence, Hoek and Marinos (2000) states that additional analyses are required to obtain a final tunnel design and support system. If results are evaluated with respect to the Hoek-Marinos classification table, the RS2, CCM and Panthi and Shresta (2018) approaches seem the more realistic ones. These results fall under the "minor squeezing" description for weakness zone 1. This description is deemed realistic. Here, the problem of the rock mass' low self-bearing capacity and degree of disintegration is deemed to be just as important as the squeezing problems.

For weakness zone 2, the descriptions in the Hoek-Marinos table seems to be more fitting, but the only parameter that has changed significantly is the vertical in-situ stress. A large part of weakness zone 2 fits the proposal of 'heavy steel set support and careful construction sequence' for all approaches. This is

more in accordance with what has actually been carried out. However, if these conditions are examined with the Singh et al. (1992) prediction criteria for squeezing problems, not one of the tunnel chainages are predicted to encounter tunnel squeezing problems. Although the Q -values of the weakness zones are within the “Very poor” class, the overburden is simply not great enough to obtain tunnel squeezing prediction from the Singh et al. (1992) empirical approach. Thus, the strain results from the methods reviewed are somewhat ambiguous when relating them to the different stability classifications. However, ignoring the Singh et al. approach, the results indicate that for weakness zone 2, moderate to severe squeezing problems will occur. This indication is deemed realistic.

On the Panthi-Shresta results

The time-independent deformation reaches its completion at about four tunnel diameters behind the tunnel face (Carranza-Torres and Fairhurst, 2000). After the face-effect has ceased, further deformation is taken as time-dependent. The Panthi and Shresta (2018) approach is the one that mostly defends the delayed installation of heavy rock support in the Ryfylke tunnel, by also considering creep-deformation. The results showed that the time-dependent part of the deformation makes up 45 and 46% of the final deformation. With respect to these results, the arched RRS may still carry substantial amounts of load after their delayed installation.

With the Panthi and Shresta (2018) approach, one has the benefit of estimating the needed support pressure both for the preliminary support and the final tunnel support, by studying the obtained time-dependent and time-independent deformation values. This approach is deemed to provide the most useful information when it comes to designing a tunnel support and support methodology.

12.2 The results indication of arched RRS support

As seen from the CCM results, indications are that the installed arched RRS far behind the tunnel face for weakness zone 1 at the Ryfylke tunnel is extravagant, and the support structure would carry little load. The Panthi-Shresta results are somewhat ambiguous with respect to this, due to the concept of time-dependent deformation. For weakness zone 2, the Panthi-Shresta results imply that arched RRS installation may be necessary. However, it is hard to quantify the additional support extent necessary, solely basing it on the support pressures and tunnel strainages. The CCM results indicates that also for weakness zone 2, arched RRS is too excessive.

As indicated from the CCM results, the needed support pressure of $\sim 0,2$ MPa was met with initial systematic bolting and an 8cm layer of shotcrete. This is much less than the support actually performed. However, the assumption of a circular cross section in hydrostatic stress, which provides an evenly distributed load deviates from the real conditions. Concentration of greater stresses may take place locally in the support materials. Also, great stresses may be put on the support elements due to longitudinal arching (Oke et al., 2021). The local failure of one support element may effectively disturb the entire supporting effect within a larger area (Li, 2017). The principle of sequential failure of rock bolts is shown in Figure 64.

Taking this effect into account, it is definitely reasonable to utilize the load-distributing capabilities of an

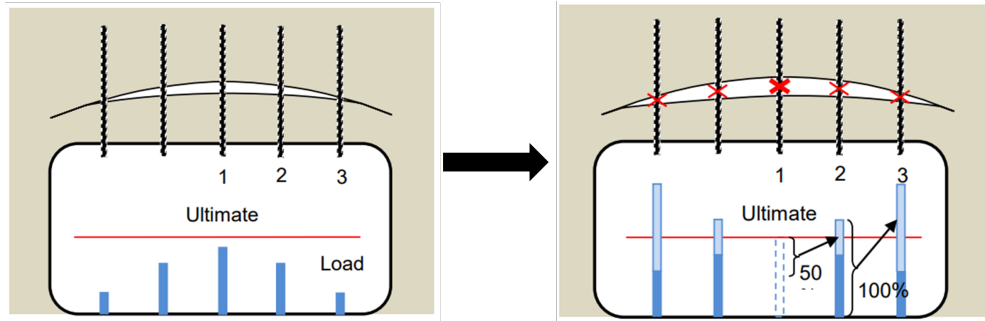


Figure 64: Sequential exceeding of the bolts support capacity. Modified after Li (2018).

arched RRS. The CCM method does not take creep-deformation into account either. The final deformation has ceased when the face-effect has ceased and the unsupported tunnel is left with a support pressure of 0. However, the safety-factor of the initial support is over 2, and alternative methods include delayed installation of more reinforcing support, or a greater capacity of the preliminary support. However, the indication that the preliminary support simulated by the CCM is adequate to stabilize the tunnel, is deemed unrealistic.

The Panthi and Shresta (2018) results indicate a substantial amount of creep deformation (time-dependent) after the face effect has ceased. These results highlight the need for rock support in two rounds; one for providing preliminary work safety and stability, and a delayed support installation to account for the creep deformation and long-term stability. This is in accordance with Grimstad (2018) proposed support methodology for very weak rock mass. Once again, the magnitudes of field stress suggests that great support capacity is not necessarily needed to obtain a sufficiently stable tunnel, as suggested by Figure 55. The Panthi-Shresta results still proposes that a higher support pressure is required to stabilize the tunnel, as compared to the CCM method. Therefore, the Panthi-Shresta results for support requirements are considered more realistic than the CCM results, but still a little uncertain.

A summary of the results' indications on tunnel stability and rock support are summarized in Table 33. In this table, "App." denotes approach, "HM" represents Hoek and Marinos (2000) approach, "Sakurai" is referring to the critical strain theory, and "PS" represents the Panthi and Shresta (2018) approach. The uncertainty evaluation ranges from very realistic- realistic- uncertain and unrealistic. For the Panthi-Shresta and the CCM method, uncertainty evaluations are given on both stability indication and support requirement indication. It can be seen that the Singh et al. (1992) approach can be rejected.

On conservativity and long-term stability and safety for road tunnels

Long term stability and safety will always be the number one priority when it comes to constructing road tunnels. Therefore, it can be argued that the construction and support methodology will be conservative by nature. When in doubt, e.g. in a transition zone of two support classes, it seems the most conservative option will always be chosen. It is also, of course, economical to avoid all possible tunnel failures and decrease comprehensive rehabilitation work to a minimum. This leads to an interesting question of whether the additional support installed will give economical gains when one is taking the full life-cycle cost of the tunnel into account. This is not studied in this thesis. An accurate analysis like that would also take more or less 100 years of data and monitoring of the tunnel and its history. Perhaps this is where the exclusively

geological field of study transits into an economical and political field.

In the light of this, the degree of conservativity of the stability assessment methods and performed support can be classified as shown in Figure 65.

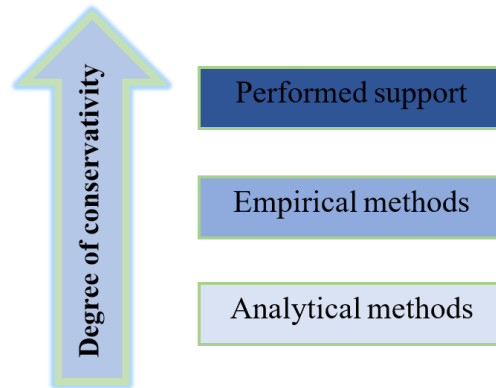


Figure 65: Degree of conservativity, illustration.

12.3 Uncertainties and limitations

Included in the stability assessment methods and the carried out calculations are some uncertainties and assumptions. The most important of them are the accuracy of the input-parameters and the main assumptions and simplifications of rock mass property estimates and stability assessment methods.

12.3.1 Input-parameters and sensitivity

The result from stability assessment methods can only ever be as accurate as the input-parameters. As mentioned, there have been no known available data on intact rock properties or stress magnitudes of the Ryfylke tunnel. Therefore, the parameters have only been crudely estimated. As a result, the accuracy of the parameters are uncertain. Consequently, the magnitude of error may increase when the parameters are incorporated in rock mass property estimation, and further increase when these are incorporated in stability assessment methods. The author is aware that the final quantitative results may be somewhat inaccurate. However, the author argues that the input-parameters utilized are realistic and of conservative nature, so that they still back up the final conclusions.

To deal with parameter uncertainty, it is possible, and recommended, to assign statistical ranges and distributions and make calculations accordingly, as carried out in e.g. Panthi (2006). In this thesis, some parameter sensitivity analyses has been carried out, but it is not representative for a full probabilistic approach. Especially the GSI sensitivity has been studied, as the GSI varies from one profile number to another while the other parameters stay more or less constant. It can be concluded that both rock mass properties and strain-values are highly sensitive to the adjustment of just a few GSI-points, which can be said to be

Table 33: Summary of result indications on stability and support requirements, with corresponding uncertainty evaluation.

App.	Zone	Indication	Evaluation	Remark/reasoning
HM	1:	Generally no squeezing problems encountered.	Uncertain	Contradicts other methods, total stress levels are lower. H-M method provides less information.
	2:	Mild-moderate squeezing problems encountered.	Realistic	Generally in accordance with other methods. Differences may be due to stress differences. H-M method provides less information.
Sakurai	1&2:	For all tunnel chainages, rock failure will happen if unsupported due to critical strain.	Very realistic	Weakness zones with low self-bearing capacity.
Singh et al.	1&2:	No tunnel chainages are predicted to encounter squeezing problems.	Unrealistic	Deviates from all other approaches regarding zone 2.
PS	1:	Moderate squeezing problems may be encountered initially, with the secondary creep deformation further increasing the deformation. Secondary support installation necessary. Arched RRS somewhat excessive.	Realistic/ Uncertain	In good accordance with other methods, although: Only method which takes creep deformation into account. This effect is deemed realistic. Also accounts for stress anisotropy.
	2:	Moderate squeezing problems may be encountered initially, with the secondary creep deformation increasing the deformation to severe squeezing. Secondary support installation necessary. Arched RRS may be needed.	Realistic/ Realistic	Squeezing levels are in good accordance with the other methods. Support indication may deviate, but again, it is the only method which accounts for creep deformation. Support indication deviates from CCM.
RS2	1:	Mild-moderate squeezing problems will be encountered. Rock fall from roof indicated.	Realistic	Predicts some more squeezing than other methods. Accounts for stress anisotropy and tunnel geometry. Roof failure without support deemed very realistic.
	2:	Moderate-severe squeezing problems will be encountered. Rock fall from roof or full collapse indicated.	Realistic	Predicts some more squeezing than other methods. Accounts for stress anisotropy and tunnel geometry. Roof failure/collapse without support deemed very realistic.
CCM	1:	Generally mild squeezing problems will be encountered. Initial support of bolts and shotcrete sufficient.	Realistic/ Uncertain	Squeezing levels a bit more than H-M and measurable Panthi-Shresta, but deemed realistic. Support indication deviates a bit from Panthi-Shresta.
	2:	Moderate-severe squeezing problems will be encountered. Initial support of bolts and shotcrete still sufficient.	Realistic/ Unrealistic	Squeezing levels a bit more than H-M and measurable Panthi-Shresta, but deemed realistic. Support indication deviates from Panthi-Shresta, and is deemed unrealistic.

within the uncertainty-range of a GSI-value assigned to a tunnel face. In addition, the results are sensitive to the D-factor, which also is said to be very difficult to quantify (Hoek, 2006). This sensitivity, in the authors opinion, has to be described as a weakness for the respective methods. Panthi (2006) estimate for rock mass properties and Panthi and Shresta (2018) squeezing estimation are the only comprehensive methods

reviewed that do not carry this weakness. As RS2 is the most sensitive method with respect to GSI, this counts as a big minus. The author argues that the difference in tunnel strainages will in reality not vary as much over small distances as shown for the RS2 results.

Regardless, when on a real project, great efforts must be made to obtain as accurate input-parameters as possible. The importance of this can not be overstated. When these are obtained, the same methodologies as those presented in this thesis can be utilized to provide realistic initial estimates on tunnel stability and preliminary support requirements.

12.3.2 Nature and basis of the assessment methods

Hoek and Marinos (2000) and CCM method assumes an isostatic stress field and a circular tunnel. This results in a uniform strain with respect to the tunnel periphery. In reality, however, there may be stress concentrations on the non-circular tunnel periphery which creates uneven strainages. Concludingly, some strain levels may exceed the ones obtained from the methods reviewed. In addition, some local pressure concentrations may exceed the capacity of the CCM simulated support, causing failure. With all the complexities of the real situation taken into account, it is only natural that the actual performed support is much heavier than the support simulated in the CCM. It can be argued that analytical solutions to complex problems with uncertain input parameters will often carry significant inaccuracy.

Having said that the Panthi (2006) estimates and the Panthi and Shrestha (2018) approach are free of subjective values, it can be questioned whether it is a strength that rock mass classification is left out. There will always be discussions about different rock mass classifications and their strengths, weaknesses and realism. Still, it is widely accepted that rock mass classification may give a good qualitative description of a rock mass, which in turn effects the magnitude of squeezing. However, the main rock mass strength parameters σ_{cm} and E_{rm} are incorporated.

13 Conclusion

In this thesis, the stability of two Ryfylke tunnel weakness zones have been examined by implementing analytical, semi-analytical, numerical and to some extent empirical approaches. The results have been summarized and compared with the actual performed support in the Ryfylke tunnel. It appears to be relatively big deviation from analytical results to the support carried out in practice. However, it has to be concluded that the magnitude of squeezing problems hardly cover every aspect of tunnel instability, which may be a far more complex topic. Following are the selected conclusions of this thesis:

1. The weakness zones in the Ryfylke tunnel, comprised of very weak phyllite rock mass, encountered mainly mild-moderate squeezing problems. Some chainages in weakness zone 2 encountered more severe squeezing problems. Substantial rock support had to be implemented to decrease deformation and maintain long-term stability. Strain levels range from $\sim 0,5 - 1,5\%$ for weakness zone 1, and $\sim 1,25 - 3,5\%$ for weakness zone 2, dependent on what method is considered. The in-situ stress levels and GSI-values greatly affect the resulting tunnel strain.
2. The analytical methods indicate that arched ribs of reinforced shotcrete was not required to prevent the tunnel squeezing problems for weakness zone 1. For weakness zone 2, the results were ambiguous as to whether arched RRS was needed or not. However, this backs up the hypothesis regarding conservative tunnel support carried out in practice. Regarding other aspects of tunnel stability, not extensively covered in this thesis, there are remaining uncertainties.
3. There seems to be a deviation between the results' indications from analytical and empirical methods, and the performed tunnel support. The performed support is the most conservative approach, and the indication from analytical methods is the least conservative approach.
4. It is evaluated that the Panthi and Shresta (2018) approach provides more information, and is more realistic in its applicability, than the other methods. Furthermore, it is also evaluated that none of the approaches reviewed are sufficient in providing an adequate representation of the total composite tunnel stability and support requirements. Additional investigations are needed. However, the methods presented in this thesis will provide a good initial idea of the magnitude of tunnel squeezing problems and perhaps preliminary rock support requirements, when accurate input-parameters are derived.

13.1 Recommendations

Selected recommendations and proposals for further studies on the topics presented in this thesis are:

1. Accurately examine input parameters in-situ and in laboratory. Assign statistical ranges and distributions for the parameters, and carry out statistical calculations.
2. Simulate the sequential rock mass deformation and support interaction of the weakness zones by comprehensive 3D numerical models, using e.g. FLAC3D.
3. By numerical modelling, both 2D and 3D, simulate how the second tube of the twin-tube tunnel affects the tunnel deformation and stability.
4. Wherever feasible, carry out more deformation and load monitoring in weakness zones where arched RRS are implemented.

References

- Alejano, L., Alonso, E., Rodriguez-Dono, A. and Fernandez-Manin, G. (2010). *Application of the convergence-confinement method to tunnels in rock masses exhibiting Hoek–Brown strain-softening behaviour*. International Journal of Rock Mechanics and Mining Sciences 47. pp. 150-160.
- Barton, N. (1995). *The influence of joint properties in modelling jointed rock masses*. Keynote lecture. 8th ISRM congress, Tokyo, Balkema, Rotterdam. 10p.
- Barton, N. (2002). *Some new Q-value correlation to assist in site characterization and tunnel design*. International Journal of Rock Mechanics and Mining Sciences 39. pp. 185-216.
- Barton, N. (2021). *Continuum or discontinuum- GSI or JRC*. Keynote lecture. From the Conference of Geotechnical Challenges in Mining, Tunnelling and Underground Structures (ICGCMTU2021), Malaysia. 67p.
- Barton, N. and Choubey, V. (1977). *The shear strength of rock joints in theory and in practice*. Rock Mechanics and Rock Engineering 10. pp. 1-54.
- Barton, N., Lien, R. and Lunde, J. (1974). *Engineering Classification of Rock Masses for the Design of Tunnel Support*. Rock Mechanics and Rock Engineering 6.4. pp. 189-236.
- Bieniawski, Z. (1989). *Engineering Rock Mass Classifications. A complete manual for engineers and geologists in mining, civil and petroleum engineering*. John Wiley & Sons, Inc. 251p.
- Bøgeberg, G. and Skretting, E. (2021). *Evaluation of the basis for rock support design for poor rock mass conditions in Norway*. Masters thesis. Norwegian University of Science and Technology (NTNU). 203p.
- Carranza-Torres, C. and Fairhurst, C. (2000). *Application of the Convergence-Confinement Method of Tunnel Design to Rock Masses That Satisfy the Hoek-Brown Failure Criterion*. Tunnelling and Underground Space Technology 15.2. pp. 187-213.
- Carter, T. G. and Marinos, V. (2020). *Putting Geological Focus Back into Rock Engineering Design*. Rock Mechanics and Rock Engineering 10.53. pp. 4487–4508.
- Deere, D. (1968). *Chapter 1: geological considerations*. Rock mechanics in engineering practice, Wiley, London (1968), pp. 1-20.
- Duncan Fama, M. E. (1993). *Numerical modelling of yield zones in weak rocks*. In: Comprehensive Rock Engineering 2. pp. 49-75.
- Fatemi Aghda, S., Ganjalipour, K. and Esmaeil Zadeh, M. (2016). *Comparison of squeezing prediction methods: A case study on nowsoud tunnel*. Geotechnical and Geological Engineering 34. pp. 1487-1512.
- Grimstad, E. (2018). *Support methods for rock mass (Norwegian). Sikringsmetoder*. Lecture notes. NBG - Applied Rock Mechanics, Trondheim. 49p.
- Grimstad, E., Kankes, K., Bhasin, R., Magnussen, A. and Kaynia, A. (2002). *Rock mass quality used in designing reinforced ribs of sprayed concrete and energy absorption*. Bergmekanikkdagen (Rock Mechanics Day) (NBG, NFF). 18p.
- Gupta, A. and Rao, K. (2000). *Weathering effects on the strength an deformational behaviour of crystalline rocks under uniaxial compression state*. Engineering geology 56. pp. 257-274.
- Hoek, E. (1994). *Strength of Rock and Rock Masses*. ISRM News Journal, 2. pp. 4-16.
- Hoek, E. (2006). *Practical rock engineering*. 341p. URL: <https://www.rocsience.com/assets/resources/learning/hoek/Practical-Rock-Engineering-Full-Text.pdf>.

- Hoek, E. and Brown, E. (1997). *Practical Estimates of Rock Mass Strength*. International Journal of Rock Mechanics and Mining Sciences 8. pp. 1165-1186.
- Hoek, E. and Brown, E. (2019). *The Hoek-Brown failure criterion and GSI, 2018 edition*. Journal of Rock Mechanics and Geotechnical Engineering 11. pp. 454-463.
- Hoek, E., Carranza-Torres, C. and Corkum, B. (2002). *Hoek-Brown failure criterion - 2002 edition*. Proceedings of the 5th North American rock mechanics symposium et al.
- Hoek, E., Carter, T. and Diederichs, M. (2013). *Quantification of the Geological Strength Index Chart*. Paper for the 47th Geomechanics Symposium. San Fransisco, CA, USA. June 23-26. 9p.
- Hoek, E. and Diederichs, M. (2006). *Empirical estimation of rock mass modulus*. International Journal of Rock Mechanics and Mining Sciences 43. pp. 203-215.
- Hoek, E. and Marinos, P. (2000). *Predicting tunnel squeezing problems in weak heterogeneous rock masses*. Tunnels and Tunnelling International 32.11. pp. 45-51.
- Høien, A. (2019). *Applicability of reinforced ribs of sprayed concrete in sections of poor quality and swelling rock mass*. Doctoral thesis. Norwegian University of Science and Technology (NTNU). 129p.
- Høien, A., Nilsen, B. and Olsson, R. (2019). *Main aspects of deformation and rock support in Norwegian road tunnels*. Tunnelling and Underground Space Technology 86. pp. 262-278.
- ISRM (1978). *Suggested methods for the quantitative description of discontinuities in rock mass*. International journal of rock mechanics, mining sciences and geomechanics abstracts 15. pp. 319-368.
- ISRM (1979). *Suggested Method for Determining the Uniaxial Compressive Strength and Deformability of Rock Materials*. International Society for Rock Mechanics and Rock Engineering. 4p.
- Kim, H., Jeon, S. and Park, E.-S. (2022). *Evaluation of monitoring items for adverse ground conditions in subsea tunneling*. Tunnelling and Underground Space Technology 32. pp 19-32.
- Lavrov, A. (2019a). *Finite element method: basic ideas*. Lecture notes. TGB4260 Numerical modelling for rock mechanics. Norwegian University of Science and Technology (NTNU). 38p.
- Lavrov, A. (2019b). *Finite element method: beyond the basic FEM*. Lecture notes. TGB4260 Numerical modelling for rock mechanics. Norwegian University of Science and Technology (NTNU). 18p.
- Lavrov, A. (2022). Personal communication, e-mail. 13.05.2022.
- Li, C. C. (2017). *Principles of rockbolting design*. Journal of Rock Mechanics and Geotechnical Engineering 9.3. pp. 396-414.
- Li, C. C. (2018). *Rock Mechanics, BC Compendium*. TGB4120 Rock Mechanics, BC. Norwegian University of Science and Technology (NTNU). 268p.
- Marinos, P. and Hoek, E. (2000). *GSI- A geologically friendly tool for rock mass strength estimation*. Proceedings of the Geological Engineering Conference, Melbourne. pp. 1422-1442.
- Marinos, V., Marinos, P. and Hoek, E. (2005). *The geological strength index: applications and limitations*. Bulletin of Engineering Geology and the Environment 55. pp. 55-65.
- Multiconsult (2009). *Zoning plan, rv.13 Ryfast and E39 Eiganes tunnel. Geological report*. 90p.
- Myrvang, A. M. (2001). *Rock mechanics (Norwegian)*. *Bergmekanikk*. Norwegian University of Science, Technology. Department of Geology and Mineral Resources Engineering, Trondheim.
- NBG (2000). *Engineering geology and rock engineering*. Norwegian Group for Rock Mechanics (NBG). Handbook no.2. 266p.
- NBG (2011). *Guide for the use of Eurocode 7 for Geotechnical Planning (Norwegian)*. *Veileder for bruk av Eurokode 7 til bergteknisk prosjektering*. Norwegian Rock Mechanics Group (NBG). 31p.

- NFF (2008). *Heavy rock support in underground constructions (Norwegian). Tung bergkriking i undergrunnsanlegg*. Norwegian Tunnelling Society (NFF). Handbook nr 5. 80p.
- NFF (2009a). *Norwegian Tunneling Technology*. Norwegian Tunneling Society (NFF). Publication 23. 218p.
- NFF (2009b). *Subsea Tunnels*. Norwegian Tunneling Society (NFF). Publication 18. 108p.
- NFF (2012). *Smoothness of drill-and-blasted tunnels (Norwegian). Konturkvalitet i sprengte tunneller*. Norwegian Tunneling Society (NFF). Technical report no12. 52p.
- NFF (2018). *The Principles of Norwegian tunnelling*. Norwegian Tunnelling Society (NFF). Publication 26. 208p.
- NGI (2015). *Using the Q-system*. Norwegian Geotechnical Institute. 56p.
- Nilsen, B. (1990). *The optimum rock cover for subsea tunnels*. Rock Mechanics Contributions and Challenges. The 31st US Symposium on Rock Mechanics (USRMS). 8p.
- Nilsen, B. (2011). *Cases of instability caused by weakness zones in Norwegian tunnels*. Bulletin of Engineering Geology and the Environment 70. pp. 7-13.
- Nilsen, B. (2014). *Characteristics of Water Ingress in Norwegian Subsea Tunnels*. Rock Mechanics and Rock Engineering 47. pp. 933-945.
- Nilsen, B. (2016). *Engineering Geology of Rocks - BC Compendium*. TGB4185 Engineering Geology, BC. Norwegian University of Science and Technology (NTNU). 278p.
- Nilsen, B. (2017). *Significance of engineering geology for planning, design and construction*. Lecture notes. TGB4190 - Engineering Geology of Rocks AC. Norwegian University of Science and Technology (NTNU). 12p.
- Nilsen, B., Palmström, A. and Stille, H. (1999). *Quality control of a sub-sea tunnel project in complex ground conditions*. International Symposium on Challenges for the 21st Century, Oslo, Norway. 9p.
- Nilsen, B., Shrestha, G. L., Panthi, K. K., Olsen, V. and Holmøy, K. H. (2003). *RMR vs Q vs RMi*. Tunnels and Tunnelling International 35. pp. 45-48.
- Norconsult (2012). *Geological report (Pre-construction) Ryfylke tunnel*. 56p.
- NPRA (2019). *Ryfylke tunnel RV13. Final geological report*. Norwegian Public Roads Administration (NPRA). 96p.
- NPRA (2021). *N500 Road Tunnels (Norwegian). N500 Vegtunneler*. Norwegian Public Roads Administration (NPRA). 88p. URL: <https://svv-cm-sv-apppublic-prod.azurewebsites.net/product/859934?filePath=b777a007-22d9-4ba5-ba06-9fb5b0aab49d.pdf>.
- NPRA (2022). *V521. Geology and rock support in tunnels (Norwegian). Geologi og bergsikring i tunnel*. Norwegian Public Roads Administration (NPRA). 88p. URL: <https://www.vegvesen.no/globalassets/fag/handboker/v521.pdf>.
- Oke, J., Vlachopoulos, N. and Diederichs, M. (2021). *Improvement to the convergence-confinement method: inclusion of support installation proximity and stiffness*. Rock Mechanics and Rock Engineering 51. pp. 1495-1519.
- Olsson, R. (2021). *Application of rock engineering in hydropower projects*. Lecture notes. TGB4212: Rock Mechanics, AC. Norwegian University of Science and Technology. 92p.
- Palmström, A. and Berthelsen, O. (1988). *The significance of weakness zones in rock tunnelling*. Proceedings from ISRM Symposium on Rock Mechanics and Power Plants, Madrid, Spain. pp. 381-388.
- Palmström, A., Nilsen, B., Pedersen, K. and Grundt, L. (2003). *Appropriate amount of ground investigations (Norwegian). Riktig omfang av grunnundersøkelser for berganlegg*. Tunnels for the society-NPRA. 137p.

- URL: https://vegvesen.brage.unit.no/vegvesen-xmlui/bitstream/handle/11250/190430/publikasjon_101.pdf?sequence=1&isAllowed=y.
- Palmström, A. and Singh, R. (2001). *The deformation modulus of rock masses: comparisons between in situ tests and indirect estimates*. Tunnelling and Underground Space Technology 16. pp. 115-131.
- Palmström, A. (1995). *RMi - a system for characterizing rock mass strength for use in rock engineering*. PhD Thesis. Oslo University. 400p.
- Palmström, A. and Broch, E. (2006). *Use and misuse of rock mass classification systems with particular reference to the Q-system*. Tunnelling and Underground Space Technology 21.6. pp 575-593.
- Panthi, K. K. (2006). *Analysis of engineering geological uncertainties related to tunnelling in Himalayan rock mass conditions*. PhD thesis. Norwegian University of Science and Technology (NTNU). 189p.
- Panthi, K. K. (2012). *Evaluation of rock bursting phenomena in a tunnel in the Himalayas*. Bulletin of Engineering Geology and the Environment 71. pp. 761-769.
- Panthi, K. K. (2021). Lecture notes. TGB4190. Engineering Geology of Rocks AC. Norwegian University of Science and Technology (NTNU). 55p.
- Panthi, K. K. (2022a). Personal communication, email. 18.04.2022.
- Panthi, K. K. (2022b). Personal communication. 01.05.2022.
- Panthi, K. K. (2022c). Personal communication. 22.04.2022.
- Panthi, K. K. (2022d). Personal communication. 19.05.2022.
- Panthi, K. K. and Shrestha, P. K. (2018). *Estimating Tunnel Strain in the Weak and Schistose Rock Mass Influenced by Stress Anisotropy: An Evaluation Based on Three Tunnel Cases from Nepal*. Rock Mechanics and Rock Engineering 51. pp. 1823–1838.
- Paraskevopoulou, C. and Boutsis, G. (2020). *Cost Overruns in Tunnelling Projects: Investigating the Impact of Geological and Geotechnical Uncertainty Using Case Studies*. Infrastructures 5.9. 35p.
- Rocscience (n.d.). *RS2 documentation*. Read 13.05.2022. URL: <https://www.rocscience.com/help/rs2/documentation/>.
- Sakurai, S. (1981). *Direct strain evaluation technique in construction of underground openings*. Symposium on Rock Mechanics (USRMS). American Rock Mechanics Association, Cambridge, Massachusetts.
- Sakurai, S. (1983). *Displacement measurements associated with the design of underground openings*. Proceedings of the International Symposium of field measurements in geomechanics, Zürich. pp. 1163-1178.
- Al-Samarray, A. (2022). Personal communication. 30.05.2022.
- Sheory, P. R. (1994). *A theory for In Situ stresses in isotropic and transverseley isotropic rock*. International Journal of Rock Mechanics and Mining Sciences & Geomechanics Abstracts 31.1. pp. 23-34.
- Singh, B. and Goel, R. (2011). *Engineering Rock Mass Classification*. Book. Publisher: Butterworth-Heinemann. Tunnelling, Foundations and Landslides. 384p.
- Singh, B., Jethwa, J., Dube, A. and Singh, B. (1992). *Correlation between observed support pressure and rock mass quality*. Tunnelling and Underground Space Technology 7.1. pp. 59-74.
- Sulem, J., Panet, M. and Guenot, A. (1987a). *Analytical solution for time dependent displacements in a circular tunnel*. International Journal of Rock Mechanics and Mining Sciences 24.3. pp. 155-164.
- Sulem, J., Panet, M. and Guenot, A. (1987b). *Closure analysis in deep tunnels*. International Journal of Rock Mechanics and Mining Sciences 24.3. pp. 145-154.
- Torgersen, E. A. (2021). *Potential use of Tunnel Seismic Prediction (TSP) in Tunnelling*. Norwegian University of Science and Technology (NTNU). Specialization project. 66p. (Not published).

- Unlu, T. and Gercek, H. (2003). *Effect of Poisson's ratio on the normalized radial displacements occurring around the face of a circular tunnel*. Tunnelling and Underground Space Technology 18. pp. 547-553.
- Vlachopoulos, N. and Diederichs, M. S. (2009). *Improved Longitudinal Displacement Profiles for Convergence Confinement Analysis of Deep Tunnels*. Rock Mechanics and Rock Engineering 42. pp. 131-146.

Appendix

A Chart for evaluating the disturbance factor D



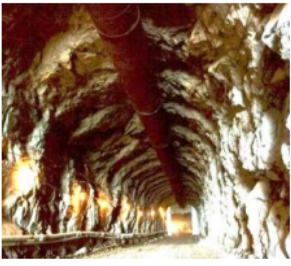


Appearance of rock mass	Description of rock mass	Suggested value of D
	Excellent quality controlled blasting or excavation by Tunnel Boring Machine results in minimal disturbance to the confined rock mass surrounding a tunnel.	D = 0
	Mechanical or hand excavation in poor quality rock masses (no blasting) results in minimal disturbance to the surrounding rock mass. Where squeezing problems result in significant floor heave, disturbance can be severe unless a temporary invert, as shown in the photograph, is placed.	D = 0 D = 0.5 No invert
	Very poor quality blasting in a hard rock tunnel results in severe local damage, extending 2 or 3 m, in the surrounding rock mass.	D = 0.8
	Small scale blasting in civil engineering slopes results in modest rock mass damage, particularly if controlled blasting is used as shown on the left hand side of the photograph. However, stress relief results in some disturbance.	D = 0.7 Good blasting D = 1.0 Poor blasting
	Very large open pit mine slopes suffer significant disturbance due to heavy production blasting and also due to stress relief from overburden removal. In some softer rocks excavation can be carried out by ripping and dozing and the degree of damage to the slopes is less.	D = 1.0 Production blasting D = 0.7 Mechanical excavation

Figure A.1: Chart for evaluating disturbance factor D. From: Hoek (2006).

B Q-system parameters and support chart

1 RQD (Rock Quality Designation)			RQD
A	Very poor	(> 27 joints per m ³)	0-25
B	Poor	(20-27 joints per m ³)	25-50
C	Fair	(13-19 joints per m ³)	50-75
D	Good	(8-12 joints per m ³)	75-90
E	Excellent	(0-7 joints per m ³)	90-100

Note: i) Where RQD is reported or measured as ≤ 10 (including 0) the value 10 is used to evaluate the Q-value
 ii) RQD-intervals of 5, i.e. 100, 95, 90, etc., are sufficiently accurate

Figure B.1: Basis for deciding the RQD in the Q-system. From: NGI (2015).

2 Joint set number		J_n
A	Massive, no or few joints	0.5-1.0
B	One joint set	2
C	One joint set plus random joints	3
D	Two joint sets	4
E	Two joint sets plus random joints	6
F	Three joint sets	9
G	Three joint sets plus random joints	12
H	Four or more joint sets, random heavily jointed "sugar cube", etc	15
J	Crushed rock, earth like	20

Note: i) For tunnel intersections, use $3 \times J_n$
 ii) For portals, use $2 \times J_n$

Figure B.2: Basis for deciding the J_n -value in the Q-system. From: NGI (2015).

3 Joint Roughness Number		J_r
a) Rock-wall contact, and b) Rock-wall contact before 10 cm of shear movement		
A	Discontinuous joints	4
B	Rough or irregular, undulating	3
C	Smooth, undulating	2
D	Slickensided, undulating	1.5
E	Rough, irregular, planar	1.5
F	Smooth, planar	1
G	Slickensided, planar	0.5
Note: i) Description refers to small scale features and intermediate scale features, in that order		
c) No rock-wall contact when sheared		
H	Zone containing clay minerals thick enough to prevent rock-wall contact when sheared	1
Note: ii) Add 1 if the mean spacing of the relevant joint set is greater than 3 m (dependent on the size of the underground opening) iii) $J_r = 0.5$ can be used for planar slickensided joints having lineations, provided the lineations are oriented in the estimated sliding direction		

Figure B.3: Basis for deciding the J_r -value in the Q-system. From: NGI (2015).

4 Joint Alteration Number		Φ_r approx.	J_a
a) Rock-wall contact (no mineral fillings, only coatings)			
A	Tightly healed, hard, non-softening, impermeable filling, i.e., quartz or epidote.		0.75
B	Unaltered joint walls, surface staining only.	25-35°	1
C	Slightly altered joint walls. Non-softening mineral coatings; sandy particles, clay-free disintegrated rock, etc.	25-30°	2
D	Silty or sandy clay coatings, small clay fraction (non-softening).	20-25°	3
E	Softening or low friction clay mineral coatings, i.e., kaolinite or mica. Also chlorite, talc gypsum, graphite, etc., and small quantities of swelling clays.	8-16°	4
b) Rock-wall contact before 10 cm shear (thin mineral fillings)			
F	Sandy particles, clay-free disintegrated rock, etc.	25-30°	4
G	Strongly over-consolidated, non-softening, clay mineral fillings (continuous, but <5 mm thickness).	16-24°	6
H	Medium or low over-consolidation, softening, clay mineral fillings (continuous, but <5 mm thickness).	12-16°	8
J	Swelling-clay fillings, i.e., montmorillonite (continuous, but <5 mm thickness). Value of J_a depends on percent of swelling clay-size particles.	6-12°	8-12
c) No rock-wall contact when sheared (thick mineral fillings)			
K	Zones or bands of disintegrated or crushed rock. Strongly over-consolidated.	16-24°	6
L	Zones or bands of clay, disintegrated or crushed rock. Medium or low over-consolidation or softening fillings.	12-16°	8
M	Zones or bands of clay, disintegrated or crushed rock. Swelling clay. J_a depends on percent of swelling clay-size particles.	6-12°	8-12
N	Thick continuous zones or bands of clay. Strongly over-consolidated.	12-16°	10
O	Thick, continuous zones or bands of clay. Medium to low over-consolidation.	12-16°	13
P	Thick, continuous zones or bands with clay. Swelling clay. J_a depends on percent of swelling clay-size particles.	6-12°	13-20

Figure B.4: Basis for deciding the J_a -value in the Q-system. From: NGI (2015).

5 Joint Water Reduction Factor		J_w
A	Dry excavations or minor inflow (humid or a few drips)	1.0
B	Medium inflow, occasional outwash of joint fillings (many drips/"rain")	0.66
C	Jet inflow or high pressure in competent rock with unfilled joints	0.5
D	Large inflow or high pressure, considerable outwash of joint fillings	0.33
E	Exceptionally high inflow or water pressure decaying with time. Causes outwash of material and perhaps cave in	0.2-0.1
F	Exceptionally high inflow or water pressure continuing without noticeable decay. Causes outwash of material and perhaps cave in	0.1-0.05
Note: i) Factors C to F are crude estimates. Increase J_w if the rock is drained or grouting is carried out ii) Special problems caused by ice formation are not considered		

Figure B.5: Basis for deciding the J_w -value in the Q-system. From: NGI (2015).

6 Stress Reduction Factor				SRF
a) Weak zones intersecting the underground opening, which may cause loosening of rock mass				
A	Multiple occurrences of weak zones within a short section containing clay or chemically disintegrated, very loose surrounding rock (any depth), or long sections with incompetent (weak) rock (any depth). For squeezing, see 6L and 6M			10
B	Multiple shear zones within a short section in competent clay-free rock with loose surrounding rock (any depth)			7.5
C	Single weak zones with or without clay or chemical disintegrated rock (depth ≤ 50m)			5
D	Loose, open joints, heavily jointed or "sugar cube", etc. (any depth)			5
E	Single weak zones with or without clay or chemical disintegrated rock (depth > 50m)			2.5
Note: i) Reduce these values of SRF by 25-50% if the weak zones only influence but do not intersect the underground opening				
b) Competent, mainly massive rock, stress problems		σ_c / σ_1	σ_θ / σ_c	SRF
F	Low stress, near surface, open joints	>200	<0.01	2.5
G	Medium stress, favourable stress condition	200-10	0.01-0.3	1
H	High stress, very tight structure. Usually favourable to stability. May also be unfavourable to stability dependent on the orientation of stresses compared to jointing/weakness planes*	10-5	0.3-0.4	0.5-2 2-5*
J	Moderate spalling and/or slabbing after > 1 hour in massive rock	5-3	0.5-0.65	5-50
K	Spalling or rock burst after a few minutes in massive rock	3-2	0.65-1	50-200
L	Heavy rock burst and immediate dynamic deformation in massive rock	<2	>1	200-400
Note: ii) For strongly anisotropic virgin stress field (if measured): when $5 \leq \sigma_1 / \sigma_3 \leq 10$, reduce σ_c to $0.75 \sigma_c$. When $\sigma_1 / \sigma_3 > 10$, reduce σ_c to $0.5 \sigma_c$, where σ_c = unconfined compression strength, σ_1 and σ_3 are the major and minor principal stresses, and σ_θ = maximum tangential stress (estimated from elastic theory)				
iii) When the depth of the crown below the surface is less than the span; suggest SRF increase from 2.5 to 5 for such cases (see F)				
c) Squeezing rock: plastic deformation in incompetent rock under the influence of high pressure			σ_θ / σ_c	SRF
M	Mild squeezing rock pressure		1-5	5-10
N	Heavy squeezing rock pressure		>5	10-20
Note: iv) Determination of squeezing rock conditions must be made according to relevant literature (i.e. Singh et al., 1992 and Bhasin and Grimstad, 1996)				
d) Swelling rock: chemical swelling activity depending on the presence of water				SRF
O	Mild swelling rock pressure			5-10
P	Heavy swelling rock pressure			10-15

Figure B.6: Basis for deciding the SRF-value in the Q-system. From: NGI (2015).

7 Type of excavation		ESR
A	Temporary mine openings, etc.	ca. 3-5
B	Vertical shafts*: i) circular sections ii) rectangular/square section * Dependant of purpose. May be lower than given values.	ca. 2.5 ca. 2.0
C	Permanent mine openings, water tunnels for hydro power (exclude high pressure penstocks) water supply tunnels, pilot tunnels, drifts and headings for large openings.	1.6
D	Minor road and railway tunnels, surge chambers, access tunnels, sewage tunnels, etc.	1.3
E	Power houses, storage rooms, water treatment plants, major road and railway tunnels, civil defence chambers, portals, intersections, etc.	1.0
F	Underground nuclear power stations, railways stations, sports and public facilities, factories, etc.	0.8
G	Very important caverns and underground openings with a long lifetime, \approx 100 years, or without access for maintenance.	0.5

Figure B.7: Basis for deciding the ESR-value in the Q-system. From: NGI (2015).

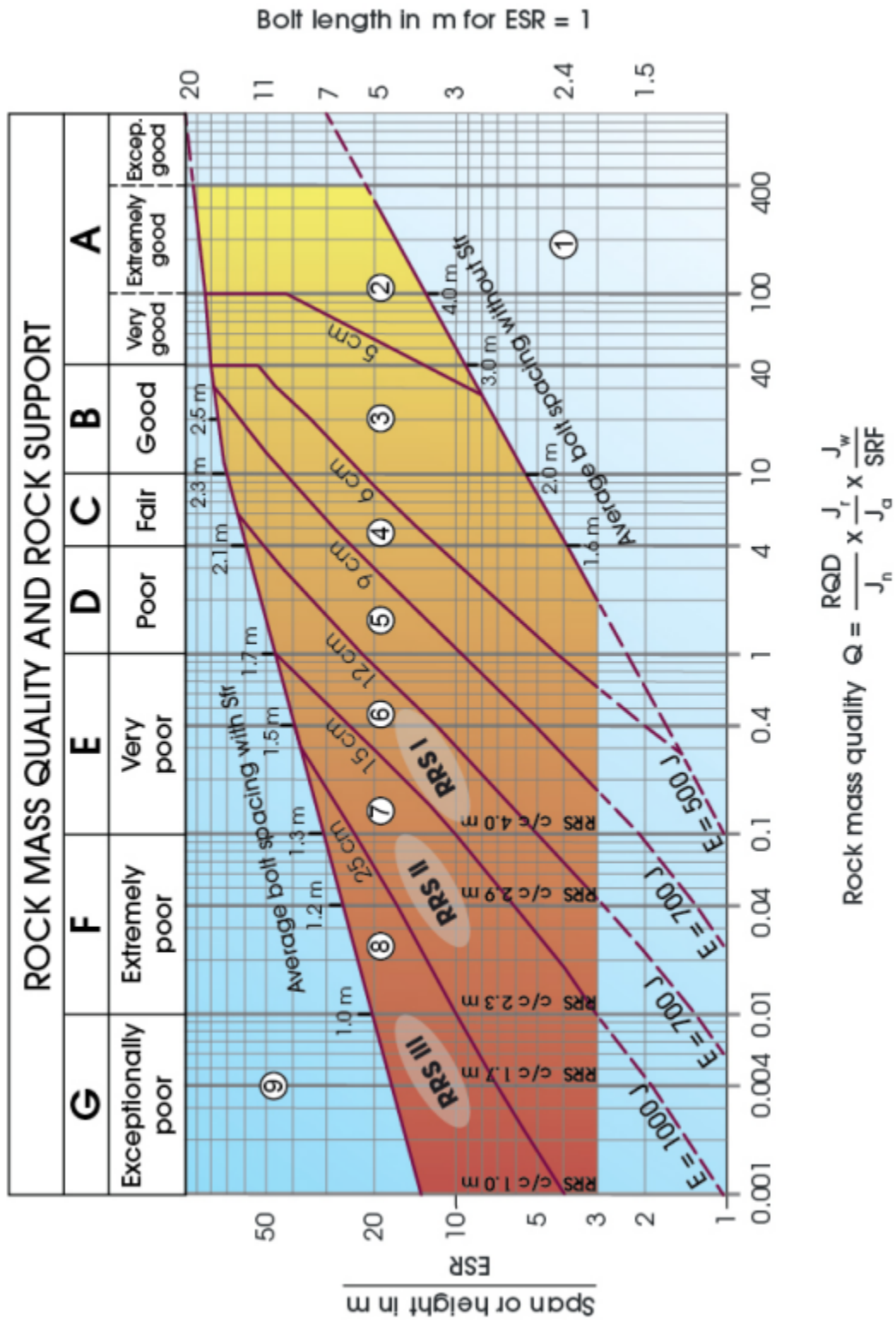


Figure B.8: Support chart for use with the Q-system. From: NGI (2015).

C Excel formulae for implementation to CCM

The following formulae to be plotted in excel are reproduced or adjusted from Carranza-Torres and Fairhurst (2000).

For the Ground Reaction Curve, *ure_grc* and *urp_grc* (elastic and plastic radial wall deformation) are plotted against *pie_grc* and *pip_grc* (elastic and plastic support pressure, decreasing with face advance).

For the Support Characteristics Curve for shotcrete and bolts, *ur_sc_b* (deformation of support) is plotted against *pi_sc_b* (support pressure provided by support system).

```

M_b=m_i*EXP((GSI-100)/(28-14*D))
S_coeff=IF(GSI>=25,EXP((GSI-100)/(9-3*D)),0)
E_rm=SQRT(sig_ci/100)*10^((GSI-10)/40)
G_rm=E_rm/2/(1+nu)
K_psi=(1+SIN(psi*PI()/180))/(1-SIN(psi*PI()/180))
S_0=sig_0/(m_b*sig_ci)+s_coeff/m_b^2
Pi_cr_s=1/16*(1-SQRT(1+16*S_0))^2
pi_cr=(Pi_cr_s-s_coeff/(m_b^2))*m_b*sig_ci
pie_grc=sig_0 (first row), =pi_cr (second row)
ure_grc=(sig_0-pie_grc)/2/(G_rm*1000)*R_t^1000
pip_grc=pi_cr*(12-pt_grc)/11
pip_r_grc=pip_grc+gamma*(xi_grc*R_t-R_t)
pip_f_grc=pip_grc-gamma*(xi_grc*R_t-R_t)
pips_grc=pip_grc/(m_b*sig_ci)+s_coeff/m_b^2
xi_grc=EXP(2*(SQRT(Pi_cr_s)-SQRT(pips_grc)))
urp_grc(((K_psi-1)/(K_psi+1))+2/(K_psi+1))*xi_grc
    ^((K_psi+1)+(1-2*nu)/4)/(S_0-Pi_cr_s)*LN(xi_grc)^2
    -((1-2*nu)/(K_psi+1))*(SQRT(Pi_cr_s))/(S_0-Pi_cr_s)
    +(1-nu)/2*(K_psi-1)/(K_psi+1)^2/(S_0-Pi_cr_s)
    *((K_psi+1)*LN(xi_grc)-(xi_grc)^(K_psi+1)+1)
    *R_t*(sig_0-pi_cr)/2/(G_rm*1000)*1000
lf_r=-4+(pt_ldp-1)*12/11
lf=lf_r*R_t
ur_ldp=ur_max*(1+EXP(-lf/1.1/R_t))-1.7
Lf_2=Lf
ur_0=ur_max*(1+EXP(-Lf/1.1/R_t))-1.7

theta_s=180/n_B
pmax_s=(3*A_s*I_s*sig_ys)/(2*S_s*R_t*theta_s*PI()/180
    *(3*I_s+D_s/1000*A_s*(R_t-t_B/1000-0.5*D_s/1000)
    *(1-COS(theta_s*PI()/180))))
K_s=1/(((S_s*R_t^2)/(E_s*1000*A_s))+(S_s*R_t^4/(E_s*1000*I_s)
    *((theta_s*PI()/180*(theta_s*PI()/180+SIN(theta_s*PI()
    /180)*COS(theta_s*PI()/180)))/(2*(SIN(theta_s*PI()/180)
    ^2))-1)+(2*S_s*theta_s*PI()/180*t_B/1000*R_t)/(E_B*1000
    *(B_s/1000)^2))
urmax_s=pmax_s/K_s*1000
pi_ss=0 (first row), =pmax_s (second and third rows)
ur_ss=ur_0 (first row), =ur_0+urmax_s (second row)
    =ur_0+urmax_s^4 (third row)
pmax_c=sig_cc/2*(1-(R_t-t_c/1000)^2/R_t^2)
K_c=E_c*1000/(1+nu_c)*(R_t^2-(R_t-t_c/1000)^2)/((1-2*nu_c)*
    R_t^2+(R_t-t_c/1000)^2)/R_t
urmax_c=pmax_c/K_c*1000
pi_sc=0 (first row), =pmax_c (second and third rows)
ur_sc=ur_0 (first row), =ur_0+urmax_c (second row)
    =ur_0+urmax_c^4 (third row)
sc_b=2*PI()*R_t/n_bolt
pmax_b=T_bf/sc_b/s_lb
K_b=1/(sc_b*s_lb)*(PI()*(d_b/1000)^2*E_bolt*1000)/(4*I_b+
    Q_b*PI()*(d_b/1000)^2*E_bolt*1000)
urmax_b=pmax_b/K_b*1000
pi_sb=0 (first row), =pmax_b (second and third rows)
ur_sb=ur_0 (first row), =ur_0+urmax_b (second row)
    =ur_0+urmax_b^4 (third row)
K_s_b=K_s+K_b
urmax_s_b=IF(urmax_s<urmax_b,urmax_s,urmax_b)
pmax_s_b=K_s_b*urmax_s_b/1000
pi_ss_b=0 (first row), =pmax_s_b (second and third rows)
ur_ss_b=ur_0 (first row), =ur_0+urmax_s_b (second row)
    =ur_0+urmax_s_b^4 (third row)
K_c_b=K_c+K_b
urmax_c_b=IF(urmax_c<urmax_b,urmax_c,urmax_b)
pmax_c_b=K_c_b*urmax_c_b/1000
pi_sc_b=0 (first row), =pmax_c_b (second and third rows)
ur_sc_b=ur_0 (first row), =ur_0+urmax_c_b (second row)
    =ur_0+urmax_c_b^4 (third row)

```

Figure C.1: Excel formulae for plotting with the CCM method. Adjusted or reproduced from Carranza-Torres and Fairhurst (2000).

D CCM Characteristic curves for all chainages reviewed

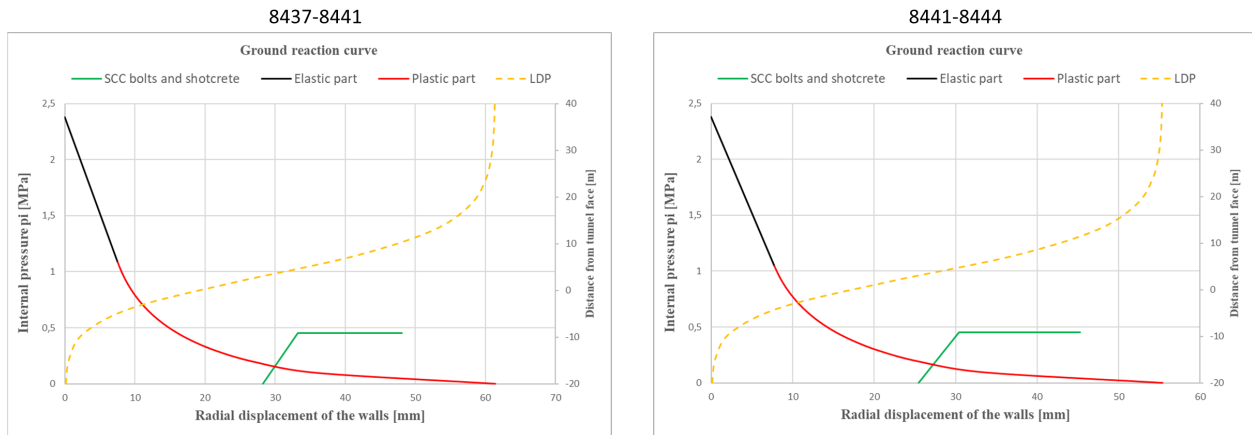


Figure D.1: Characteristic curves for chainage 8437-8444.

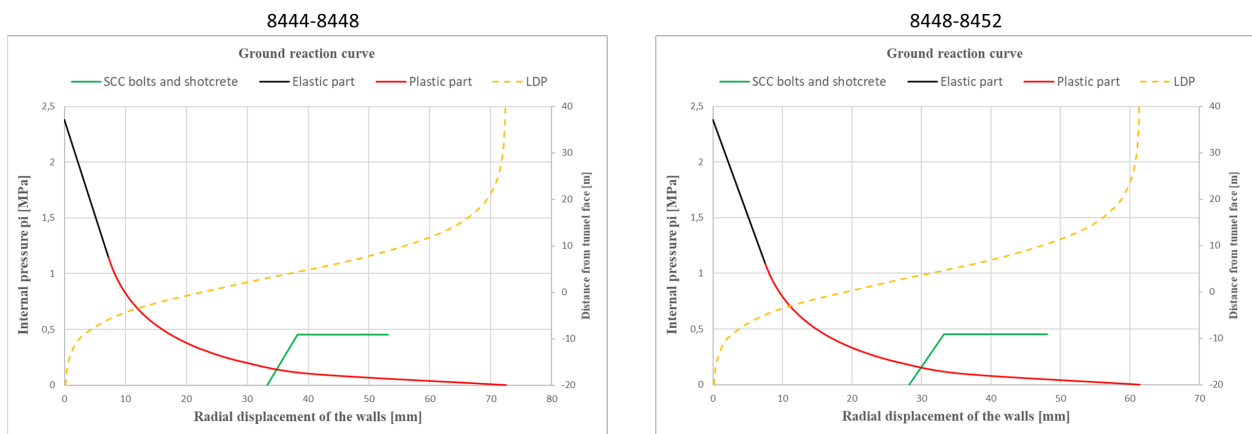


Figure D.2: Characteristic curves for chainage 8444-8452.

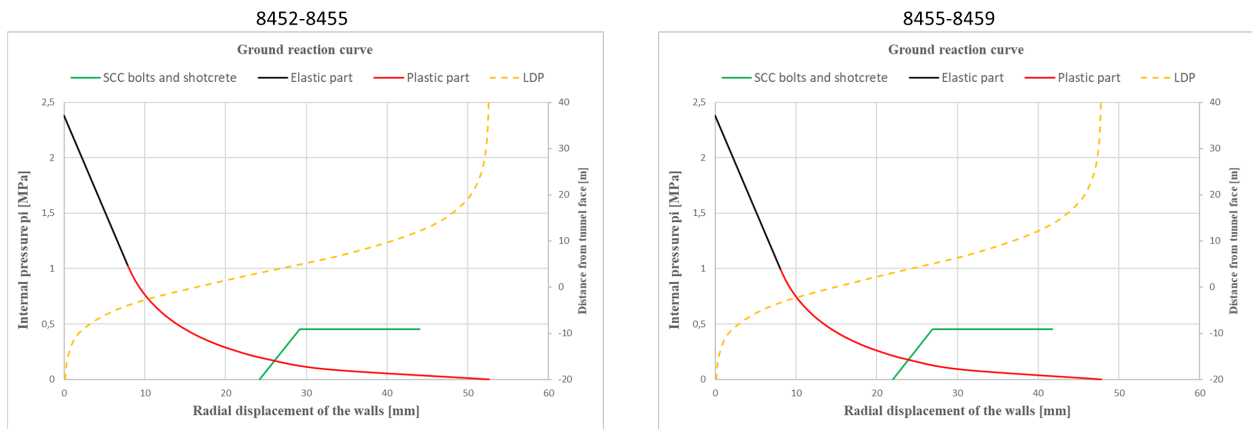


Figure D.3: Characteristic curves for chainage 8452-8459.

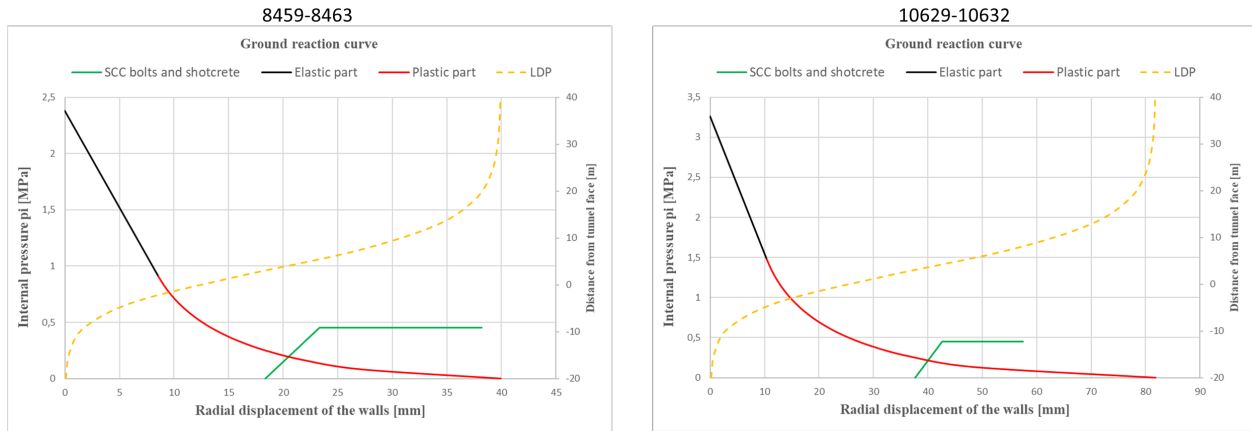


Figure D.4: Characteristic curves for chainage 8459-8463 and 10629-10632.

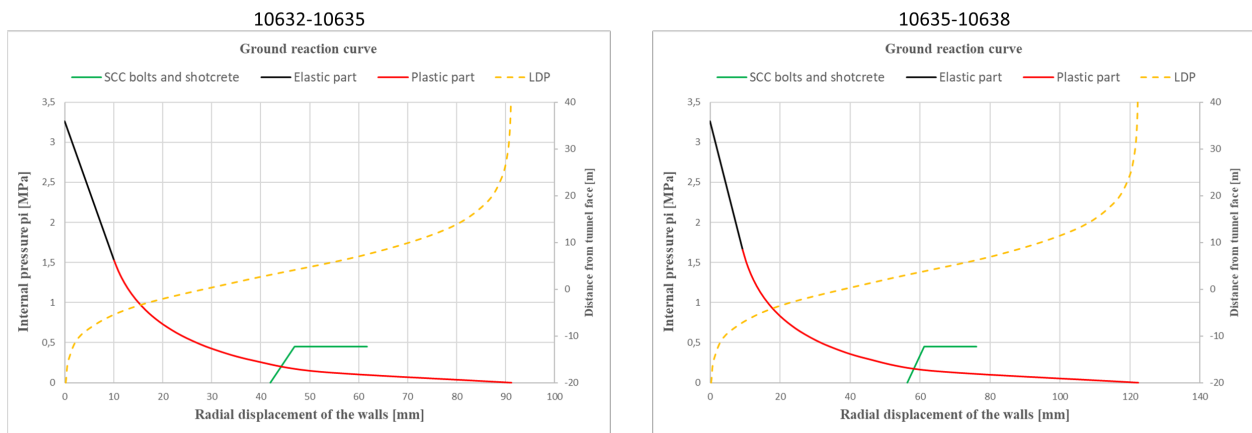


Figure D.5: Characteristic curves for chainage 10632-10638.

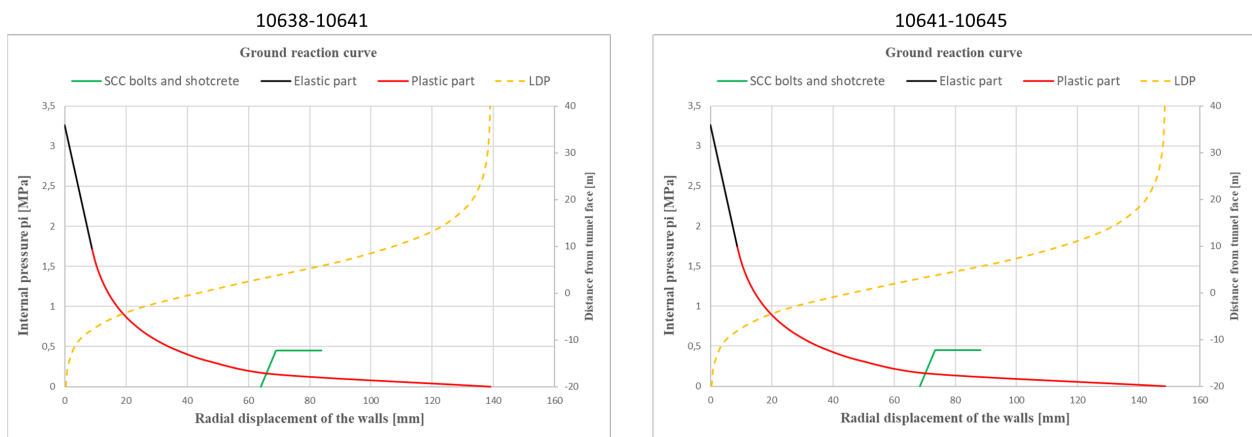


Figure D.6: Characteristic curves for chainage 10638-10645.

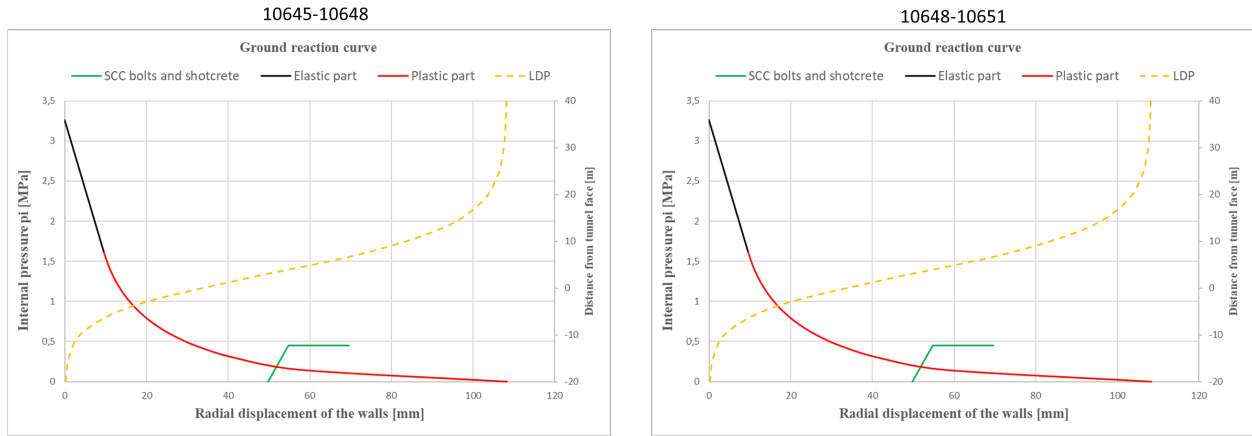


Figure D.7: Characteristic curves for chainage 10645-10651.

